

PALEOSEISMOLOGY, SLIP BUDGET, AND FAULT BEHAVIOR ALONG THE
PARKFIELD SEGMENT OF THE SAN ANDREAS FAULT

by

Nathan A. Toké

A Thesis Presented in Partial Fulfillment
of the Requirements for the Degree
Master of Science

ARIZONA STATE UNIVERSITY

December 2005

PALEOSEISMOLOGY, SLIP BUDGET, AND FAULT BEHAVIOR ALONG THE
PARKFIELD SEGMENT OF THE SAN ANDREAS FAULT

by

Nathan A. Toké

has been approved

November 2005

APPROVED:

_____, Chair

Supervisory Committee

ACCEPTED:

Department Chair

Dean, Division of Graduate Studies

ABSTRACT

Historically, the Parkfield segment of the San Andreas Fault (SAF) has represented a transition in fault behavior between steady fault creep to the northwest and segments to the southeast (e.g., the Cholame segment) that have not slipped since the Great 1857 Fort Tejón earthquake. Since 1857, slip from ~M6 earthquakes and creep has been observed at Parkfield. However, Parkfield's prehistoric fault behavior and thus its importance in great SAF ruptures remained previously unexplored.

Two fault-perpendicular paleoseismic excavations along the central Parkfield segment exposed five fault zones deforming >2000 years of fluvial and sag pond stratigraphy. Four of these fault zones extend into the uppermost stratigraphy indicating recent rupture and fault creep. Several antithetic faults and one fault zone displayed upward terminations, but strong indicators of large-magnitude ruptures (e.g., filled fissures and colluvial scarp deposits) were not observed. Their absence does not preclude the possibility of larger ruptures at Parkfield. However, all deformation exposed here can be explained through repeated ~M6 rupture and creep. The 2004 M6 Parkfield earthquake ruptured this paleoseismic site. Comparison between 2004 vertical offsets and those within the exposed stratigraphy suggests M6 recurrence between 8 and 248 years.

Assuming the following slip budget: *Accumulated slip deficit = (long-term slip rate [33mm/yr] * time) – (historical slip)*, nearly 5m of slip deficit has accumulated along the Cholame segment since 1857. This is approximately the mean of 1857 offsets measured there. The slip deficit is much greater than the few 1857 offsets in the southeastern Parkfield segment. Thus, the slip deficit in southeast Parkfield and Cholame may be as great as or may have surpassed the slip released along these segments in 1857.

The slip deficit abruptly decreases to the northwest across the central Parkfield segment. It is 1-2 m near Parkfield, California and 0-1 m northwest of Middle Mountain. A ~M7 event, rupturing Cholame and the southeastern portion of the Parkfield segment could release the accumulated slip deficit and is plausible. Importantly, the slip budget shows that the change in the pattern of strain release occurs in the middle of the Parkfield segment, rather than at its ends.

ACKNOWLEDGMENTS AND BACKGROUND

I received my B.S. in geology from the University of Vermont where Dr. Paul Bierman mentored me through my first thesis writing process as a John Dewey Honors student. I recognize that experience as being pivotal in my growth as a student of science. I also thank my family, friends, and past teachers for their encouragement throughout my educational experience.

As an M.S. student at Arizona State University (ASU), I would like to acknowledge professors S.J. Reynolds, M.J. Fouch, and E.J. Garnero for service on my thesis committee. I also acknowledge the Department of Geological Sciences staff members for their logistical assistance throughout my time at ASU. This research was financially-supported by Dr. J Ramón Arrowsmith's NSF research grant (EAR-0310357).

Fellow members of the Active Tectonics, Quantitative Structural Geology and Geomorphology Research Group <http://activetectonics.la.asu.edu> at ASU provided a much appreciated collaborative support team during this research. I would like to acknowledge Jeff Conner and Chris Crosby for their technical support of this project. Chris Crosby gathered much of the California and San Andreas Fault GIS data used here in and has and continues to maintain the Parkfield research webpage <http://activetectonics.la.asu.edu/Parkfield>.

In March of 2004 Ramón, Dallas Rhodes, and Jeff Kilpatrick introduced me to the San Andreas Fault (SAF) and geology along the Carrizo, Cholame, and Parkfield segments of the SAF. In April, I began my field research in Parkfield. Maurits Thayer introduced me to the geology of Middle Mountain. Ramón and Jeri Young helped me refine my geomorphic mapping skills as I documented tectonically-produced landforms

associated with the main trace of the San Andreas Fault. Ramón, Jeri, and Chris Crosby provided expert guidance in paleoseismic techniques as I opened my first paleoseismic trenches in the summer of 2004. Later that summer, Kenneth Jones provided much-needed field assistance as I was completing my work. My interpretations were aided by the September 28th 2004 Parkfield earthquake, Ramón and I had the opportunity to help document the ground rupture at Parkfield while collaborating with Michael Rymer and John Tinsley of the USGS and Jerry Treiman of the California Geological Survey. I would like to acknowledge Jim Lienkaemper, Heidi Stenner and Jessica Murray of the USGS for their suggestions and access to research data as I was interpreting the results of my study. I would like to thank Ramón, Jeri, and Chris for their continued collaboration as I submitted these two papers to the Bulletin of the Seismological Society of America's special issue about the 2004 Parkfield Earthquake (due to be published in September, 2006). Finally, I would like to thank my advisor, J Ramón Arrowsmith, for his enthusiasm, encouragement, and engagement in my research. His enthusiasm fosters an excellent working environment within our research group and made my experience at ASU very enjoyable.

TABLE OF CONTENTS

	Page
LIST OF TABLES.....	x
LIST OF FIGURES.....	xi
PREFACE.....	xii
CHAPTER	
1 PALEOSEISMIC IMPLICATIONS FOR FAULT BEHAVIOR ALONG THE PARKFIELD SEGMENT OF THE SAN ANDREAS FAULT.....	1
Abstract.....	1
Introduction.....	2
Paleoseismology of Creeping Faults.....	10
Methods.....	10
Paleoseismic Site.....	12
Stratigraphy.....	15
MST Stratigraphy.....	15
PT Stratigraphy.....	29
Radiocarbon Age Constraints.....	32
MST Age Constraints.....	32
PT Age Constraints.....	35
Deformation Styles.....	35
MST Fault Zone 1.....	35
MST Fault Zone 2.....	37

CHAPTER	Page
1 Continued	
MST Fault Zone 3.....	38
MST Fault Zone 4.....	38
PT deformation.....	38
2004 Ground Rupture at MST and PT.....	39
Discussion.....	44
M6 Earthquake Recurrence.....	44
Deformation styles.....	46
Rupture style Implications.....	49
Uncertainty and Recommendations.....	50
Conclusions.....	50
Acknowledgments.....	51
References.....	52
2 REASSESSMENT OF A SLIP BUDGET ALONG THE PARKFIELD SEGMENT OF THE SAN ANDREAS FAULT.....	59
Abstract	59
Introduction.....	60
SAF Slip Budget.....	66
Long-Term slip Rate	66
Aseismic Slip Since 1857.....	67
Coseismic Slip Since 1857.....	68

CHAPTER	Page
2 Continued	
The Slip Deficit.....	72
Slip Deficit Development	73
Slip Deficit and 1857 Offsets.....	73
Discussion.....	77
Conclusions.....	79
Acknowledgments.....	79
References.....	80
CONCLUSIONS AND RECOMMENDATIONS.....	84
APPENDIX	
A TECTONIC GEOMORPHOLOGY.....	86
B PALEOSEISMIC STRATIGRAPHY.....	95
C RADIOCARBON SAMPLES.....	103
D ASEISMIC SLIP CALCULATIONS.....	105
E COSEISMIC SLIP CALCULATIONS.....	108
F SLIP DEFICIT CALCULATIONS.....	119

LIST OF TABLES

TABLE	Page
1.1 Deformation observations from MST and PT.....	20
1.2 Radiocarbon data and analysis from MST and PT.....	33
1.3 M6 Parkfield recurrence rate calculations.....	45

LIST OF FIGURES

FIGURE	Page
1.1 Parkfield segment location and SAF behavior map.....	3
1.2 Felt effects from central SAF earthquakes.....	6
1.3 Paleoseismic site location in space and time.....	8
1.4 Paleoseismic site location.....	13
1.5 Geomorphology of the paleoseismic site.....	14
1.6 Trench stratigraphy and radiocarbon ages.....	16
1.7 Explanation of paleoseismic logs.....	19
1.8 MST logs.....	21
1.9 MST fault zones 1 and 2.....	23
1.10 MST fault zones 3 and 4.....	25
1.11 PT log.....	30
1.12 2004 M6 ground rupture through the paleoseismic site.....	41
1.13 M6 model for sag pond development.....	47
2.1 Parkfield segment location and SAF behavior map.....	61
2.2 Felt effects from central SAF earthquakes.....	63
2.3 Constructing slip budgets along the central SAF.....	69
2.4 Slip deficit growth along the central SAF since 1857.....	74
2.5 Accumulated slip deficit and 1857 offsets.....	75

PREFACE

This research provides a contribution of knowledge about earthquake geology along the central San Andreas Fault (SAF). The paleoseismic excavations I present herein are among the first along the Parkfield segment of the SAF. My research follows previous efforts by Dr. Arrowsmith's research group to extend the earthquake geology record of the SAF northwestward from the Carrizo segment. The slip budgets I present are based upon previous studies and place my paleoseismic results in the context of an accumulating slip deficit along this portion of the fault. For more information on these topics look to the references within these chapters, contact the author or visit the following website: <http://activetectonics.la.asu.edu>.

CHAPTER 1. PALEOSEISMIC IMPLICATIONS FOR FAULT BEHAVIOR ALONG THE PARKFIELD SEGMENT OF THE SAN ANDREAS FAULT (SAF)

Abstract

Parkfield is considered a transitional segment between continuous fault creep to the NW and segments that only rupture in great earthquakes to the SE. Historically, fault creep and recurring M6 events have been observed at Parkfield, but its role in great SAF ruptures has remained uncertain. A paleoseismic study conducted along the central Parkfield segment of the San Andreas fault provides a > 2000 year record of tectonically deformed fluvial terrace and sag pond stratigraphy. Two fault-perpendicular excavations across a sag pond and a pressure ridge ~200 m north of Carr Hill exposed five primary fault zones displaying apparent vertical offsets, upward splaying clay shear bands, and warped stratigraphy. Four of five fault zones extended into the uppermost stratigraphy suggesting recent rupture and recent aseismic fault creep. Several antithetic fault splays and one primary fault zone displayed upward terminations, but strong indicators of large-magnitude coseismic ruptures such as filled fissures and colluvial scarp deposits were not observed. The absence of unequivocal evidence for large-magnitude ground rupture does not preclude the possibility of 1857-style ruptures extending into the Parkfield segment. However, all deformation exposed within these trenches can be explained through repeated ~M6 ground rupture and aseismic fault creep. The 2004 M6 Parkfield earthquake ruptured through the site and activated at least three of the five fault zones exposed in our excavations. Comparison between 2004 vertical offset and vertical offsets

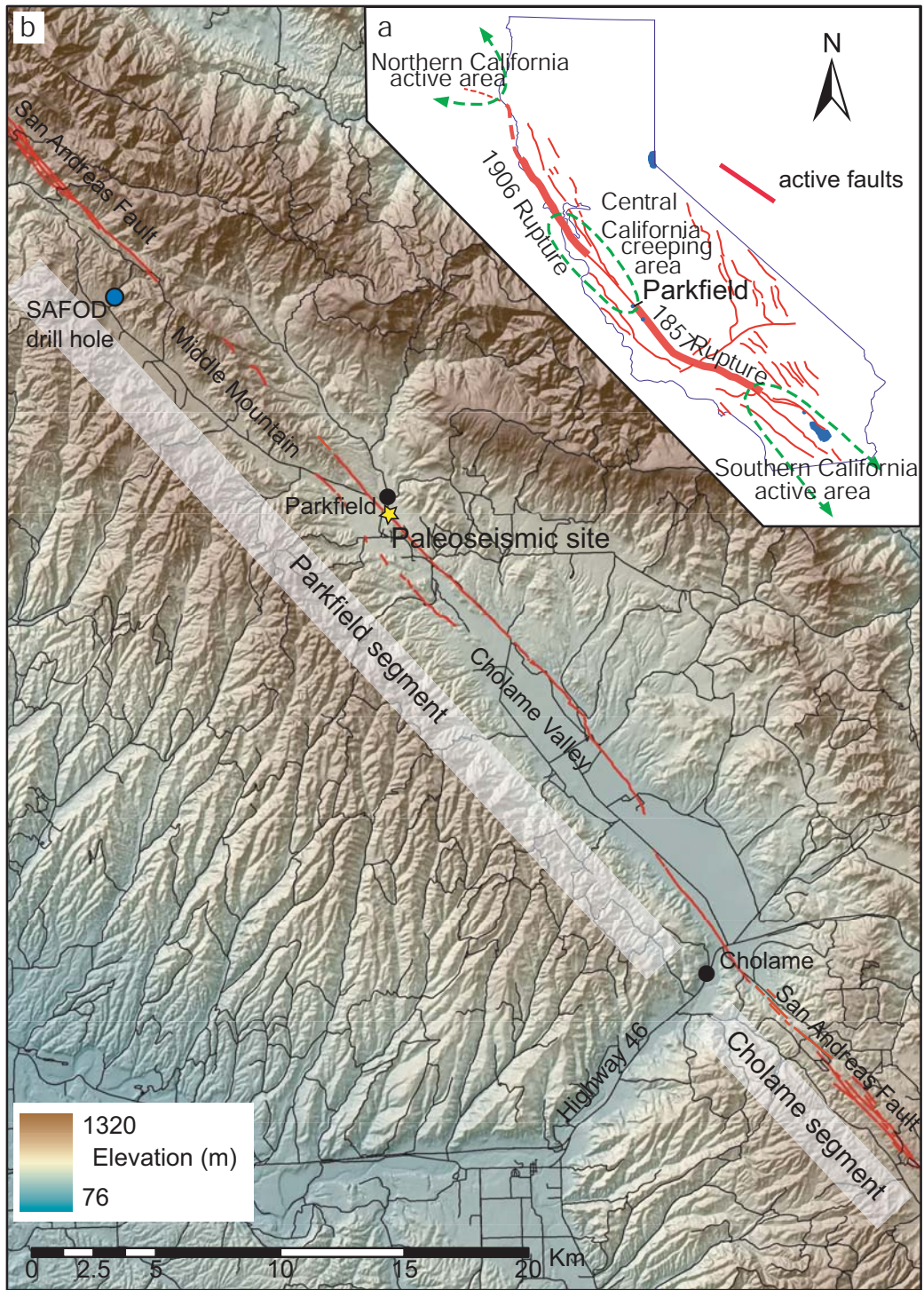
within the exposed stratigraphy suggests a prehistoric M6 recurrence interval between 8 and 248 years at Parkfield.

Introduction

The Parkfield segment of the San Andreas Fault (SAF) is situated between the aseismic creeping segment and the apparently-locked Cholame segment to the NW and SE, respectively (figure 1.1). Historically, Parkfield is characterized by the occurrence of both ~M6 earthquakes and fault creep that decreases from a rate > 25 mm/yr NW of Middle Mountain (e.g., Savage and Burford, 1973; Murray et al., 2001; Titus et al., 2005) to 0 mm/yr at CA Highway 46 (figure 1.1; e.g., Burford and Harsh, 1980; King et al., 1987; Murray et al., 2001). Parkfield has received much attention from the seismological community because of the recurrence of at least six ~M6 earthquakes (1881, 1901, 1922, 1934, 1966 and 2004) at semi-regular intervals of time since the Great 1857 Fort Tejon ~M8 earthquake (e.g., Bakun and McEvilly, 1984; Bakun and Lindh, 1985; Roeloffs and Langbein, 1994; Topozada et al., 2002). Despite the community's recent success in capturing both geophysical and geodetic data on the segment through most of a M6 earthquake cycle (e.g., Langbein et al., 2005), only one previous study (Sims, 1987) has been successful in exploring Parkfield's longer earthquake history, over time scales as long as the recurrence of great SAF earthquakes.

Historical accounts of felt effects and geomorphic offset studies have provided some insight about the 1857 event. Prior to the 1857 main shock, at least two prominent foreshocks were felt in central California (Sieh, 1978a; Meltzner and Wald, 1999). The

Figure 1.1. Parkfield segment location and SAF behavior: A) A transition between contrasting zones of SAF behavior is found along the Parkfield segment (modified from Allen, 1968). The creeping segment creeps at a rate > 25 mm/yr (e.g., Titus et al, 2005; Murray et al, 2001). Along the Parkfield segment both fault creep and repeating historical \sim M6 earthquakes occur. Southeast of Parkfield, the creep rate drops to zero and no historic earthquake ruptures have been documented SE of California Highway 46 since 1857 (e.g. Allen, 1968; Segall and Harris, 1986; Harris and Archuleta, 1987; Arrowsmith et al., 1997; Murray et al., 2001). B) Hill shading over a 10m DEM with overlays of historic surface traces of the SAF (Jennings, 1997; Zielke and Arrowsmith, in progress) and the 1966 Parkfield segment rupture trace (Brown, 1970; Crosby, 2004). The 2004 rupture followed the 1966 rupture pattern closely (Langbein et al., 2005). Our paleoseismic excavations were located just S of the town of Parkfield.

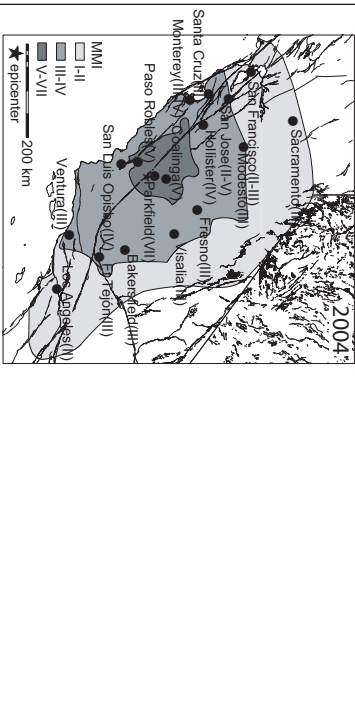
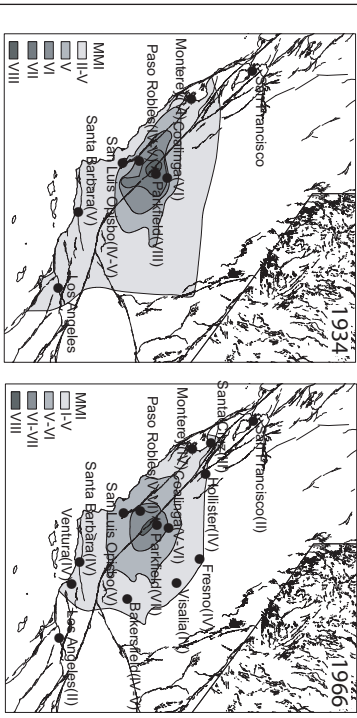
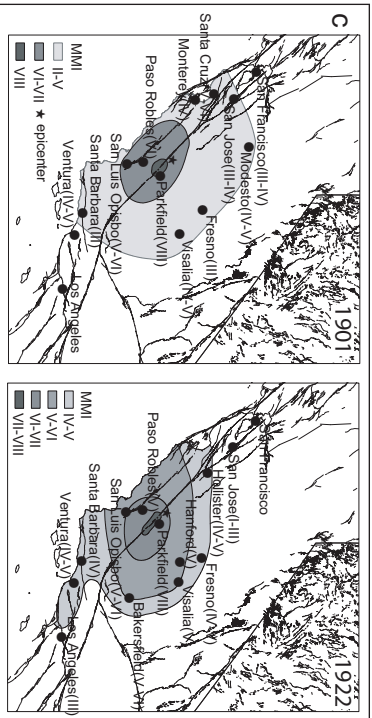
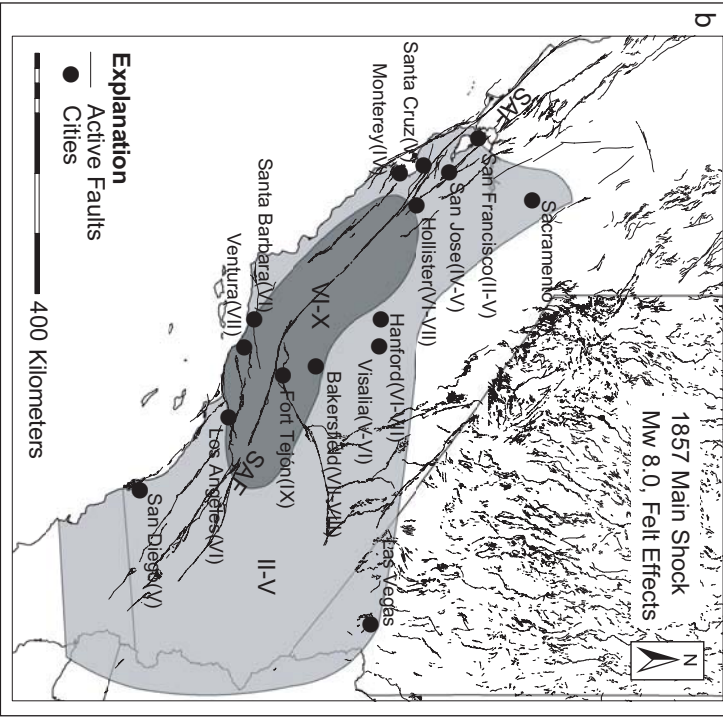
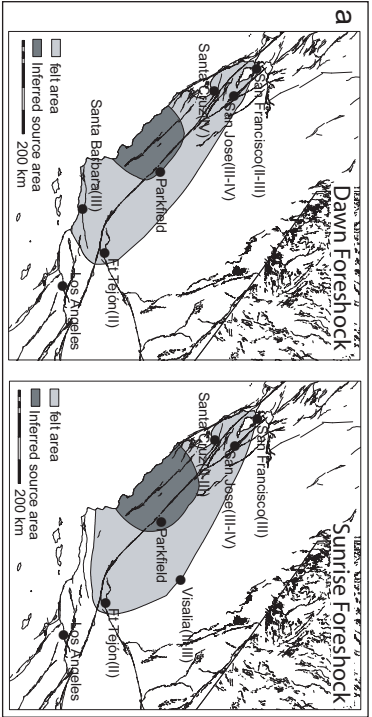


distribution of felt effects from these foreshocks were very similar to the distributions of the felt effects from the 1901, 1922, 1934, 1966 and 2004 Parkfield earthquakes (figure 1.2). This suggests that the 1857 foreshocks were of similar magnitude and location as the Parkfield events (Sieh, 1978a). If we also consider the distribution and duration of felt effects of the 1857 main shock (Agnew and Sieh, 1978; figure 1.2), the 1857 event probably ruptured from the northwest to the southeast with an epicenter near or along the Parkfield segment (Sieh, 1978a). These observations suggest that the Parkfield segment played a role in both the nucleation and rupture of the 1857 event and may do so again in future great central California earthquakes (e.g., Arrowsmith et al., 1997). However, the sparse population in 1857 and relatively little scientific response left a high level of uncertainty about the extent of the rupture within the Parkfield segment.

The paleoseismology community has had success in exposing earthquake records at seven sites along the portion of the SAF that last ruptured in 1857 (figure 1.3; Las Yeguas, Young et al., 2002; Carrizo Plain, Liu et al., 2004, Sims 1994, Grant and Sieh, 1994; Frasier Mountain, Lindvall et al., 2002; Three Points, Rust, 1982; Littlerock, Schwartz and Weldon, 1986; Pallett Creek, Salyards et al., 1992, Biasi et al., 2002, Sieh et al, 1989; and Wrightwood, Biasi et al, 2002, Fumal et al., 2002b, Weldon et al, 2002). Large gaps in the recent earthquake record along this portion of the fault allow for numerous plausible interpretations about SAF behavior (Weldon et al., 2004; figure 1.3).

With little reliable data from the 1857 event and no prehistoric data from the Parkfield segment (figure 1.3), it remains uncertain how the Parkfield segment interacts with the locked SAF segments to the southeast during large central California

Figure 1.2. Felt effects from central SAF earthquakes: A) Felt (light grey) and source areas (dark grey) of the 1857 dawn and sunrise foreshocks (Sieh, 1978a). Both foreshocks were felt sparsely from the Bay area southeast to Ft. Tejón. The felt areas were centered near the Parkfield segment of the SAF. B) MMI Felt intensity distributions of the ~M8 1857 main shock (Sieh, 1978a; Agnew and Sieh 1978). The 1857 main shock was felt throughout central and southern California as well as Nevada, Arizona, and Mexico. C) Estimated epicenters (stars; Topozada et al., 2002) and felt MMI intensities from the 1901, 1922, 1934, 1966, and the 2004 ~M6 Parkfield events (Sieh 1978a). Similar to the 1857 foreshocks, the Parkfield earthquakes are felt from the San Francisco Bay to the Los Angeles Basin and the greatest intensities (darker grey) center on the Parkfield segment of the SAF.



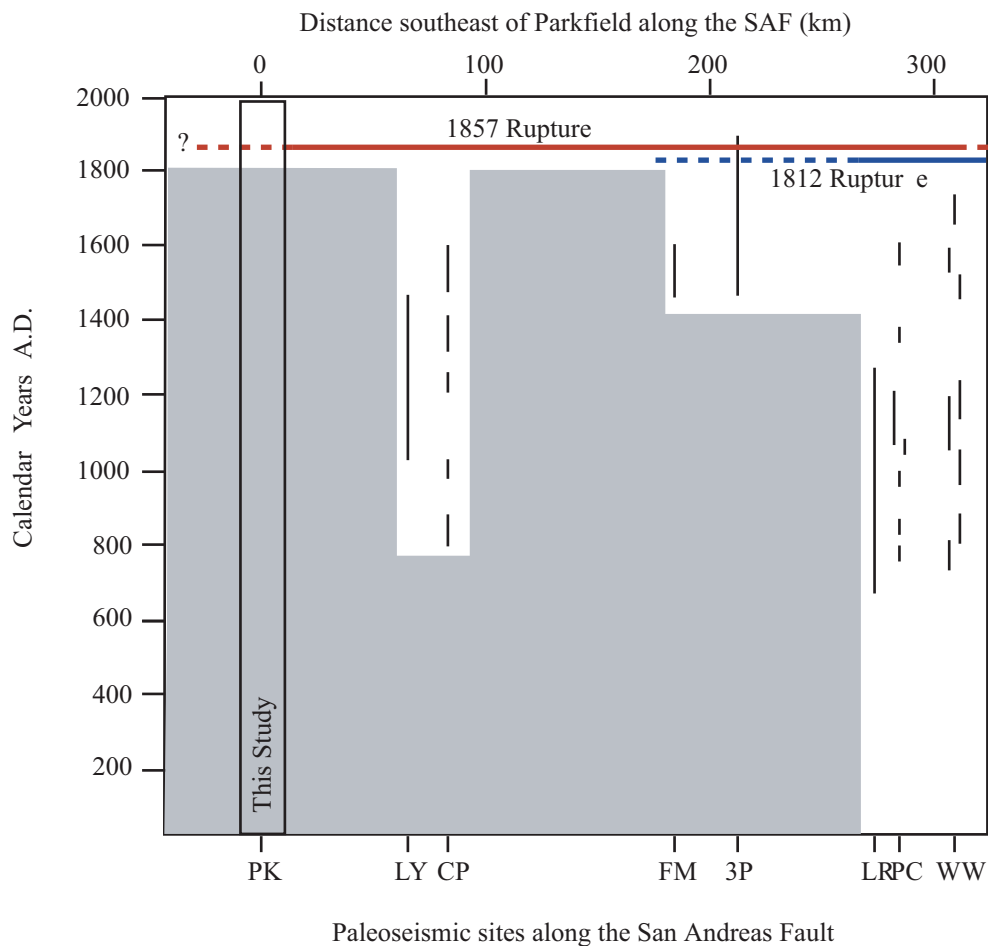


Figure 1.3 . Paleoseismic records of earthquakes along the portion of the San Andreas fault which is thought to have ruptured in 1857. PK = Parkfield, LY = Las Yeguas, CP = Carrizo Plain, FM = Frasier Mountain, 3P = Three Points, LR = Littlerock, PC = Pallett Creek, WW = Wrightwood (see text for citations). Earthquake events at each site are shown as solid black vertical lines with the length equal to the bracketed ages of the event. Parkfield is thought to be near the northwestern terminus of the 1857 rupture. Our study is the first to expose a record northwest of Las Yeguas.

earthquakes such as 1857. Understanding the interaction between these segments provides insight into overall SAF behavior, fault mechanics, and will have significant implications for earthquake hazards along the central SAF.

At the paleoseismic site we studied (figure 1.4), the SAF creeps at a rate of 10-20 mm/yr (Murray et al., 2001). This site is also the location of small ground-rupturing earthquakes (e.g., 2004; 1966, 1934...), yet there appears to be a small slip deficit, ~1 m of slip, since 1857. A slip deficit along the Parkfield segment is inferred in previous work (e.g., Harris and Archuleta, 1988; Lienkaemper and Prescott, 1989; Arrowsmith et al., 1997) and is reassessed here in chapter 2. This deficit could be recovered via large ground-rupturing earthquakes, such as a repetition of the 1857 event. However, this deficit could also be recovered by an increase in the aseismic creep rate, additional M6 Parkfield events, or some combination of these. Multiple mechanisms of strain release make paleoseismic interpretations challenging at Parkfield because we must distinguish between deformation produced from creep, M6 events, and large surface ruptures such as 1857 events.

To expose Parkfield's prehistoric earthquake record, we conducted a paleoseismic excavation along the central Parkfield segment (figures 1.1, 1.4 and 1.5). Our excavations (figures 1.6-1.11) showed no unequivocal evidence for large-magnitude surface-ruptures along the central Parkfield segment. Ground-rupture observations from the 2004 Parkfield event help us to infer that > 2000 years of tectonic deformation exposed within these trenches can be explained by a combination of repeating M6-style ruptures and fault creep.

In this paper, we present the results of our paleoseismic investigation (figures 1.4-1.11) followed by observations of the 2004 M6 Parkfield earthquake rupture at our paleoseismic site. Tectonic models for the formation of the site's present day geomorphology are indicated by the 2004 rupture pattern. Finally, we discuss earthquake recurrence at Parkfield and implications for fault behavior during large central SAF earthquakes.

Paleoseismology of Creeping Faults

Previous studies have attempted to differentiate creep from ground-rupture in trench exposures along strike-slip faults known to experience fault creep, however results were ambiguous and left the community with few unequivocal lines of evidence for differentiating creep from rupture (e.g., Stenner and Ueta, 2000; Kelson and Baldwin, 2001; Lienkaemper et al., 2002). Evidence for paleodeformation along faults include: 1) vertical displacement of stratigraphy, 2) folding and tilting of stratigraphy (resulting in angular unconformities), 3) abrupt variations in stratigraphic thickness, 4) abrupt facies change across strata, 5) upward terminations in stratigraphic displacement, 6) liquefaction, 7) filled fissures, and 8) colluvial scarp deposits (Kelson and Baldwin 2001). Because variations in fault creep through time may produce indicators 1-5, these are not definitive for ground rupturing earthquakes. However, filled fissures and colluvial scarp deposits are unequivocal evidence of significant ground-rupture.

Methods

Our paleoseismic effort consisted of geomorphic mapping; paleoseismic excavation and logging; and total station surveys of topography, trench features, and the

2004 earthquake rupture after our trenches were closed. To maximize the likelihood of exposing an interpretable paleoseismic record, we conducted tectonic geomorphic mapping from Middle Mountain to Carr Hill (Appendix A) in search of sites along the main SAF trace which met the following criteria: 1) a well delineated expression of the SAF for precise trench location, 2) a sufficient rate of Holocene deposition for recording ground deformation, and 3) sites with a significant scarp where colluvial wedge and filled fissure deposits from large ground ruptures might be preserved. Based upon these criteria, we excavated two fault-perpendicular trenches in an abandoned late Pleistocene terrace of the Little Cholame Creek (figure 1.4 and 1.5): Miller Sag Pond Trench (MST) and Phoebe's Trench (PT). MST was excavated across a tectonically-generated depression and was ~30 m long by 1-2 m deep. PT was excavated into a pressure ridge along the active trace and was 30 m long by 1-3 m deep.

Trenches walls were scraped, cleaned, and a 0.5 m² grid was erected. Stratigraphic units were characterized based upon physical properties of texture, color, grain size, sorting, thickness, and other properties such as organic content and bioturbation (Appendix B). All stratigraphic and deformation patterns were initially mapped at 1:20 scale and the SE wall of MST was logged at 1:10 within the fault zones (figures 1.6, 1.8-1.10, Appendix B). PT-northwest was logged throughout the fault zone (figure 1.11, Appendix B). Additionally, we documented the MST southeast wall with a photo mosaic (figure 1.8). Attitudes of faults were taken when possible and sense of motion was recorded if evidence were available (table 1.1).

Abundant charcoal was collected within the units of these trenches (Appendix C). Thirteen of these samples (9 from MST and 4 from PT) were selected for AMS radiocarbon analysis (table 1.2; figures 1.6, 1.8-1.11) by the NSF Arizona AMS facility. Age calibration was performed using OxCal v3.9 (Bronk Ramsey, 1995; Bronk Ramsey 2001) and the correction of Stuiver and Polach, (1977).

We surveyed the trench site with a Leica Total Station for topographic characterization and precise trench and fault zone locations (figure 1.5). On October 1st, 2004 we returned to Parkfield and surveyed the fractures from the 2004 earthquake at the site for length, opening, and slip. These data were projected into the previous trench site survey (figure 1.12).

Paleoseismic Site

Mapping revealed that three of the most pronounced tectonic geomorphic features along the central Parkfield segment are found on the Miller Brothers Inc. agricultural field, 21 km northwest of Highway 46, between Carr Hill and the Parkfield-Coalinga Rd Bridge (figures 1.1, 1.4, and 1.5). The Miller's field, our paleoseismic site, lies on an abandoned Late Pleistocene terrace of the Little Cholame Creek (figure 1.5; Sims, 1990). The terrace has been deformed by slip along the SAF resulting in three tectonic landforms. A terrace riser, just SE of the bridge, appears to be right-laterally offset more than 5 meters. However, cattle use this feature as a natural path to the creek, perhaps enhancing the apparent offset. Southeast of the offset riser, an elongate sag pond about 80 m long, parallel to the SAF, and about 30 m wide has apparently formed by extension across a right-step in the surface trace of the SAF. The pond is fed by springs along a < 1



Figure 1.4. Our paleoseismic trench site (orange hill shaded DEM over the SE Parkfield USGS DOQQ) is located less than 1 km south of the town of Parkfield along the main SAF trace. Prior to our excavation (June, 2004) the site was last ruptured in the M6 Parkfield event of 1966 (black line, Crosby, 2004). The Southwest fracture zone also ruptured in 1966 and paralleled the main rupture about 1 km to the SW. See figure 1.1 for regional overview and figure 1.5 for a detailed view of the paleoseismic site.

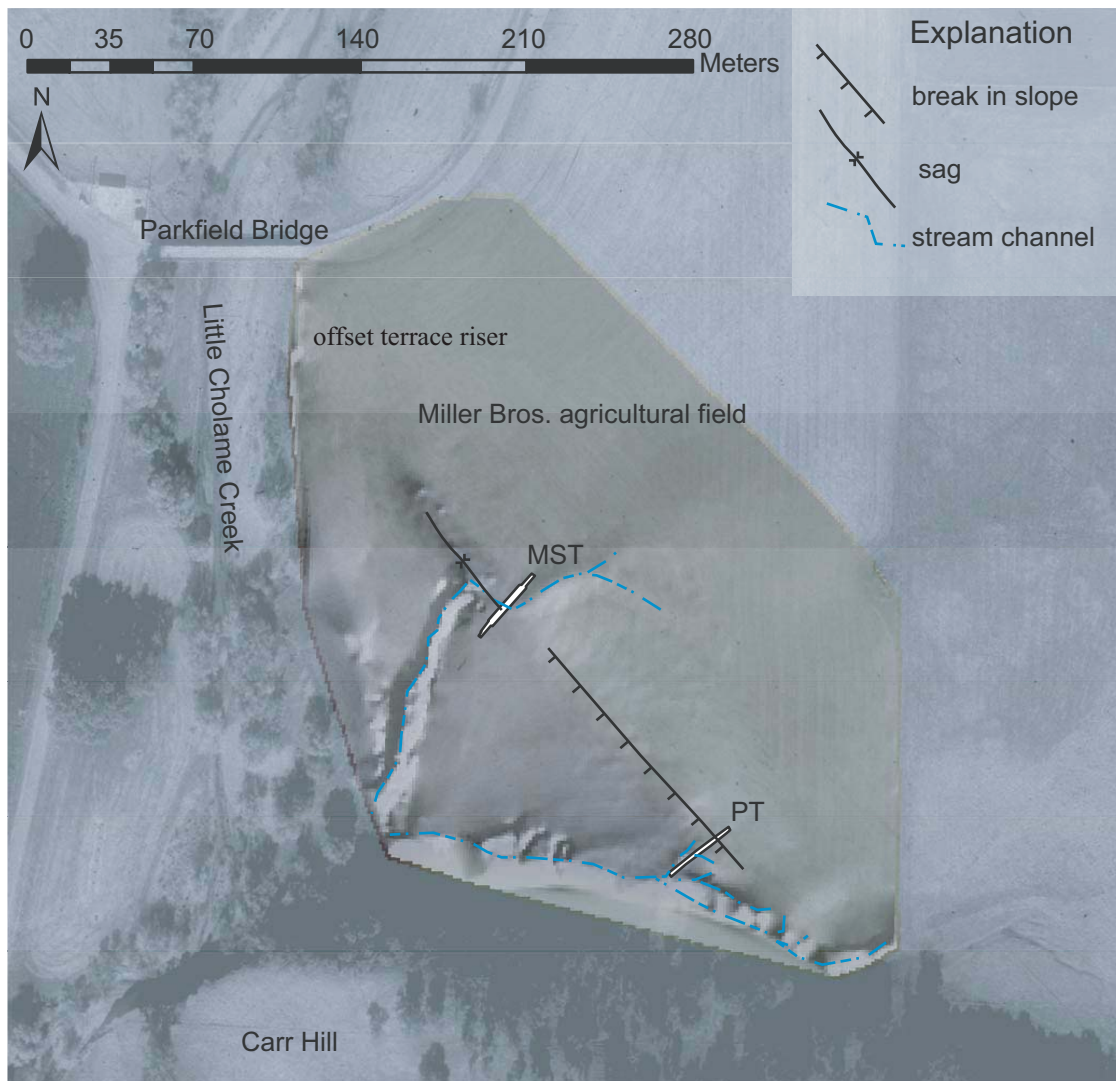


Figure 1.5. We excavated two fault-perpendicular trenches in the Miller Bros. Agricultural field just north of Carr Hill. MST was excavated across the SE end of the Miller Sag Pond and bisected the geomorphic expression of an offset ephemeral stream channel. PT was excavated across the SE end of the pressure ridge near the base of Carr Hill. See figures 1.1 and 1.4 for location and figure 1.12 for the 2004 rupture at this site. 1:6000 aerial photography is overlain by shaded relief map from our topographic survey.

m scarp on the northeast side of the depression and a small ephemeral channel that approaches the sag pond from the east and is right-laterally deflected ~15 m across the SAF. The third feature is a 1.5-2.5 m tall pressure ridge that extends southeast from the sag pond to a stream channel that runs along the base of Carr Hill. The pressure ridge appears to be the result of slip along a small left restraining bend in the surface trace of the SAF at Carr Hill (figures 1.4 and 1.5). The southwest side of the pressure ridge is lushly vegetated with springs emanating along the break in slope.

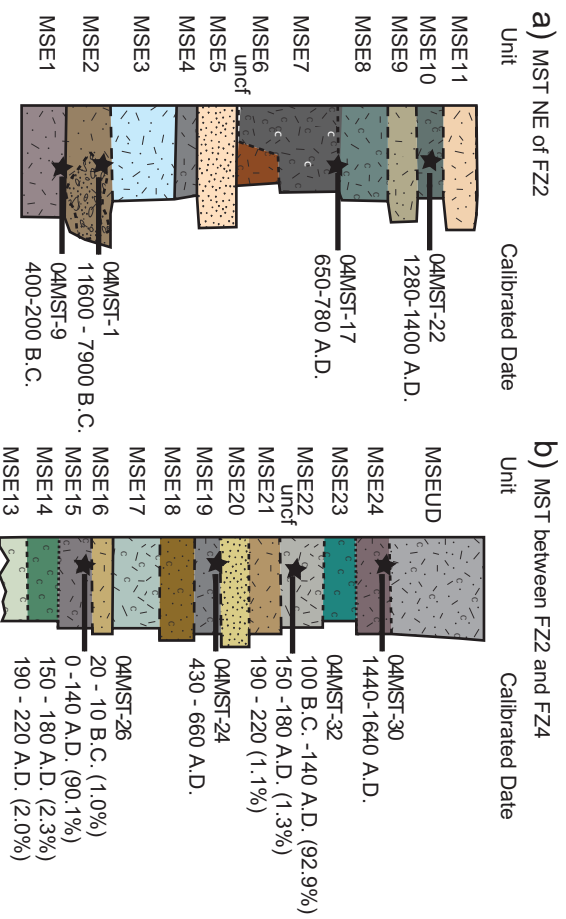
Stratigraphy

The Miller sag pond trench (MST) and Phoebe's Trench (PT) exposed well-preserved tectonically deformed stratigraphy. In following section, we first describe the basic stratigraphy of each trench across the major deformation zones, then we describe radiocarbon age constraints, and finally we describe the deformation observed. All stratigraphic units are displayed in figure 1.6 and described in supplemental tables 1.1 and 1.2. MST trench logs are displayed in figures 1.8-1.10, the PT trench log is displayed in figure 1.11, and important deformation measurements and observations are listed in table 1.1. Radiocarbon samples are described in supplemental table 1.3, sample locations are shown in figures 1.6, 1.8-1.11 and results are shown in figure 1.6 and table 1.2.

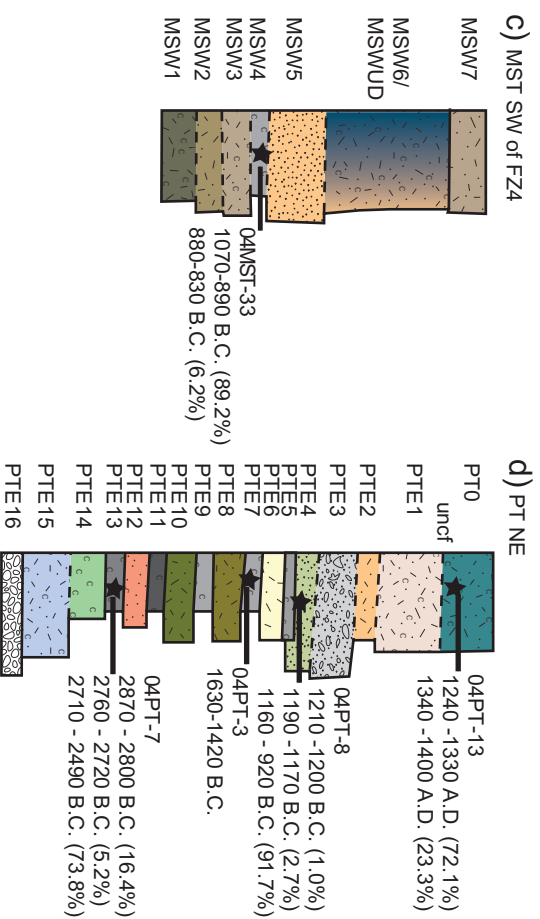
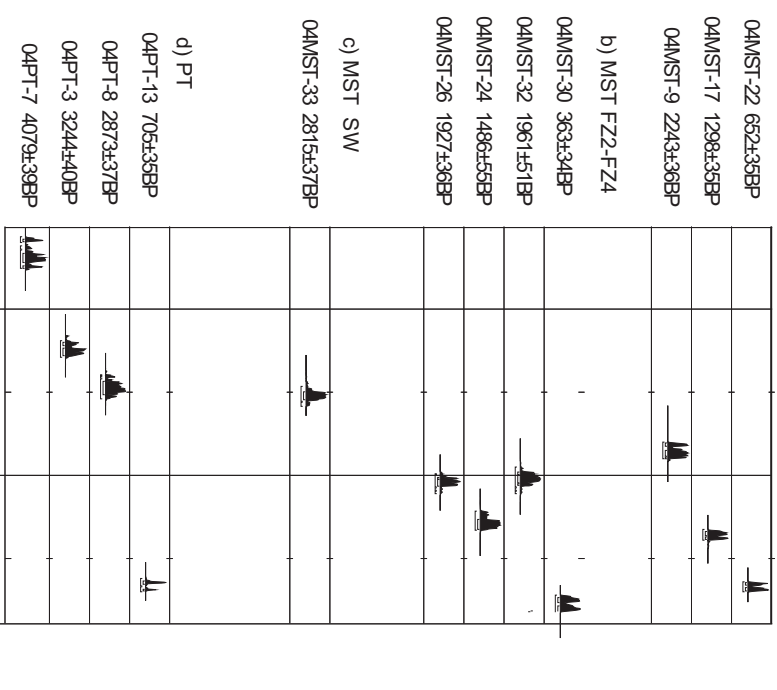
MST Stratigraphy

MST was excavated across the southeast end of the sag pond, perpendicular to the geomorphic expression of the SAF, and bisecting the apparent offset of the stream channel at the southeast end of the Miller Sag Pond (figure 1.5). The MST excavation exposed four zones of deformation distributed beneath the geomorphic expression of the

Figure 1.6. Stratigraphic unit relationships and radiocarbon ages of the SE exposure of the Miller Trench: A) NE of fault zone 2 (FZ2), B) Between fault zones 2 and 4, and C) SW of fault zone 4. Miller Sag Trench (MST) is divided into three stratigraphic sequences because there is no apparent unit correlation across deformation zones 2 and 4 in MST (figures 1.8-1.10). D) Stratigraphic relationships of Phoebe's trench (figure 1.11). Explanations of patterns are provided in figure 1.7. E) Two sigma probability distributions for calendar dates determined from the radiocarbon age for each sample using OxCal v3 (Bronk Ramsey, 1995; Bronk Ramsey, 2001) and atmospheric data from Stuiver et al., (1998). The age of sample 04MST-1 is stratigraphically inconsistent with other samples suggesting it is detrital and the probability distribution is not shown here. Table 2 presents radiocarbon analyses; figures 1.8-1.11 show trench relationships.



e) 2 sigma radiocarbon sample ages and probability distribution curves



sag pond (figures 1.8-1.10). We refer to these deformation zones as fault zone 1 (FZ1), the most northeastern deformation zone, through fault zone 4 (FZ4), the southwestern-most deformation zone. Stratigraphic units and deformation styles were consistent between the two trench walls (figure 1.8; Appendix B). We describe the units by their position relative to the four fault zones. Units are divided into two sections. Those that outcrop NE of FZ4 are referred to as MSE1-MSE24 and units to the SW of FZ4 are MSW1-MSW7; numbers correspond to stratigraphic position with 1 representing the lowest (oldest) unit exposed in the section. Stratigraphic interpretations were complicated by the accumulation of pedogenic clay, disturbance from agricultural tilling, root bioturbation, and burrowing by ground squirrels (primarily outside of the fault zone because of soil moisture within the sag pond) (figures 1.8-1.10, Appendix B).

Northeast of FZ1 (Figures 1.6, 1.8, and 1.9) the lowest unit exposed, MSE1, is a very fine sand and silt with some clay accumulation. It is overlain by thin laminated clay with sparse charcoal; we interpret that MSE1 is an over-bank deposit from the Little Cholame creek and the laminar clay and charcoal are the result of an in situ burn horizon over MSE1, which was once the vegetated terrace surface. MSE1 is overlain by fine clayey silt, MSE2. Coarse sands and moderately sorted gravel lenses heavily dissect this unit. MSE2 was probably laid down by over-bank deposits from the Little Cholame creek. Later, these flood deposits were eroded by paleochannels of the Little Cholame Creek or by the small stream that is offset across the sag pond. The channel deposits of MSE2 include locally derived clasts from the Franciscan, Etchegoin, and Monterey formations (Sims, 1990). Knapped chert flakes were observed within one of the

Explanation of Paleoseismic Logs

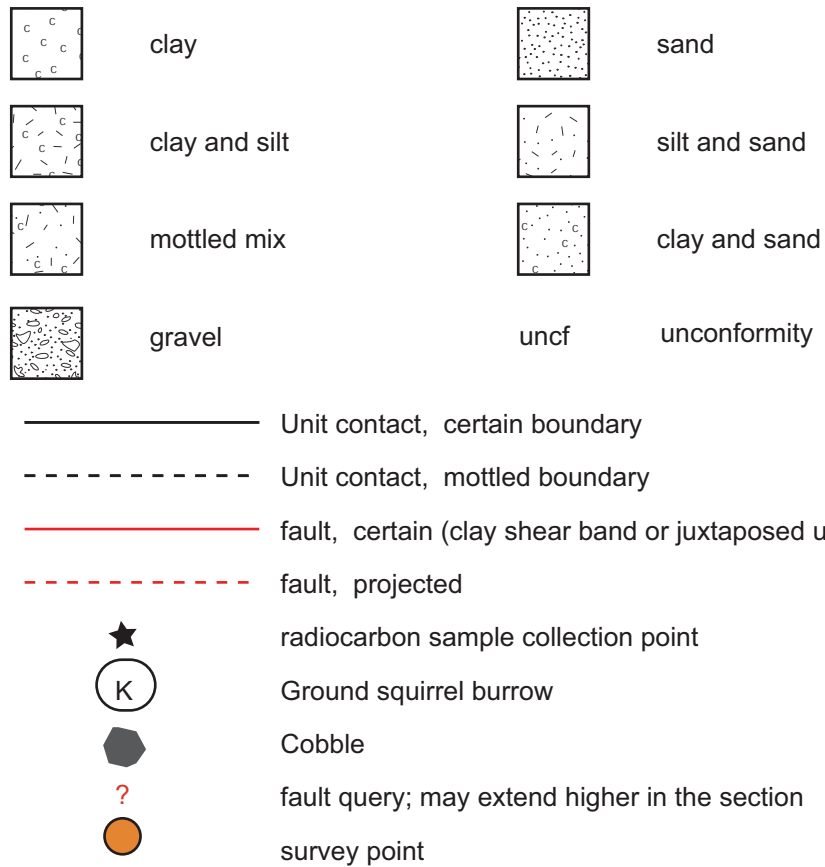


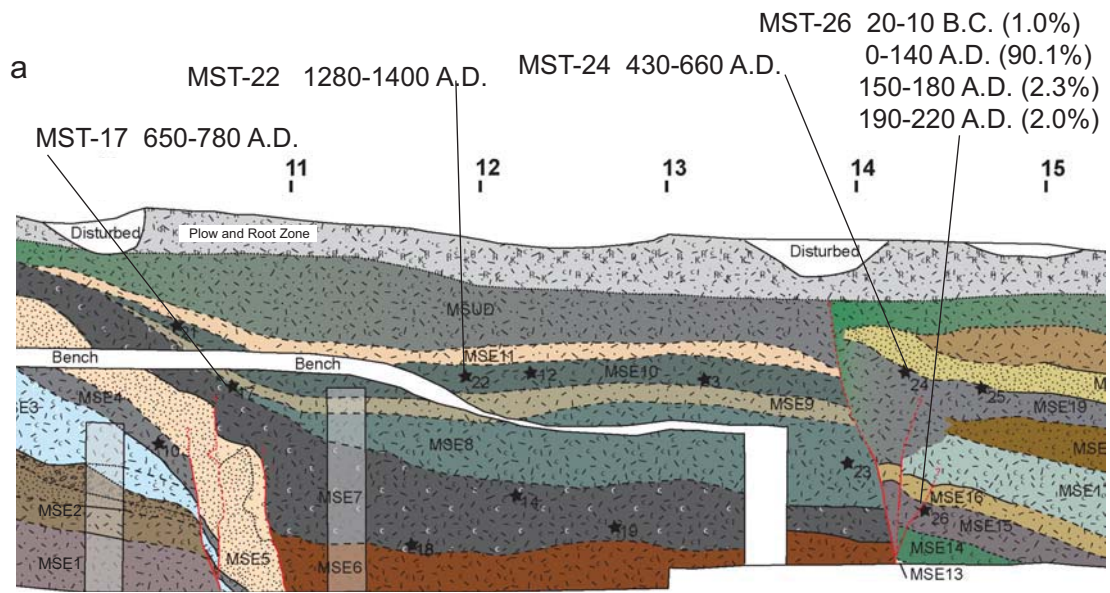
Figure 1.7. Explanation to accompany the trench logs (figures 1.8-1.11) and the stratigraphy (figure 1.6). For detailed descriptions of each unit see Appendix B.

Table 1.1. Key deformation observations from MST (figures 1.8-1.10) and PT (figure 1.11).

Trench	Fault Zone	Observation	Measurement
MST	FZ1	Pebbles from MSE2 are entrained in FZ1 (figures 1.8-1.9)	NA
MST	FZ1	MSE 5 is mixed with clay at offsets on the top of the unit (figure 1.8 and 1.9)	NA
MST	FZ1/FZ4	Fracture trend (figure 1.12)	313°
MST	FZ2	Shear zone orientation on NW wall	Strike and Dip: 161°/68°SW
MST	FZ2	Shear zone orientation on SE wall	Strike and Dip: 170°/64°SW, rake =87° NW
MST	FZ2	Deformation appears to reach the surface (figures 1.8-1.9)	NA
MST	FZ3	Units MSE17-MSE21 maintain thicknesses along 4 faults with apparent normal offset, faults can be traced into the undifferentiated MSEUD unit (figures 1.8 and 1.10)	NA
MST	FZ4	Numerous clay shear bands can be traced to near the surface of the trench (figures 1.8 and 1.10)	NA
PT	FZ splays	Fault splays appear to bend with deeper depth towards main deformation zone (figure 1.11)	NA
PT	FZ main	Pockets of sands, pebbles and some small cobbles are found within the undifferentiated unit often near clay shear zones (figure 1.11)	NA
PT	FZ main	PTW1.5 offset is associated with clay shear bands, which approach the surface and merge at depth (figure 1.11)	NA
PT	SW of FZ main	Double triangle shaped clay feature extends from the base of the trench (figure 1.11)	NA

Figure 1.8. Overview of MST logs (A) and calibrated radiocarbon ages for northwest and southeast walls; 1:1 scale in meters. B) Trench log (zoomed view) of MST SE faults and corresponding photo mosaic. Four zones of localized faulting were exposed within MST (FZ1-FZ4). Each of these fault zones contained several fault splays that were characterized by clay shear bands and offset units. FZ1 does not reach the surface. FZ2 through FZ4 extend into the uppermost-disturbed trench stratigraphy and may come to the surface. FZ1 and FZ3 show apparent vertical offset and are overlain by sag deposits. FZ2 and FZ4 juxtapose sag units against older fluvial deposits. See figure 1.7 for unit and symbol explanation, figures 1.9 and 1.10 for zoomed fault zone views, and figures 1.1, 1.4, and 1.5 for trench site location.

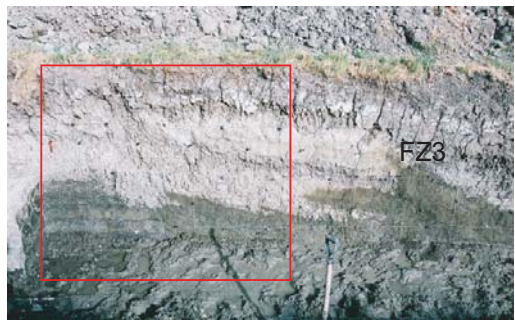
Figure 1.9. Southeast MST Trench log blow up of fault zones 1 and 2 (A) and photographs of the two fault zones (B-E). FZ1 (B and C) consists of three fault splays that displace downward MSE1-MSE5 (fluvial over bank deposits) and MSE6 and MSE7 (organic-rich sag pond units). FZ1 does not reach the surface of the trench. FZ2 (D and E) juxtapose MSE6-MSE11 (sag pond units) against fluvial over bank deposits (MSE12-21) and apparently deforms the uppermost units of the trench. See figure 1.8 for position of FZ1 and FZ2 within the trenches, figure 1.7 for explanation of logs, and figure 1.6 for stratigraphic relationships.



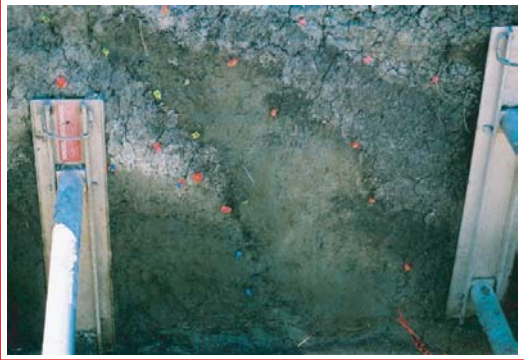
b Fault Zone 1



d Fault Zone 2



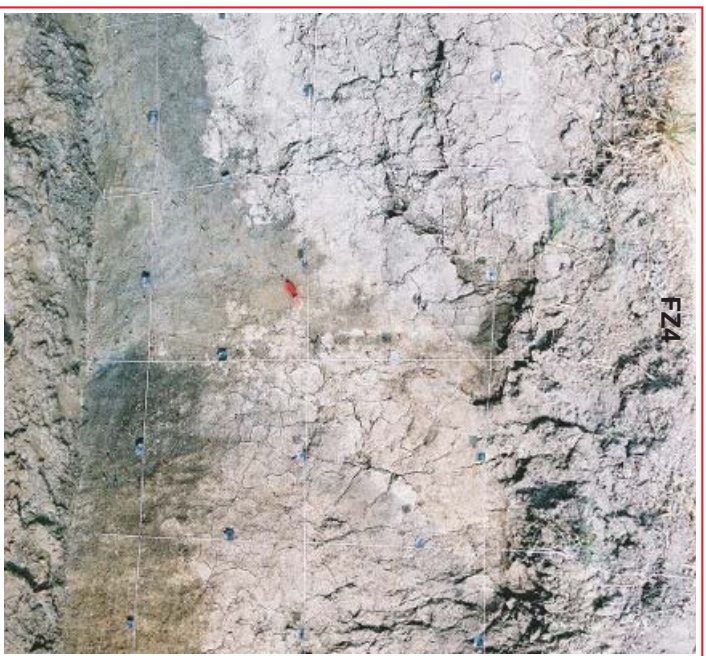
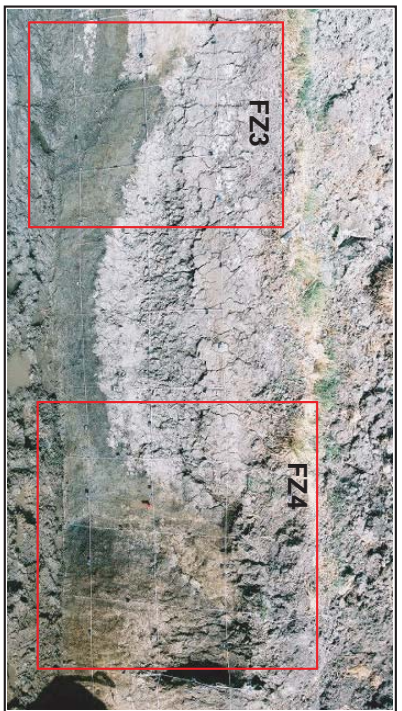
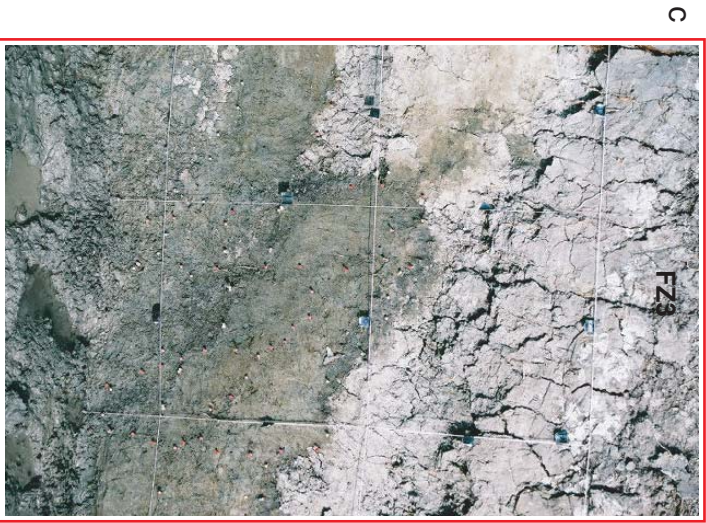
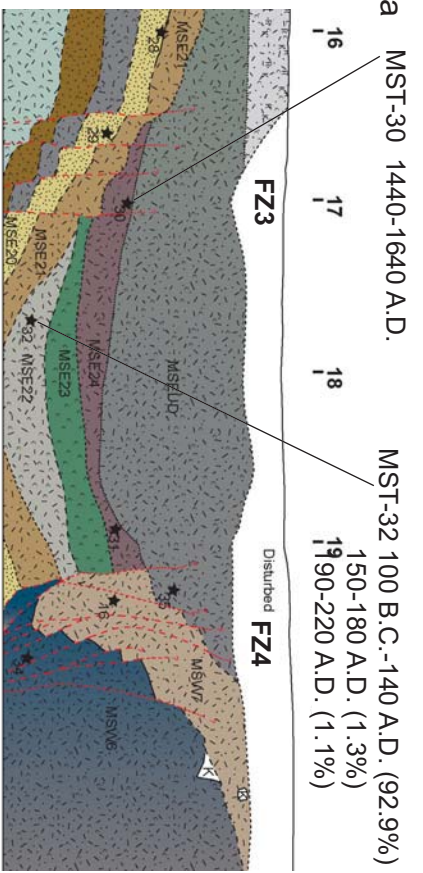
c



e



Figure 1.10. Zoomed in trench log of MST fault zones 3 and 4 (A) and corresponding photographs (B-D) of the two fault zones . FZ3 consists of 4 fault splays that displace MSE17-MSE22 downward to the SW. The fault splays may extend to the surface, but relationships are unclear within the sag units MSE23-MSEUD. FZ4 consists of numerous clay shear bands and juxtaposes sag units (MSE22-MSE24) against older fluvial deposits that are down warped into the fault zone. See figure 1.8 for position of FZ1 and FZ2 within the trench, figure 1.7 for explanation of logs, and figure 1.6 for stratigraphic relationships.



channel deposits. MSE3 is a thick clayey sand and silt over-bank deposit that has a mixed lower interface, probably from bioturbation. MSE4 overlies MSE3 and is similar in grain size, but is darker with more organic content. Above MSE4, MSE 5 is a well-sorted deposit of very fine sand and silt from over-bank deposition of Little Cholame Creek. Units MSE1-MSE5 are tabular, but have been warped and faulted by FZ1 (figure 1.9).

Between FZ1 and FZ2 (figure 1.8-1.9) MSE6-MSE11 thicken towards the center of the sag pond suggesting that they are growth-strata that formed as space was created by down-faulting along the southwest side of FZ1. MSE6 is silty clay that is juxtaposed against the southwest side of FZ1. MSE 7 is slightly darker clayey silt that thickens to the southwest and is warped down across FZ1. MSE6 and MSE7 are probably the result of many small influxes of silty material as the sag was developing, but here they are lumped because the material is so similar that it was impossible to consistently map subunits. Despite the large scarp across FZ1, we did not observe material from MSE5 (sand) within MSE6 and MSE7. MSE8 is southwest-thickening clayey silt, which is topped by thin clay with sparse charcoal. MSE9 overlays this burn horizon; it is a thin unit of sandy silt that thickens to the southeast. Overlying MSE9 is a layer of southwest-thickening organic-rich silty clay that contains abundant charcoal, MSE10, and a thin layer of tan sand and silt, MSE11. Units MSE6-MSE11 are truncated by and cannot be correlated across FZ2 (figures 1.8-1.9). The sag units MSE6-MSE11 were probably deposited near the locus of sag pond subsidence, but have since been offset to their current position NE of the deepest portion of the sag pond.

Southwest of FZ2, a sequence of silt, clay and sand deposits, MSE12-MSE21, are disturbed by splays of FZ2 (figure 1.9), down-dropped and warped by FZ3 (figure 1.10), and truncated by FZ4 (figure 1.10). These units maintain their thickness across the exposure (figure 1.8) and include several relatively thick homogeneous fine sands and silts (MSE16, MSE18, MSE20, and MSE 21) suggesting that they are over-bank deposits from Little Cholame Creek. Between MSE19 and MSE20 and MSE20 and MSE21 are thin layers of laminated clay with charcoal. The apparent vertical deformation of MSE12-MSE21 across FZ3 created space and an unconformity, which has been covered and filled by dark, clay-rich material: MSE 22-24 and MSEUD. These four units are located below the region of maximum depth of the sag pond, thicken beneath the locus of the active sag, and are the youngest units of the trench. MSEUD is undifferentiated because it is highly bioturbated by roots of the thick sag pond grasses; this unit also contained a discarded piece of worked stone. MSE 20-24 are truncated to the southwest by FZ4 (figure 1.10). We interpret that these as growth strata from the actively forming sag.

Southwest of FZ4 is a heavily bioturbated sequence of units, MSW1-MSW7 (figures 1.8 and 1.10). These units include (from bottom to top) dark clay, silty sand, clayey silt, laminated clay with charcoal, coarse sand and gravel lenses, dark clayey silt and brown sandy silt. We interpret these as a sequence of fluvial deposits from Little Cholame Creek, including some over bank deposits, channel deposits, and an in situ burn horizon (MSW4). All of these units are all tilted toward FZ4. MSW6 and MSW7 are heavily sheared and truncated by FZ4. Southwest of fault zone 4 the units become more

bioturbated by burrows apparently because soil moisture decreases outside of the sag expression.

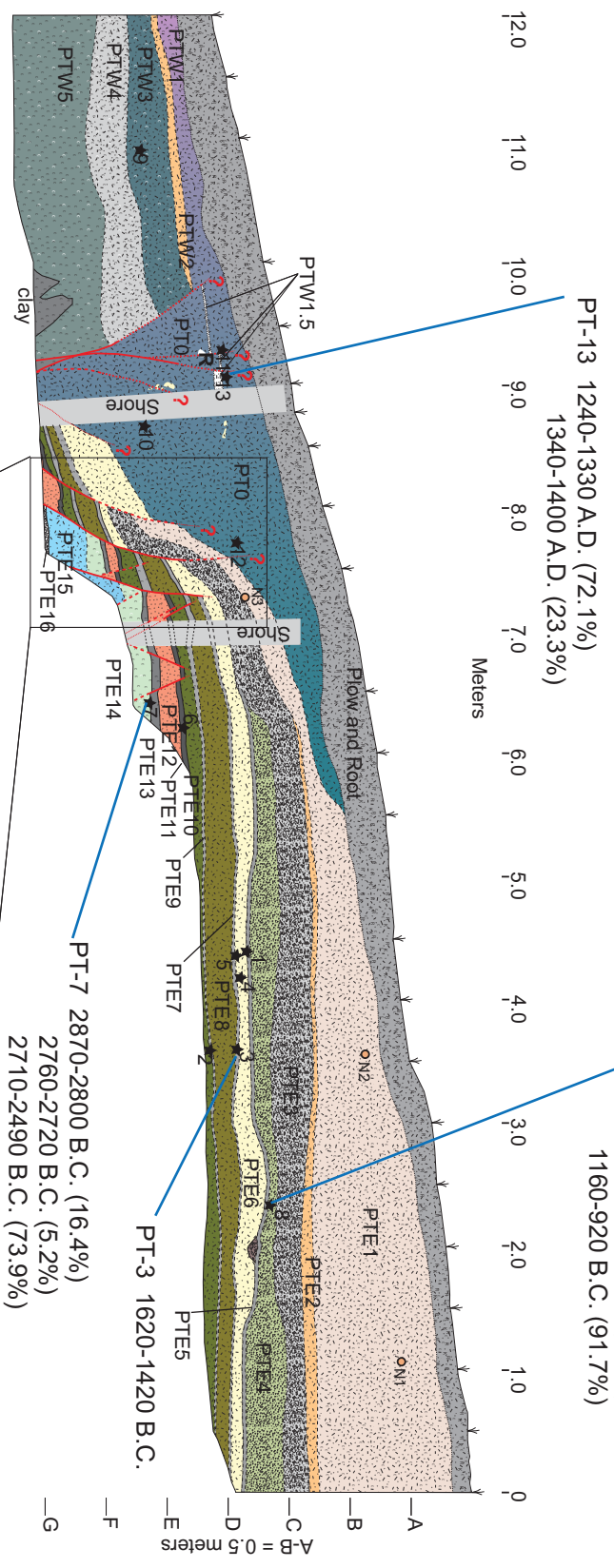
PT Stratigraphy

PT was located across the pressure ridge and associated spring line near Carr Hill (figure 1.5). Deformation within the PT trench was localized below the break in slope along the pressure ridge. Units on the NE side of the pressure ridge are referred to as PTE1-PTE16 and units on the SW side are PTW1-PTW5; numbers correspond to stratigraphic position with 1 representing the stratigraphically highest (youngest) unit in the section. Units exposed to the southwest side of the pressure ridge (PTW1-PTW5) were tabular and did not show evidence of tectonic deformation. We only logged near the main deformation zone (figure 1.11). PT units on the northeast side of the pressure ridge (figure 1.11, supplemental table 1.2), PTE1-PTE16, are a sequence fluvial deposits. The sequence alternates between fine sand and silt overlain by thin layers of laminated clay with in situ charcoal, PTE5-PTE13. This sequence apparently represents a history of repeated over bank flood deposits followed by periods of vegetation growth and fire. Other units included coarse sands and gravels (PTE3; PTE4; PTE16). These were apparently deposited by paleotributaries or paleochannels of the Little Cholame Creek.

Along the southwest slope of the pressure ridge, the stratigraphy is complicated by intense root bioturbation, a large amount of pedogenic clay, and deformation from the SAF. We were unable to differentiate many units in this portion of the exposure, with the exception of PTW1.5, which is a thin layer of leaves, sand, and pebbles, that were faulted near the top of the exposure (figure 1.11).

Figure 1.11. Phoebe's northwest trench log and photo mosaic of the apparent vertical offset along the fault splays of the pressure ridge. PTE0 is an undifferentiated dark grey unit consisting of a mix of materials including sand, silt, pebbles, small cobbles, leaves, and roots, but dominated by clay. At least 4 clay shear bands were located within this unit. To the SW of PTE0, units are tabular and show no tectonic warping. To the NE lies a sequence of alternating fluvial over bank sands, silts and clay-rich burn horizons. These deposits are offset (0.01-1m) along many fault splays that bend with depth toward the main deformation zone of PTE0. Some of these offsets show reverse motion, but much of the offsets display apparent normal offset. See figure 1.7 for symbol explanations, figure 1.6 for further stratigraphic relationships and supplemental table 1.2 for unit descriptions.

3 Phoebe's Trench (PT) northwest wall



Oblique view of Fault Splays

Radiocarbon Age Constraints

We collected 48 samples of the abundant charcoal from the MST and PT trenches (Appendix C and table 1.2). The excavations exposed several sequences of well-preserved thinly laminated silts and clay that contain thin, horizontally-continuous charcoal laminae. Because these charcoal layers are horizontally continuous we interpret them to be in situ; the charcoal was likely formed as a result of a fire on the paleoterrace surface and preserved by subsequent burial from over-bank flood deposition. Therefore, we have high confidence that ages from these burn horizons are representative of the age of the stratigraphy at that position within the exposure. Other charcoal samples were collected as individual pieces from organic-rich sag deposits, within over-bank sands, or from paleochannel gravels of the Little Cholame Creek. The age of such individual charcoal pieces may be older than the layer from which they were collected because of transport prior to deposition (detrital history). The NSF Arizona AMS Facility analyzed 13 charcoal samples: 9 from MST and 4 from PT (table 1.2, figures 1.6-1.11). Calibration was performed using OxCal v. 3.9; here, we quote the 2σ -calibrated ages.

MST Age Constraints

We analyzed 2 samples from the units northeast of FZ1, 04MST-1 and 04MST-9. 04MST-9 was collected from the laminar clay at the top of MSE1, the lowest unit in the northeast section of MST. This sample yielded a calibrated age of 400-200 B.C. (table 1.2). The sample 04MST-1 was collected near the top of a gravel lens from unit MSE2, yielding an age of 11600-7900 B.C. This age is stratigraphically inconsistent by > 5000 years (figure 1.6), indicating a long transportation prior to deposition.

Table 1.2. Radiocarbon data and analysis from MST and PT paleoseismic sites. Pretreatment and analyses were performed by the NSF-Arizona AMS facility at the University of Arizona. This facility uses the background correction of Stuiver and Polach, (1977). Stratigraphic and sample age relationships are shown in figure 1.6, further description is provided in Appendix C.

Sample ID ¹	NSF-AMS# ²	Sample Description	$\delta^{13}\text{C}$	Fraction Modern	+/- ³	¹⁴ C age (years BP)	+/- ⁴	2 σ calibrated age (cal A.D. / B.C.) ⁵
04PT-3	AA61381	charcoal from thin charcoal and clay in situ burn horizon	-26.1	0.6677	0.0033	3244	40	1620-1420 B.C.
04PT-7	AA61382	bulk sample from thick charcoal-rich in situ burn horizon	-24.84	0.6018	0.0029	4079	39	2870-2800 B.C. (16.4%) 2760-2720 B.C. (5.2%) 2710-2490 B.C. (73.8%)
04PT-8	AA61383	large charcoal ember collected from charcoal laden clayey silt unit	-22.72	0.6993	0.0032	2873	37	1210-1200 B.C. (1.0%) 1190-1170 B.C. (2.7%) 1160-920 B.C. (91.7%)
04PT-13	AA61384	charcoal collected from a thin, discontinuous layer with detrital leaves	-25.22	0.916	0.0039	705	35	1240-1330 A.D. (72.1%) 1340-1400 A.D. (23.3%)
04MST-1	AA61385	small charcoal sample collected from gravel lens	-24.64	0.28	0.023	10230	660	11600-7900 B.C.
04MST-9	AA61386	charcoal from thin charcoal and clay in situ burn horizon	-24.82	0.7563	0.0034	2243	36	400-200 B.C.
04MST-17	AA61387	charcoal from thin burn horizon	-24.6	0.8508	0.0037	1298	35	650-780 A.D.
04MST-22	AA61388	small charcoal sample collected within a sandy clay	-28.22	0.9221	0.004	652	35	1280-1400 A.D.
04MST-24	AA61389	small charcoal pieces collected from a laminated silt layer	-19.94	0.8311	0.0056	1486	55	430-660 A.D.
04MST-26	AA61390	bulk sample from thick charcoal rich unit	-26.39	0.7867	0.0035	1927	36	20-10 B.C. (1.0%) 0-140 A.D. (90.1%) 150-180 A.D. (2.3%) 190-220 A.D. (2.0%)
04MST-30	AA61391	charcoal pieces collected from top-most distinguishable active sag unit	-24.04	0.9558	0.0041	363	34	1440-1640 A.D.
04MST-32	AA61392	charcoal from sandy clay sag unit	-24.61	0.7833	0.0049	1961	51	100 B.C.-140A.D. (92.9%) 150-180 A.D. (1.3%) 90-220 A.D. (1.1%)
04MST-33	AA61393	charcoal from laminated silt and clay in situ burn horizon	-25.64	0.7044	0.0033	2815	37	1070-890 B.C. (89.2%) 880-830 B.C. (6.2%)

- (1) Assigned sample number based upon: A) the year collected (2004), B) the trench of collection - Miller Sag Trench (MST) or Phoebe's Trench (PT), and C) the order of collection in each trench.
- (2) NSF- Arizona AMS facility tracking number.
- (3) Error value (2 σ) assessed in the calculation of the modern fraction.
- (4) Error value (2 σ) assessed in the calculation of ¹⁴C years before present.
- (5) Determined with OxCal 3.9 using the atmospheric data of Stuiver et al., (1998).

Two samples were analyzed from the sag units between FZ1 and FZ2. 04MST-17 was collected at the interface between MSE7 and MSE8, a thin layer of laminated clay and sparse charcoal, probably an in situ burn horizon. The age of this sample is 650-780 A.D., which is stratigraphically consistent with other sample ages (figure 1.6, 1.8, 1.9 and table 1.2). 04MST-22 was collected from the middle of MSE10, a sandy clay unit. It yielded an age of 1280-1400 A.D.

Between FZ2 and FZ4, four samples were analyzed; two from fluvial terrace deposits and two from the growth strata sequence below the present-day active sag. 04MST-26 was collected from a charcoal rich portion of the MSE 15 silty clay. This sample yielded an age of 20 B.C. – 220 A.D. The next sample in the section, 04MST-24 was collected from laminated silty clay at the top of unit MSE19 and yielded an age of 430-660 A.D. The lowest sample from the active sag sequence was 04MST-32. It was collected from a layer of sandy clay, MSE22, and yielded an age of 100 B.C. – 220 A.D. This age is similar to the age of the MSE15 unit and older than the age from MSE19; apparently 04MST-32 is detrital. The youngest age in MST was 04MST-30, 1440-1640 A.D. This sample was collected from the uppermost distinguishable sag unit, MSE24 (figures 1.6, 1.8, 1.10 and table 1.2). Southwest of FZ4, only one sample was analyzed, 04MST-33, it was collected from the MSW4 in situ burn horizon and yielded an age of 1070-830 B.C.

Sample 04MST-1, 04MST-9 and 04MST-33 are the oldest in MST (table 1.2, figure 1.6), which is consistent with the interpretation that the units northeast of FZ1 and southwest of FZ4 are old fluvial terrace deposits (figure 1.8). 04MST-26 is also old,

supporting the interpretation that the units between FZ2 and FZ3 are also terrace units (figure 1.8). The relatively young ages of 04MST-17 and 04MST-22 support the interpretation that the sequence of units (MSE6-MSE11) between FZ1 and FZ2 are younger sag pond units (figures 1.8 and 1.9). These overlapping sag units are slightly older than the youngest units in the trench, MSE22-MSE24. These are also interpreted to be sag pond growth strata. These two young sequences are separated by FZ2 and FZ3, which are oriented obliquely to the SAF trend, suggesting MSE6-MSE11 are slightly older sag deposits that have been faulted into place and out of the locus of active deposition.

PT Age Constraints

Four samples were analyzed from the PT trench. One sample was collected from a sandy unit, PTE 4 (04PT-8), two samples were taken from the sequence of repeating in situ burn horizons (04PT-3 and 04PT-7), while the fourth sample was taken from the thin leaf litter-rich fault disrupted unit, PTW1.5 (04PT-13; figures 1.6 and 1.11). All four PT sample ages were stratigraphically consistent (figure 1.6). The leaf litter sample, 04PT-13 yielded an age of 1240-1400 A.D., while the samples from the sequence of terrace deposits (04PT-8, 04PT-3 and 04PT-7) yielded ages of 1210-920 B.C., 1620 -1420 B.C., and 2870-2490 B.C., respectively.

Deformation Styles

MST Fault Zone 1

Four localized zones of faulting are distributed across the extent of the sag pond exposure. Each fault zone includes multiple fault splays (fault splays are < 2 cm wide zones of clayey material that typically define boundaries between offset strata), which

accommodate the offset. Fault zone 1 (FZ1) contains three distinct fault splays (figures 1.8 and 1.9) and is parallel with the regional SAF trend: $\sim 313^\circ$ (table 1.1). MSE1-MSE4 are down warped, thinned, and they show 10-20 cm of apparent normal offset along the northeastern-most fault splay (figures 1.9 and 1.8). These units are also down-faulted ~ 10 cm by splay 2. Splay 2 merges with splay 1 near the bottom the exposure. Slip along the merged splays sends the thinned units below the trench exposure. Splays 1 and 2 also contain entrained pebbles from MSE2 (table 1.1). MSE5 is a package of clean sand and silt, which is also down faulted by fault splays 1 and 2; however, it does not show significant thinning. MSE5 is faulted a third time; about 20 cm to the southwest. Splay 3 juxtaposes MSE5 against clayey deposits: MSE6 and MSE7. These units overly and thicken above the splay 3 scarp unconformably (figures 1.6, 1.8-1.9). This suggests that MSE6 and MSE7 were deposited while offset was occurring along FZ1. Because the top of MSE 7 does not show signs of offset, we interpret that offset along FZ1 ceased sometime during the deposition of MSE7. An age from the top of MSE7 is 650-780 A.D. (04MST-17; table 1.2, figures 1.6-1.9), so we can assume FZ1 deactivated prior to this time and has not ruptured or experienced creep since then.

The units deformed by FZ1 display ~ 1 m of cumulative apparent normal offset. Because units above MSE7 thicken to the southwest (figure 1.8) we infer that a scarp existed along FZ1 while these sag units were deposited; we observe a relict of this scarp in the topography today (figures 1.5 and 1.8). MSE5 shows mixing with clay along its interface with MSE6 and MSE7 (figures 1.8-1.9 and table 1.1), suggesting that these offsets are related to coseismic rupture that caused ground cracking in to which clay and

silt accumulated. However, these are not large fissure fills. Moreover, we do not recognize any slope colluvial wedge deposits within MSE6 or MSE7 along fault splay 3's scarp. If this scarp formed in a few large events we would expect the sandy unit MSE5 to easily erode, likely injecting sandy colluvial material into the dark clayey units of MSE6 and MSE7. We did not observe such material within these units, so we interpret that this scarp must have formed over a period of time with repeated deformation from moderate coseismic ruptures (e.g., < 10 's of cm/event) and aseismic creep.

MST Fault Zone 2

Fault zone 2 (FZ2) is oriented obliquely to the local trend of the SAF (table 1.1, figure 1.5). Also, FZ2 appears to bend across the trench; on the northwest wall it strikes 170 degrees, but on the southeast wall it strikes 161 degrees. The southeast wall exposes three fault splays. The splays merge near the bottom of the trench exposure (figure 1.8). The northeastern-most fault splay truncates the sag units to the northeast (MSE6-MSE11) and juxtaposes them against the terrace deposits to the southwest (MSE12-MSE21). This fault splay extends to the surface of the trench (figure 1.8; photo mosaic). This observation is consistent with recent fault creep and recent M6 rupture along this fault zone (see below). The terrace units exposed to the southwest of FZ2 are cut by two fault splays, which kink the units slightly (figure 1.9). These fault splays do not reach the surface of the trench. The fault surface of FZ2 was exposed during trenching and was characterized by a clay coating, which showed steep dip-slip/oblique-slip striae (table 1.1). This is consistent with the apparent normal sense of motion observed across the trench and suggests that FZ2 helps to accommodate extension across the sag.

MST Fault Zone 3

Fault zone 3 (FZ3) is composed of four steeply dipping fault splays that down-drop the MSE17- MSE21 terrace units exposed between FZ2 and FZ4 (figure 1.8 and 1.10). The normal slip across FZ3 apparently created space that was subsequently filled by the MSE22-MSE24 sag deposits. Each fault appears to have accommodated several cm to more than 10 cm of normal slip. Units maintain thickness across these faults and the faults are traceable up into MSEUD, so the faults may reach the surface and be creeping or may have recently ruptured in 1966 and/or earlier historical earthquakes.

MST Fault Zone 4

Fault zone 4 (FZ4) juxtaposes the MSE22-MSE24 sag units against the southwestern terrace deposits MSW6 and MSW7 (figure 1.8 and 1.10). FZ4 is characterized by numerous clay shear bands that each show small apparent vertical offset and collectively they probably accommodate significant right-lateral offset. The shear bands appear to reach the TR unit, suggesting that they may accommodate creep as well as recent M6 events. The units on the northeast side of FZ4 show a small amount of warping as they approach FZ4 and the southwestern fluvial units are warped down, apparently dipping more than 50° to the northeast. FZ4 is parallel to the SAF and FZ1.

PT Deformation

Deformation exposed in PT is on the southwest side of the pressure ridge and is accommodated by two styles of faulting: a main shear zone that probably accommodates most of the slip and a series of splaying, listric-style, dip-slip faults that crisply displace the NE terrace units (PTE1-PTE16; figure 1.11). Splays bend towards the main

deformation zone with depth, suggesting that they probably merge below the exposure. The splays are < 2cm clay shear bands that truncate and vertically offset terrace units. Apparent vertical displacements range from ~1 cm to several 10's of cm along the more dominant splays. However, the fault splays do not appear to reach the upper terrace stratigraphy.

The main fault zone is characterized by a deformed PT0 unit that contains a mixture of clay, silt, sand, pockets of sand, small cobbles and pebbles and many clay shear bands (figure 1.11). At least three of these shear bands displace unit PTW1.5 (1240-1440 A.D.) both up and down by as much as 10 cm. If we assume that PTW1.5 is a colluvial deposit, the offsets of PTW1.5 do not appear to be related to large events because of the preservation of the fragile and tabular leaf litter and small pebble layer. However, sand and silt pockets are exposed deeper in the section. These could be related to fissure fill, but their size and orientation does not necessarily require ground rupture. They could be related to soil slump and fill or burrowing. Another interesting feature is an angular dark clay structure deep within the PT section. We are uncertain of its origin. It could be a buried and altered block of soil that slumped due to instability along the spring line of the fault; however, we cannot rule out that it may have formed via large ground rupture. The main fault zone of PT is not well understood stratigraphically or structurally because of deformation and bioturbation.

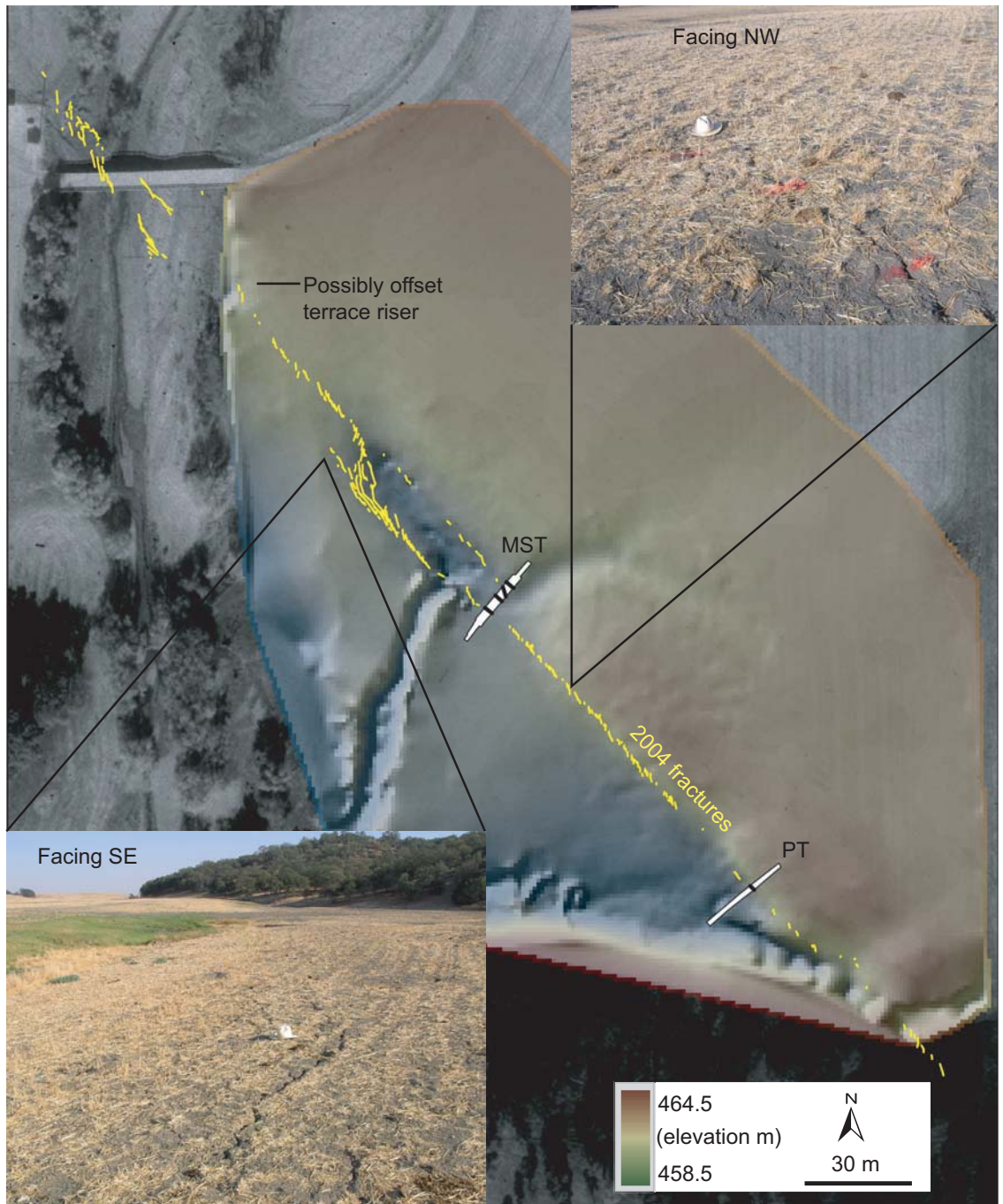
2004 Ground-Rupture at MST and PT

Three days following the September 28th, 2004 Parkfield earthquake, we surveyed the rupture through the backfilled paleoseismic site (figure 1.12). The general rupture

pattern consisted of left-stepping, opening mode, en echelon fractures. Fractures ranged in length from 0.5-5 m and steps ranged from 0.5-2 m. Openings ranged from 0.5-4 cm. Right-lateral slip tended to be quite small, but exceeded 2 cm on some of the fractures. At the sag pond, up to 2 cm of normal slip was observed.

The fractures trended NW-SE along the geomorphic expression of the SAF (~315°). Individual fractures trended 340°-000°. A single set of fractures opened between Carr Hill and the sag pond. Along the SE side of the pressure ridge the fracture set bends to the left. The fracture set trends across the main deformation zone of PT (figure 1.12 and 1.11). This same fracture set aligns with FZ4 of MST and continues along the SW side of the sag (figure 1.12 and 1.8). At the NW end of the sag, the fracture set broadens into a wide set of fractures that bend right, joining a second set of fractures that run along the NE side of the sag. The NE fracture set is parallel to the SW set and aligns with FZ3 of MST. The NE fractures continue NW past the sag. The fractures align cut along the apparently offset terrace riser at the edge of the Miller's field. In the Little Cholame Creek bed, the fractures break into two parallel sets. One set is aligned with the NE fracture set and the other set is stepped to the left. These fractures converge in a wide zone under the Parkfield Bridge and continue their trend to the NW (figure 1.12). The 2004 fracture pattern illuminates the surface geometry of the SAF through the paleoseismic site (figure 1.12) and provides clear explanations for the geomorphology there. The pressure ridge near Carr Hill is associated with a left bend in the 2004 rupture pattern. This step acts as a restraining bend and the persistence of such a bend through time and slip along the fault has resulted in uplift, forming the pressure ridge on the NE

Figure 1.12. 2004 M6 earthquake fractures (yellow) over a hillshade map of the paleoseismic site and 1:6000 aerial photography. Fractures were left-stepping en echelon opening mode with a small component of right lateral motion. Fractures along the sag pond showed up to 2 cm of normal offset. Trench footprints are shown in white and contain the locations of fault zones in black. The trend of fractures near the trench footprints suggests that FZ2 and FZ4 of MST and the main fault zone of PT were activated in 2004. Two photographs show the fractures on October 1st, 2004. See figures 1.8-1.11 for trench logs and fault zones and figure 1.13 for a M6 earthquake deformation model.



side of the fault. Uplift is not observed on the SW side of the fault, probably because erosion from a stream and several springs outpace the uplift rate. The Miller sag was ruptured on both its NE and SW sides across a right step in the 2004 ground rupture. This right step has resulted in extension between the step-over through time, forming the depression. The 2004 fractures appear to have accommodated as much as 2 cm of normal slip along FZ2 and FZ4 of MST. This is consistent with the apparent normal component of slip observed within the MST (figures 1.8-1.10).

The caveat of our slip measurement is that it was a minimum because of the role of delayed aseismic creep following the 2004 event (after slip). We observed an increase in fracture numbers and opening around the NW step-over of the sag pond during the two days that we surveyed. Our measurements were taken 2-3 days following the earthquake. After slip has persisted since the 2004 event and has resulted in ~20 cm of total dextral slip at the Parkfield Bridge (measured over ~100m apertures by Lienkaemper et al., in review). On October 1st, 2004 6.3cm of dextral slip was measured by Lienkaemper et al., in review; suggesting that ~1/3 of the total event slip was released by October 1st, 2004. On the same day, we measured 2cm of horizontal and vertical slip at the aperture of individual fractures at the sag pond of our paleoseismic site. The total event slip over these smaller apertures was probably more than 2cm; perhaps as much as 6cm if we assume that we proportionally measured 1/3 of the slip at MST during our survey. Also, it is plausible that after slip could have later activated FZ1 and FZ3. Although, non-activation of FZ1 was consistent with trench relationships suggesting this fault zone has not been active recently (figures 1.8-1.9 and 1.12).

Discussion

This study provides an important prehistoric record of deformation along the Parkfield segment of the San Andreas Fault. We did not observe any unequivocal evidence of large magnitude ground rupture. Observations from MST, PT, and the 2004 earthquake suggest that the Parkfield segment may be characterized by moderate magnitude ground rupture and aseismic fault creep for > 2000 years.

M6 Earthquake Recurrence

Vertical offset measurements from the 2004 event may provide insight into the recurrence of M6 events along the Parkfield segment. If we compare the 2004 vertical offset measurements at the Miller sag with vertical offsets observed within the MST stratigraphy (figures 1.8-1.10) we are able to estimate the number of 2004-sized events required to create the MST offsets. With the addition of radiocarbon age constraints we can estimate recurrence.

Three offsets observed within MST allow us to perform such estimations (table 1.3). An example is recurrence estimate 1 (RE1; table 1.3): Sag unit MSE24 has a 2σ age of 1440-1640 A.D. and was offset ~90cm below the surface of the trench. This suggests MSE24 was offset 90 cm over the past 364-564 years. If we assume that the vertical offset observed in 2004 at MST (2-6 cm) is typical of such events, then it suggests that between 15-45 events are required to create the 90 cm offset. Dividing the number of events by time of offset suggests an average recurrence of 8-38 years is required to fit the data observed from RE1. RE2 and RE3 are calculated in the same manner:

- 1) MST offset observation / 2004 offset (2-6cm) = # M6 events,
- 2) Estimated age of MST offset / #M6 events = average recurrence

Table 3. M6 Parkfield recurrence rate calculations: E.g., Recurrence estimate 1 (RE1) utilizes the offset between the sag unit MSE24 and the MST surface and age constraints provided by MST-30.

	RE1	RE2	RE3
Units compared	MSE24 and surface	MSE24 and MSE22	MSE10 and MSE9
Radiocarbon samples ^a	MST-30	MST-30, MST-32	MST-22, MST-17
Upper unit min age (Umin)	2004 A.D.	1640 A.D.	1400 A.D.
Upper unit max age (Umax)	2004 A.D.	1440 A.D.	1280 A.D.
Lower unit min age (Lmin)	1640 A.D.	220 A.D.	780 A.D.
Lower unit max age (Lmax)	1440 A.D.	100 B.C.	650 A.D.
Estimated offset ^b	90 cm	44 cm	25 cm
Min time (Tmin) = Umax - Lmin	364 yrs	1220 yrs	500 yrs
Max time (Tmax) = Umin - Lmax	564 yrs	1740 yrs	750 yrs
Events (Emin), Offset / (6cm ^c /event)	15	7	4
Events (Emax), Offset / (2cm ^c /event)	45	22	14
Min recurrence rate ^d = Tmin / Emax	8	55	36
Max recurrence rate = Tmax / Emin	38	249	188

^a For radiocarbon sample locations and analyses refer to table 2 and figures 6-10

^b Offsets measured via relative vertical positions of radiocarbon samples

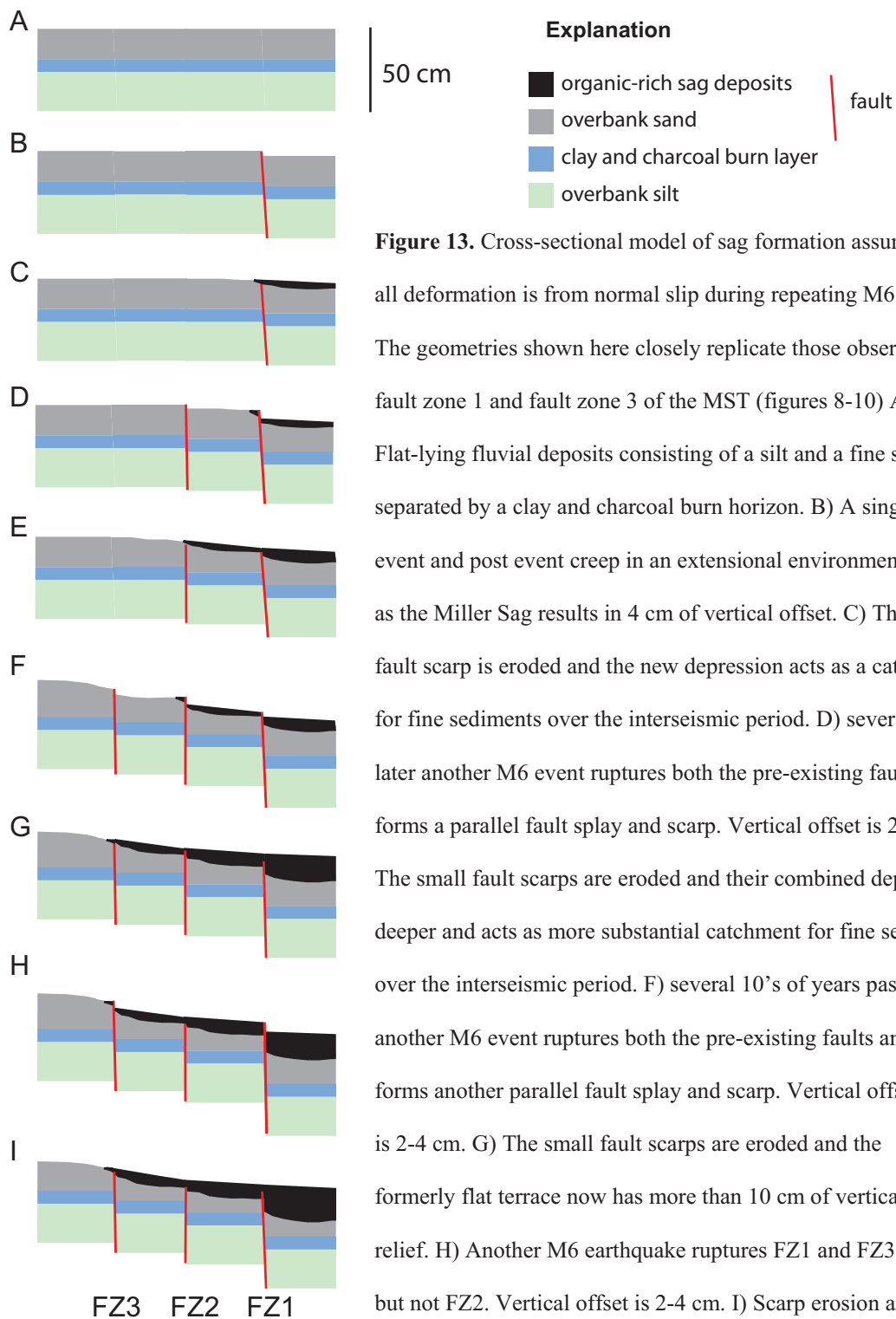
^c In 2004 we measured 2 cm of normal slip 3 days following the event, with after slip this slip could have been as much as 6cm.

^d If we assume all vertical deformation is attributed to M6 deformation.

These offset calculations suggest a M6 recurrence between 8 and 249 years on the Parkfield segment (table 1.3). This range of recurrence estimates includes the historically observed range of 8-38 year M6 recurrence at Parkfield. A recurrence of 249 years is probably an overestimate of the recurrence because of the suspected detrital history of sample MST-32 (figure 6). The caveats of these estimations are that we assume that all vertical offset is attributed to M6 events and we assume that all previous events produced a similar amount of vertical offset as 2004. The additional contribution of vertical offset due to fault creep or larger events would necessitate a longer time between M6 events.

Deformation Styles

If we assume that the 2004 offset and deformation styles observed at our paleoseismic site are typical of M6 events at Parkfield, then we are able to develop a speculative model of deformation and sag pond formation at our site (figure 1.13). The Miller sag is underlain by a base of originally flat lying fluvial terrace stratigraphy, in figure 1.13a we represent this by a thin in situ clay and charcoal burn layer surrounded by thicker fine silt and sand layers. In the series of cartoons (figure 1.13b-i) we show how repeating M6 events with 2-6 cm vertical offset would generate a sag pond environment. We assume that earthquakes may have ruptured one or more fault splays during each event. If the activation of these splays varies between events, then the subsequent vertical offset on each splay would vary. After several earthquake cycles of this behavior, a sag depression forms and may be filled by fine sediments (figure 1.13e). At MST, with springs and an ephemeral channel, it is clear how the sag would become wet and vegetated. Lush



vegetation would contribute to the deposition of decaying organic material (represented by the black unit in figure 1.13). Because each splay may have different activity histories, with subsidence greatest at the locus of the sag, the depth of sag deposits would increase across each fault splay (figure 1.13i). This result corresponds to our observations from MST FZ1 (figures 1.8 and 1.9) and FZ3 (figures 1.8 and 1.10). Both FZ1 and FZ3 down drop terrace units along multiple splays with increasing amounts of vertical offset toward the center of the sag depression. Overlying the terrace units are organic-rich sag deposits that thicken across each fault splay.

Interseismic surface creep has been inferred across the site at a rate of ~ 9 mm/yr (<http://quake.wr.usgs.gov/research/deformation/monitoring/longterm/pk/xmm1.html>). The M6 deformation model we present (figure 1.13) does not include aseismic creep; however, the addition of creep to the model should increase the rate of subsidence and aid in the formation of the sag. It would also be a mechanism for warping and tilting the terrace units such as MSE5 (figures 1.8-1.10).

Our trenches did not reveal direct evidence for earthquake ruptures greater than M6. The absence of filled fissures and colluvial wedge deposits does not preclude the possibility of larger ground ruptures through the central Parkfield segment. However, we located both of our trenches along tectonic escarpments where colluvial wedges would be expected to form and where slope instabilities would likely enhance fissuring from large earthquakes. 1857 anecdotal reports suggest ground-rupture extended as much as 80 km north of Highway 46 (Johnson, 1905 cited in Wood, 1955 and Sieh, 1978b). However, the 1857 rupture along the Parkfield segment may not have been a result of the 1857

main shock. If the two 1857 foreshocks were Parkfield events (figure 1.2), then they would have likely ruptured Parkfield in a manner similar to 2004, resulting in the reports of ground-rupture. Moreover, studies of offset landforms (Sieh, 1978b and Lienkaemper, 2001) suggest that the offset from 1857 were only 1-2 meters near Highway 46. This is 2-5 meters less than offsets measured along the Cholame segment.

Rupture Style Implications

Our data suggests that ruptures along the central Parkfield segment may not have exceeded the deformation expected from ~M6 earthquakes for > 2000 years. The absence of larger ground ruptures north of the Cholame Valley step-over supports the notion that M6 earthquakes characterize the Parkfield segment. Moreover, our prehistoric recurrence estimate is consistent with the historical recurrence of M6 events at Parkfield. If large ground ruptures do not extend into the central Parkfield segment, it suggests that the SAF rupture behavior changes significantly across the Cholame Valley.

Our results are also consistent with the variable rupture model of Kanamori and McNally, 1982. The variable rupture model states that simultaneous ruptures may occur along contiguous segments of a fault or the segments may fail individually (Working Group on the Probabilities of Future Large Earthquakes in Southern California, 1995). This suggests that the absence of large surface deformation along the central Parkfield segment does not mean that Parkfield cannot participate in a great earthquake rupture such as 1857. In fact, if we consider the 1857 foreshocks (figure 1.2), anecdotal accounts of the 1857 rupture extending 80km northwest of highway 46 (e.g., Wood, 1955; Sieh, 1978b), the 2-5 m decrease in geomorphic offset measurements northwest of Highway 46

(Sieh, 1978b; Lienkaemper 2001), and this study's lack of evidence for large magnitude ground rupture 21 km northwest of Highway 46, then a variable (or cascading) rupture fits what we know about the 1857 event at Parkfield. If this is the case, then future Parkfield events may warrant concern over a cascading rupture to the southeast as reviewed in Arrowsmith et al., 1997.

Uncertainty and Recommendations

We cannot preclude the possibility of larger ground-rupture at Parkfield because we have not ruled out the possibility that evidence for large ground ruptures exist elsewhere along the segment. We did not trench the Southwest fracture zone (figure 1.4) or the other faults that ruptured in 2004. However, this study shows that interpretable stratigraphy exists along the Parkfield segment. Clearly, to better understand the segment and the implications for fault mechanics and seismic hazards in central California, more excavations should be conducted along the main SAF trace of the segment and the southwest fracture zone. However, suitable sites must be found to resolve the intricate relationships between evidence for M6 rupture, creep, and larger ruptures if they are present.

Conclusions

Paleoseismic investigation within the central portion of the Parkfield segment suggests that the segment is characterized by repeated deformation from M6 earthquakes and fault creep for > 2000 years. This result is consistent with historical observations of strain release along the segment. We found no unequivocal evidence for large magnitude ground rupture in our paleoseismic trenches. 2004 M6 ground rupture was consistent

with the trench site geomorphology and ruptured through at least two preexisting faults that were mapped within our trenches. Vertical slip measurements from 2004 and age constraints along trench-exposed vertical offsets suggest that the recent Holocene recurrence rate of M6 events is between 8-249 years. This is consistent with the observed range of historical recurrence intervals of 8-38 years.

Acknowledgements

We thank Michael Rymer and Andy Snyder of the USGS, Kenneth Jones of ASU, and the residents of Parkfield, CA, especially the Miller family for cooperation during our research and Bob Fredericks for skillful backhoe work. We also thank Jim Lienkaemper and Heidi Stenner for their correspondence and suggestions. The US National Science Foundation (EAR-0310357) funded this investigation.

References

- 1994 Working Group on the Probabilities of Future Large Earthquakes in Southern California (1995). Seismic hazards in Southern California: probable earthquakes, 1994 to 2024, *Bulletin of the Seismological Society of America* **85**, 379-439
- Agnew, D.C. and K.E. Sieh (1978). A Documentary Study of the Felt Effects of the Great California Earthquake of 1857, *Bulletin of the Seismological Society of America* **68**, 1717-1729.
- Allen, C. R. (1968). The tectonic environments of seismically active and inactive areas along the San Andreas Fault system, *Proceedings of conference on geologic problems of San Andreas Fault system*, (edited by W. R. Dickinson and A. Grantz), *Stanford University Publications in the Geological Sciences* **11**, 70-82.

- Arrowsmith, JR., K. McNally, and J. Davis (1997). Potential for Earthquake Rupture and M7 Earthquakes along the Parkfield, Cholame, and Carrizo Segments of the San Andreas Fault, *Seismological Research Letters* **68**, no. 6, 902-916.
- Bakun, W.H. and A.G. Lindh (1985). The Parkfield California, Earthquake Prediction Experiment, *Science* **229**, 619-624.
- Bakun, W.H. and T.V. McEvilly (1984). Recurrence Models and Parkfield, California Earthquakes, *Journal of Geophysical Research* **89**, 3051-3058.
- Biasi, G.P., Weldon, R.J., Fumal, T.E., and Seitz, G.G. (2002). Paleoseismic event dating and the conditional probability of large earthquakes on the southern San Andreas fault, California, *Bulletin of the Seismological Society of America* **92**, 2761-2781.
- Bronk Ramsey C. (1995). Radiocarbon Calibration and Analysis of Stratigraphy: The OxCal Program, *Radiocarbon* **37**, no. 2, 425-430.
- Bronk Ramsey C. (2001). Development of the Radiocarbon Program OxCal, *Radiocarbon* **43**, 2A, 355-363.
- Brown, R.D. (1970). Map showing recently active breaks along the San Andreas and related faults between the northern Gabilan Range and Cholame Valley, California, scale: 1:62,500, *U.S. Geol. Surv. Misc. Geol. Invest. Map*, I-575.
- Burford, R.O. and Harsh, P.W. (1980). Slip on the San Andreas fault in central California from alignment array surveys, *Bulletin of the Seismological Society of America* **70**, p. 1233-1261.
- Crosby C.J. (2004). Digital database of faulting accompanying the 1966 Parkfield, California earthquake, *US Geological Survey Open File Report* **2004-1437**.

- Fumal, T.E., Weldon, R.J., Biasi, G.P., Dawson T.E., Seitz, G.G., Frost, W.T., and Schwartz D.P. (2002b). Evidence for large earthquakes on the San Andreas fault at the Wrightwood, California paleoseismic site: A.D. 500 to Present, *Bulletin of the Seismological Society of America* **92**, 2726-2760.
- Grant, L.B. and Sieh, K. (1994). Paleoseismic evidence of clustered earthquakes on the San Andreas fault in the Carrizo Plain, California, *Journal of Geophysical Research* **99**, 6819-6841.
- Harris, R.A. and R.J. Archuleta (1988). Slip Budget and potential for a M7 earthquake in Central California, *Geophysical Research Letters* **15**, 1215-1218.
- Jennings, C. W., (1977). Geologic map of California, *California Division of Mines and Geology*, Geologic Data Map No. 2, scale 1:750,000
- Johnson, H.R., (1905). Unpublished Field Notebook #3354, *U.S. Geological Survey Archives*, Denver, Colorado.
- Kanamori, H. and K.C. McNally (1982). Variable rupture mode of the subduction zone along the Ecuador-Columbia coast, *Bulletin of the Seismological Society of America* **72**, 1241-1253.
- Kelson, K.I. and J.N. Baldwin (2001). Can paleoseismic techniques differentiate between aseismic creep and coseismic surface rupture?, *Seismological Research Letters* **72**, no. 2, 263-264.
- King, N.E., P. Segall, and W. Prescott (1987). Geodetic Measurements near Parkfield, California, 1959-1984, *Journal of Geophysical Research* **92**, 2747-766.

- Langbein, J., R. Borchardt, D. Dreger, J. Fletcher, J.L. Hardebeck, M. Hellweg, C. Ji, M. Johnson, J.R. Murray, R. Nadeau, M.J. Rymer, and J.A. Treiman (2005). Preliminary report on the 28 September 2004, M 6.0 Parkfield, California Earthquake, *Seismological Research Letters* **76**, no. 1, 10-26.
- Lienkaemper, J.J. (2001). 1857 Slip on the San Andreas Fault Southeast of Cholame, California, *Bulletin of the Seismological Society of America* **91**, no. 6, 1659-1672.
- Lienkaemper, J.J., T.E. Dawson, S.F. Personius, G.G. Seitz, L.M. Reidy, and D.P. Schwartz (2002). A Record of Large Earthquakes on the Southern Hayward Fault for the Past 500 Years, *Bulletin of the Seismological Society of America* **92**, no. 7, 2637-2658.
- Lienkaemper, J.J., Baker, B., and McFarland, F.S. (in review). Surface Slip Associated with the 2004 Parkfield (CA) Earthquake Measured on Alinement Arrays.
- Lindvall, S.C., Rockwell, T.K., Dawson, T.E., Helms, J.G., and Weaver, K.D. (2002). Evidence for two surface ruptures in the past 500 years on the San Andreas fault at Frasier Mountain, California, *Bulletin of the Seismological Society of America* **92**, 2689-2703.
- Liu, J., Klinger, Y., Sieh, K., and Rubin C. (2004). Six similar sequential ruptures of the San Andreas fault, Carrizo Plain, California, *Geology* **32**, 649-652.
- Meltzner, A.J. and D.J. Wald (1999). Foreshocks and Aftershocks of the Great 1857 California Earthquake, *Bulletin of the Seismological Society of America* **89**, 1109-1120.

- Murray, J., P. Segall, P. Cervelli, W. Prescott, J. Svarc (2001). Inversion of GPS Data for Spatially Variable Slip-rate on the San Andreas Fault near Parkfield, CA, *Geophysical Research Letters* **28**, 359-362.
- Roeloffs, E. and J. Langbein (1994). The Earthquake Prediction Experiment at Parkfield, California, *Reviews of Geophysics* **32**, no. 3, 315-336.
- Rust, D.J. (1982). Radiocarbon dates for the most recent large prehistoric earthquakes and Holocene slip rates: San Andreas fault in part of the Transverse Ranges north of Los Angeles, *Geological Society of America Abstracts with Programs* **14**, 229
- Salyards, S.L., Sieh, K.E., and Kirschvink, J.L. (1992). Paleomagnetic measurements of non-brittle deformation across the San Andreas fault at Pallett Creek, *Journal of Geophysical Research* **97**, 12457-12470.
- Savage J.C. and Burford, R.O. (1973). Geodetic determination of relative plate motion in central California, *Journal of Geophysical Research* **78**, p. 832-845.
- Schwartz, D.P. and Weldon R. (1986). Late Holocene slip rate of the Mohave segment of the San Andreas fault zone, Littlerock, California: Preliminary results, *Eos (Transactions American Geophysical Union)* **67**, 906.
- Segall, P. and R. Harris (1986). Slip Deficit on the San Andreas Fault at Parkfield, California, as Revealed by Inversion of Geodetic Data, *Science* **233**, no. 4771.
- Sieh, K.E., (1978a). Central California Foreshocks of the Great 1857 Earthquake, *Bulletin of the Seismological Society of America* **68**, 1731-1749.
- Sieh, K.E. (1978b). Slip along the San Andreas Fault associated with the great 1857 earthquake, *Bulletin of the Seismological Society of America* **68**, 1421-1448.

- Sieh, K.E., Stuiver, M., and Brillinger, D. (1989). A more precise chronology of earthquakes produced by the San Andreas fault in southern California, *Journal of Geophysical Research* **94**, 603-623.
- Sims, J.D., (1987). Late Holocene slip rate along the San Andreas Fault near Cholame, California, *Geological Society of America Abstracts with Programs*, 451.
- Sims, J.D. (1990). Geologic map of the San Andreas Fault in the Parkfield 7.5 Minute Quadrangle, Monterey and Fresno Counties, California. 1:24,000. Map MF-2115USGS, 1990.
- Sims, J.D., (1994). Stream channel offset and abandonment and a 200-year average recurrence interval of earthquakes on the San Andreas fault at Phelan Creeks, Carrizo Plain, California, *Proceedings of the Workshop on Paleoseismology: U.S. Geological Survey Open-File Report* **94-568**, 793-812.
- Stenner, H.D. and K, Ueta (2000). Looking for evidence of large surface rupturing events on the rapidly creeping Calaveras fault, California, in *Active Fault Research for the New Millennium: Proceedings of the Hokudan International Symposium and School on Active Faulting*, K. Okumura, K. Takada, and H. Goto (Editors), Hokudan Co. Ltd., Hokudan, Hyogo, Japan, 479-486.
- Stuiver, M. and H.A. Polach (1977). Discussion: Reporting of ^{14}C data, *Radiocarbon* **19**, 355-63.
- M. Stuiver, P. J. Reimer, E. Bard, J. W. Beck, G. S. Burr, K. A. Hughen, B. Kromer, F. G. McCormac, J. Plicht, and M. Spurk (1998) INTCAL98 Radiocarbon age calibration 24,000 - 0 cal BP, *Radiocarbon* **40**, 1041-1083.

- Titus, S.J., C. DeMets, B. Tikoff (2005). New slip rate estimates for the creeping segment of the San Andreas Fault, California, *Geology* **33**, no. 3, 205-208.
- Toké et al. (in review). A slip budget along the Parkfield segment of the San Andreas fault: a slip deficit since 1857.
- Topozada, T.R., D.M. Branum, M.S. Reichle, and C.L. Hallstrom (2002). San Andreas Fault Zone, California: M>5.5 Earthquake History, *Bulletin of the Seismological Society of America* **92**, 2555-2601.
- Weldon, R.J., Fumal, T.E., Powers, T.J., Pezzopane, S.K., Scharer, K.M., and Hamilton, J.C. (2002). Structure and earthquake offsets on the San Andreas fault at the Wrightwood, California, paleoseismic site, *Bulletin of the Seismological Society of America* **92**, 2704-2725.
- Weldon, R.J., K. Scharer, T. Fumal, and G. Biasi (2004). Wrightwood and the earthquake cycle: what a long recurrence record tells us about how faults work, *GSA Today* **14**, no. 9, 4-10.
- Wood, H.O. (1955). The 1857 Earthquake in California, *Bulletin of the Seismological Society of America* **45**, 47-67.
- Young, J. J., JR. Arrowsmith, L. Colini, and L.B. Grant (2002). 3-D excavation and measurement of recent rupture history along the Cholame segment of the San Andreas Fault, *Bulletin of the Seismological Society of America: Special Issue on Paleoseismology of the San Andreas fault* **92**, 2670-2688.
- Zielke, O. and JR. Arrowsmith (In Progress). Digital database of active breaks in the SAF along the 1857 rupture

U.S. Geological Survey, Earthquake Hazards Program (2002). Long term plots for

xmm1: <http://quake.wr.usgs.gov/research/deformation/monitoring/longterm/pk/xmm1.html>

CHAPTER 2. REASSESSMENT OF A SLIP BUDGET ALONG THE PARKFIELD SEGMENT OF THE SAN ANDREAS FAULT

Abstract

Historically, the Parkfield segment has represented transition in fault behavior along San Andreas Fault (SAF). Despite the ~ 33 mm/yr long-term slip rate along the SAF, no slip has been observed on the Cholame segment since the great 1857 Fort Tejón earthquake. During that time, the Parkfield segment has experienced slip from six $\sim M6$ earthquakes and from fault creep. Data from aseismic slip rate studies and historical earthquake studies allow us to estimate the total slip released along this portion of the SAF since 1857. The slip deficit along the northwestern Cholame segment (to the SE of Parkfield) is about 5 m. This is approximately the mean of the range of 1857 offsets measured there. The slip deficit is much greater than the few 1857 offsets in the southeast portion of the Parkfield segment. Thus, the slip deficit in southeast Parkfield and Cholame may be as great as or may have surpassed the slip accommodated along these segments in 1857. The slip deficit abruptly decreases to the northwest across the central Parkfield segment. It is 1-2 m near the town of Parkfield and 0-1 m northwest of Middle Mountain. A $\sim M7$ event rupturing the all or part of the Cholame segment and the southeastern Parkfield segment (slip decreasing to the NW) would release the accumulated slip and is plausible. Importantly, this result also shows that the change in the pattern of strain release occurs in the middle of the Parkfield Segment, rather than at its ends.

Introduction

The Parkfield segment of the SAF spans from where California Highway 46 crosses the SAF to Slack Canyon, 48 km to the northwest (figure 2.1). Southeast of Parkfield is the Cholame segment of the SAF that last ruptured in the great 1857 Fort Tejón earthquake (e.g., Sieh, 1978b) and where at least one large prehistoric rupture is documented (Young et al., 2002). However, slip has not been observed along the Cholame segment of the SAF since 1857. In contrast, northwest of Parkfield, the Creeping segment, has experienced small to moderate historical earthquakes (e.g. Topozada et al., 2002) and continuous fault creep as long as historical measurements have been recorded (e.g., Burford and Harsh, 1980; Titus et al, 2005), but apparently did not rupture in the 1857 earthquake.

At least six \sim M6 earthquakes since 1857 have occurred along the Parkfield Segment (1881, 1901, 1922, 1934, 1966 and 2004; e.g., Bakun and McEvilly, 1984; Topozada et al., 2002; Langbein et al., 2005) and fault creep increases from 0 mm/yr at CA Highway 46 to >25 mm/yr northwest of Slack Canyon (figure 2.1, e.g., Burford and Harsh 1980; King et al., 1987; Murray et al., 2001; Murray and Langbein, this issue). Apparently, Parkfield is a \sim 50 km long transition zone between the historically-locked Cholame segment of the SAF, which experiences large magnitude earthquakes, and the steadily-slipping Creeping segment to the northwest.

Additionally, Parkfield appears to have played a role in the great 1857 rupture: Prior to the 1857 main shock, at least two prominent foreshocks were felt in central

Figure 2.1. A) A transition between contrasting zones of fault behavior occurs along the Parkfield segment of the SAF (modified from Allen, 1968). The Central California Creeping segment creeps at a rate > 25 mm/yr (e.g., Burford and Harsh, 1980; Titus et al, 2005). Along the Parkfield segment, both fault creep and repeating historical $\sim M6$ earthquakes accommodate fault motion. Southeast of Parkfield, the creep rate drops to zero and no historic earthquake ruptures have been documented SE of California Highway 46 since 1857. B) Hill shading over a 10m DEM with overlays of historic surface traces of the SAF (Jennings, 1997; Zielke and Arrowsmith, in progress) and the 1966 Parkfield segment rupture trace (Crosby, 2004). Yellow stars are estimated epicenters of post-1857 earthquakes: (Toppozada et al., 2002).

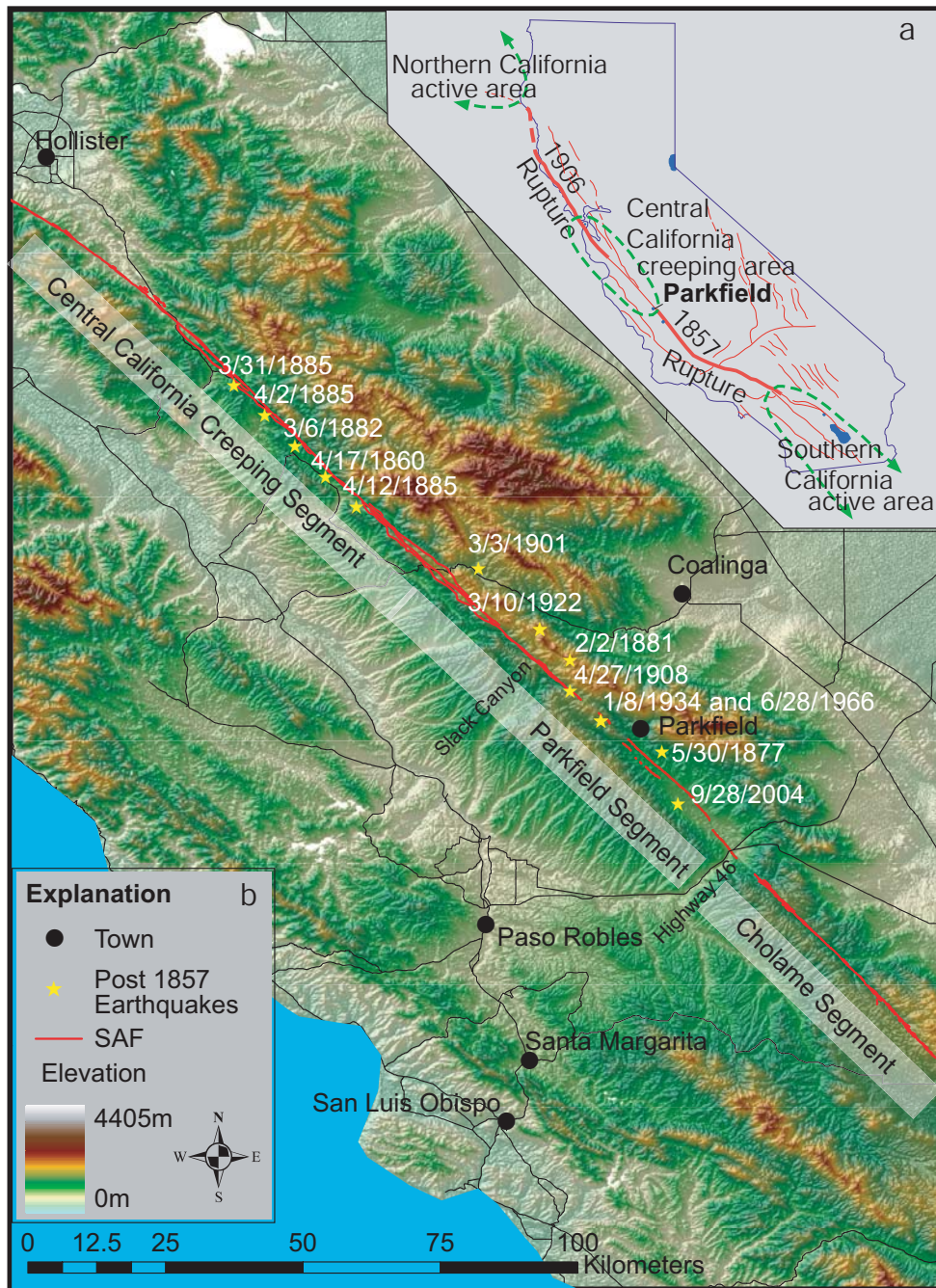
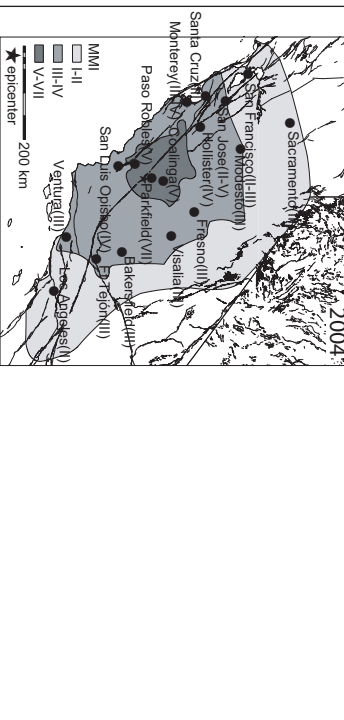
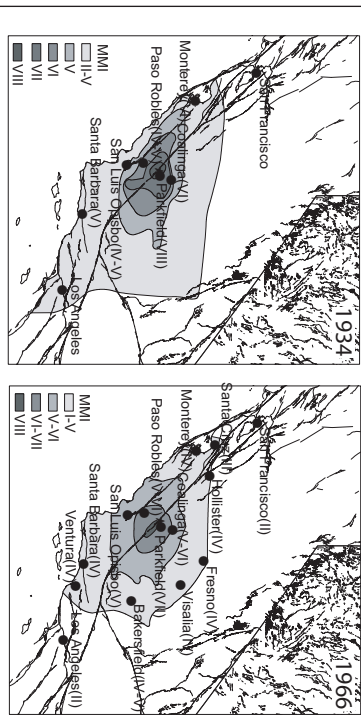
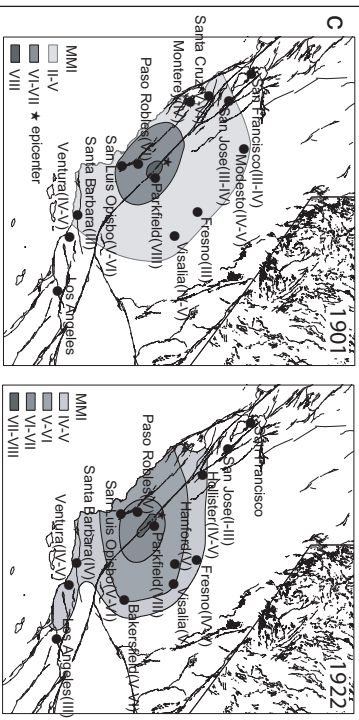
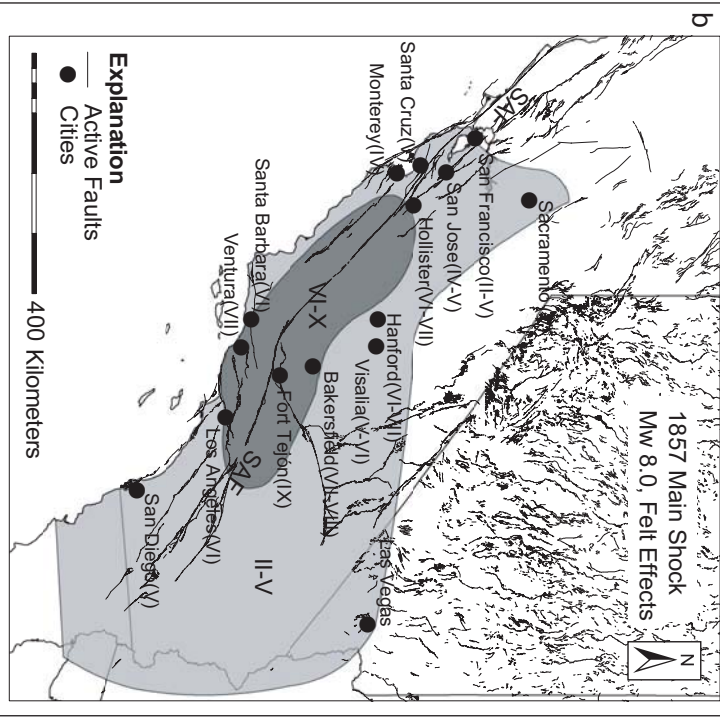
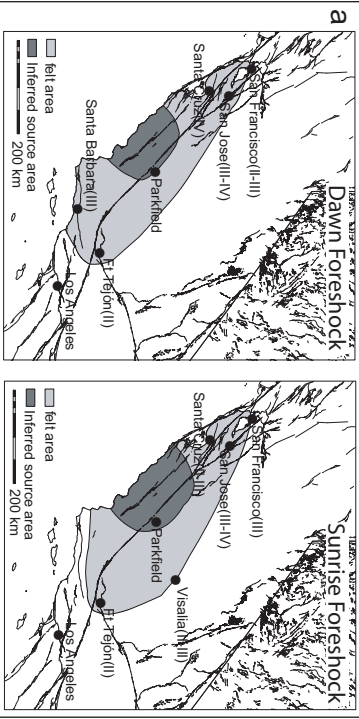


Figure 2.2. Felt effects from central SAF earthquakes: A) Felt (light grey) and source areas (dark grey) of the 1857 dawn and sunrise foreshocks (Sieh, 1978a). Both foreshocks were felt sparsely from the Bay area southeast to Ft. Tejón. The felt areas were centered near the Parkfield segment of the SAF. B) MMI Felt intensity distributions of the ~M8 1857 main shock (Sieh, 1978a; Agnew and Sieh 1978). The 1857 main shock was felt throughout central and southern California as well as Nevada, Arizona, and Mexico. C) Estimated epicenters (stars; Topozada et al., 2002) and felt MMI intensities from the 1901, 1922, 1934, 1966, and the 2004 ~M6 Parkfield events (Sieh 1978a). Similar to the 1857 foreshocks, the Parkfield earthquakes are felt from the San Francisco Bay to the Los Angeles Basin and the greatest intensities (darker grey) center on the Parkfield segment of the SAF.



California (Sieh, 1978a; Meltzner and Wald, 1999). The distribution of felt effects from these foreshocks were similar to the distributions of the felt effects from the 1901, 1922, 1934, 1966 and 2004 Parkfield earthquakes (figure 2.2). The 1857 foreshocks were of similar magnitude and location as the Parkfield events (Sieh, 1978a). If we also consider the distribution and duration of felt effects of the 1857 main shock (Agnew and Sieh, 1978; figure 2), the 1857 event probably ruptured from the northwest to the southeast with an epicenter near Parkfield (Sieh, 1978a). These observations suggest that the Parkfield segment played a role in both the nucleation and rupture of the 1857 event and may do so again in future large central California earthquakes (e.g., Sieh and Jahns, 1984; Harris and Archuleta, 1988; Arrowsmith et al., 1997).

Questions about the Parkfield segment's role in the rupture of large SAF earthquakes are even more urgent if one considers previous slip budget calculations along the SAF near Parkfield (Sieh and Jahns, 1984; Segall and Harris, 1986; Segall and Harris 1987; Harris and Archuleta, 1988; Lienkaemper and Prescott, 1989; Arrowsmith et al., 1997; Murray et al., 2001, Murray and Langbein, this issue). These studies enumerated the existence of a large slip deficit along the Carrizo and Cholame segments and a diminishing slip deficit across the Parkfield segment prior to the 2004 Parkfield earthquake. Furthermore, Arrowsmith et al., 1997 and Harris and Archuleta, 1988 showed that the slip deficits along the Parkfield and Cholame segments are greater than measurements of offset along landforms that last slipped in the 1857 rupture, as measured by Sieh, 1978b and Lienkaemper, 2001. Moreover, both studies use moment calculations to hypothesize that these two segments could co-rupture in a $\sim M7$ event.

This study reassesses the spatial distribution of the central SAF slip deficit after the 2004 Parkfield earthquake by constructing a slip budget using data from aseismic slip rate studies (Burford and Harsh, 1980; Murray et al., 2001; Titus et al., 2005) and historical earthquake studies (Lienkaemper and Prescott, 1989; Segall and Du 1993; Topozada et al., 2002; Lienkaemper et al., this issue). The slip deficit decreases abruptly across the central portion of the Parkfield segment. Additionally, this work highlights the requirement of a change from historically observed fault behavior to balance the SAF slip budget assuming a long-term slip rate of 33 mm/yr.

In this paper, we present three slip budget calculations (figure 2.3) that vary by the amount and extent of coseismic slip released. We discuss the current distribution of this slip deficit along the Parkfield segment (figure 2.3c) and the development of the slip deficit from Cholame to the Creeping segment of the SAF since 1857 (figure 2.4). We conclude by placing these results into context of slip from the 1857 rupture (figure 2.5), long term slip rate studies, and recent paleoseismic data.

$$\text{SAF Slip Budget} = (\text{long term slip-rate} * \text{time}) - (\text{aseismic slip} + \text{coseismic slip})$$

Long-Term Slip Rate

If the slip budget along a fault is to be balanced, the cumulative slip from aseismic slip and coseismic slip should equal the long-term slip rate multiplied by the time span considered. Therefore, the slip deficit is highly dependant upon the long-term slip rate. Along the central SAF, it is generally considered to be about 31-37 mm/yr (e.g., Sieh and Jahns, 1984; Murray et al., 2001; Noriega et al., in press). However, Sims, 1987 used a trench exposure of an offset alluvial fan, just northwest of Highway 46, to determine a

late Holocene SAF slip rate of $26.3 +3.9/-3.3$ mm/yr. Although the long-term slip rate of the SAF is still debatable, here we follow Murray et al., 2001 who used geodetic models, with a seismogenic transition depth of 14km, to determine a long-term slip rate of ~ 33 mm/yr. This rate suggests that nearly 5 m of slip should have accumulated since 1857 (black line: figure 2.3a).

Aseismic Slip Since 1857

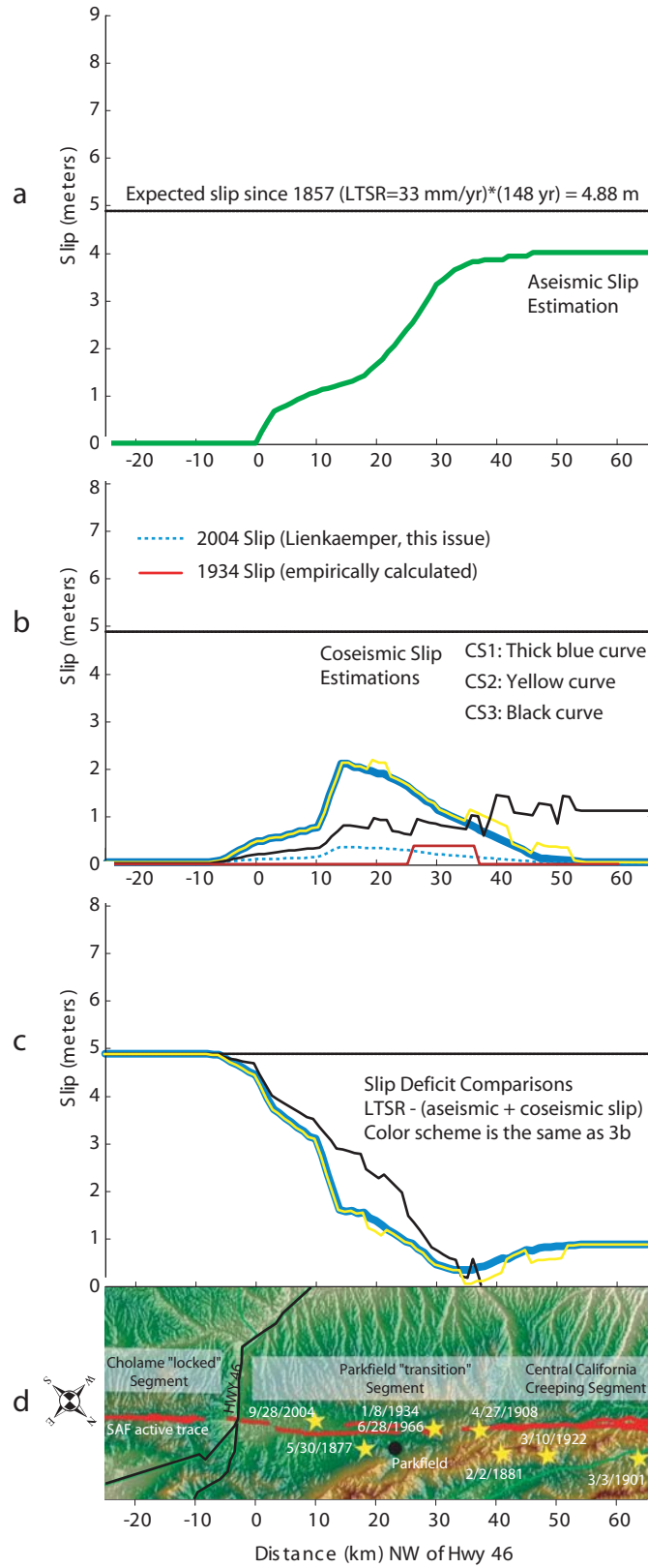
To estimate the slip released aseismically along the SAF since 1857 we used data from recent geodetically-based aseismic slip rate studies. Although geodetic studies do not span the entire time since 1857, we assume that recent aseismic slip rate measurements are representative for this time period: Along the Cholame segment, aseismic slip has not been observed (e.g., Segall and Harris 1987; Murray et al., 2001) so we assume a aseismic slip rate of 0 mm/yr for this portion of the SAF. Along the Creeping segment, we assumed a steady aseismic slip rate of 27 mm/yr, consistent with geodetically-determined aseismic slip rate studies (e.g., Burford and Harsh, 1980; Titus et al., 2005). Along the Parkfield segment, we depth-averaged the spatially-variable aseismic slip rates from the Murray et al., 2001 model. We divided the SAF into 1 km increments and interpolated these aseismic slip rates linearly in order to obtain an aseismic slip rate for each 1 km increment of the fault (Appendix D). We then multiplied the each aseismic slip rate by the time since 1857 ($2005-1857 = 148$ years) to obtain an estimate of aseismic slip released along the SAF since 1857 (green curve: figure 2.3a). Note that the creep rate as currently measured apparently is insufficient to keep up with the long term slip accumulation along the Creeping segment.

Coseismic Slip Since 1857

Coseismic slip along this portion of the SAF has been released in at least six ~M6 Parkfield earthquakes (e.g., Langbein et al., 2005). However, Topozada et al., 2002 suggests that there may have been additional moderate historic events near Parkfield that have been overlooked. Because of this debate over the number of Parkfield earthquakes, their relative sizes, and locations, we provide three differing estimations of the cumulative coseismic slip released since 1857 (see below; figure 2.3b).

The relative distribution of surface slip attributed to the 2004 Parkfield earthquake and post-seismic after slip was similar to the 1966 event (Lienkaemper et al., in review). Apparently the only major differences were that slightly more slip was recorded in 1966 and the 1966 rupture extend slightly further southeast than 2004. In our first estimation of cumulative coseismic slip (CS1; thick blue curve: figure 2.3b) we considered only the six accepted Parkfield events. We used the surface slip distributions measured by Lienkaemper and Prescott, 1989 and Lienkaemper et al., (in review) for the 1966 and 2004 earthquakes, respectively. For the 4 events prior to 1966 we assumed that slip was exactly the same as 2004. We then summed the slip from these 6 event estimations (figure 2.3c; Appendix E). All of the distributions were interpolated at 1 km intervals along the SAF. For reference, we present the total slip from the 2004 event (thin dashed blue curve: figure 2.3b).

Figure 2.3. A) Cumulative aseismic slip along the SAF since 1857 assuming the current aseismic slip rates of Murray et al., 2001, Burford and Harsh, 1980, and Titus et al., 2005. Refer to Appendix D for aseismic slip calculations. B) Estimations (CS1-CS3) of cumulative coseismic slip along the SAF since 1857; see Appendix E and the text. Also shown is the along fault surface slip from the 2004 Parkfield earthquake (dashed blue curve; Lienkaemper et al., this issue) and estimated slip for the 1934 Parkfield earthquake (using the empirical relationships of Wells and Coppersmith, 1994 as described in the text) C) Varying slip deficit estimations (expected slip – (cumulative aseismic slip + cumulative coseismic slip)). Slip deficit curve color corresponds to different estimations of coseismic slip in figure 2.3b. D) Distance northwest of Highway 46 along the SAF and important geographic features.



Toppozada et al., 2002 suggest that there have been several more earthquakes along the Parkfield segment and they document a number of nearby moderate magnitude Creeping segment events. In the second estimation (CS2; yellow curve: figure 2.3b) we consider these extra events (using the inferred locations and magnitudes from Toppozada, et al, 2002) in addition to the 6 similar Parkfield events as calculated above. To estimate the coseismic slip from these additional events, we used empirical relationships between magnitude, rupture length, and average displacement (Wells and Coppersmith 1994; modified for strike slip earthquakes in California by Arrowsmith et al., 1997). For these calculations, we assumed constant slip distributed along symmetric ruptures extending from the estimated epicenters and we assumed a rupture depth of 10 km. The addition of slip from these events is shown in figure 2.3b (yellow curve) and Appendix E.

Despite the similarities between the 1966 and 2004 earthquakes (e.g., Lienkaemper et al., in review; Langbein et al., 2005), historical analysis of previous Parkfield events (Toppozada et al., 2002) has suggested that these events have varied in magnitude and may have varied in location. In the third estimation of cumulative coseismic slip (CS3; black curve: figure 2.3b) we take into account the estimated differences in the magnitudes and locations of the Parkfield events considered by Toppozada et al., 2002. In this case, we used the empirical relationships mentioned above to estimate the coseismic slip from each of the events prior to 1966 (Appendix E). To compare the estimated rupture size of events calculated using the empirical methods, we show the rectangular coseismic slip distribution estimated for the 1934 event (red curve: figure 2.3b). The CS3 calculation results in a more distributed cumulative coseismic slip

curve because Parkfield epicenters reported in Topozada et al., 2002 are distributed along the segment and because the empirical rupture patch calculations result in shorter ruptures than historically observed (e.g., 1934 vs. 2004: figure 2.3b).

The Slip Deficit

Assuming a long-term slip rate of 33 mm/yr, we expect that nearly 5m of slip should have been released along the SAF since 1857. By summing the cumulative coseismic and aseismic slip we observe that varying amounts ($< 5\text{m}$) of slip has been released along the SAF since 1857; the slip budget is not balanced (figure 2.3c). Because no slip has been released along the Cholame segment since 1857, the slip deficit there is equal to the accumulated slip, nearly 5m. Slight differences in the slip deficit are suggested from comparison of the CS1-CS3 calculations (figure 2.3c). Assuming CS1 (figure 2.3c: thick blue curve), the slip deficit decreases at the SE end of the 1966 coseismic slip (just SE of Highway 46). The addition of increased aseismic slip rates and increased coseismic slip northwest of Highway 46 results in a rapid drop in the slip deficit across the southeast portion of the Parkfield segment. 10 km northwest of Highway 46, the slip deficit has decreased to 3m. Near the town of Parkfield (about 22 km northwest of Highway 46) the slip deficit is 1-2 m and it drops below 1 m 30 km northwest of Highway 46. It remains less than 1 m into the Creeping segment (Appendix F). The addition of the smaller events identified by Topozada et al., 2002 (CS2; figure 2.3c: yellow curve) lowers the slip deficit slightly in three regions along the Parkfield segment. Because the CS3 calculation (Appendix E) results in more distributed coseismic slip release (figure 2.3b, black curve), it also results in a slip deficit that is slightly higher

along the southeast and central portions of the Parkfield segment (where slip in 1966 and 2004 was the greatest). CS3 also implies that there is no slip deficit on the southeastern Creeping segment (figure 2.3c: black curve and Appendix E). In general, these calculations suggest the following: 1) The slip deficit decreases abruptly across the SE portion of the Parkfield segment, from a high of nearly 5m on the Cholame segment down to 1-2 meters near the town of Parkfield. 2) Northwest of the town of Parkfield, the slip deficit is generally less than 1 meter and may be 0 along the Creeping segment of the SAF (figure 2.3c).

Slip Deficit Development

Assuming the aseismic slip rates, presented above, and coseismic slip release as described in CS2 (Appendix E), we show the slip deficit's development in 10 year time steps since 1857 (figure 2.4). This figure shows that the slip deficit to the southeast of the town of Parkfield has grown through time despite Parkfield events and some aseismic creep. Continued accommodation of slip like that observed historically (creep and moderate earthquakes) will result in continued growth of this slip deficit. Along the northwest portion of the Parkfield segment, an increased aseismic slip rate and the six Parkfield events have slowed the growth of the slip deficit through time. Additionally, northwest of Slack Canyon, a creep rate of 27 mm/yr has kept the slip deficit below 1m.

Slip Deficit and 1857 Offsets

The slip deficit on the Cholame segment is nearly 5 m because of an absence of slip since 1857. This is approximately the mean of the range of offsets attributed to the

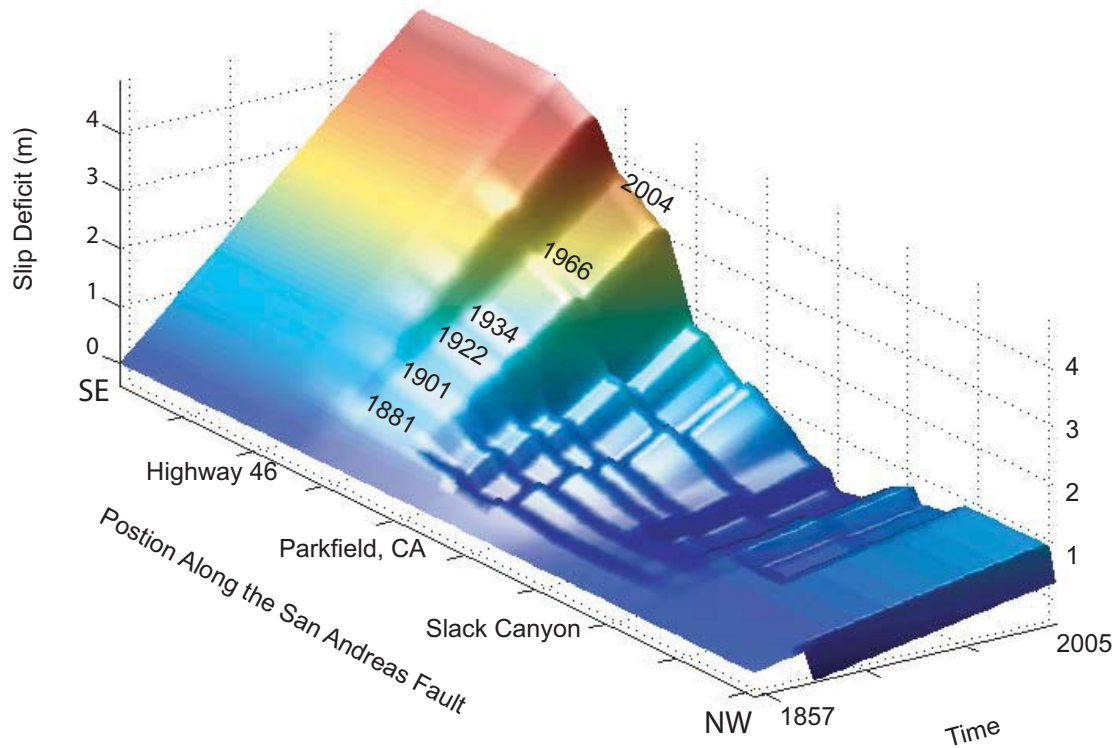
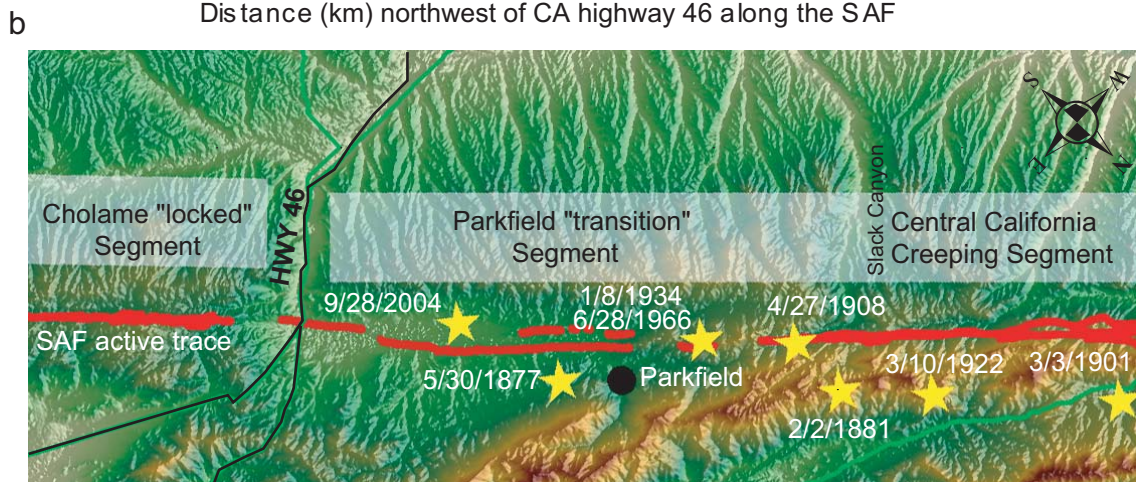
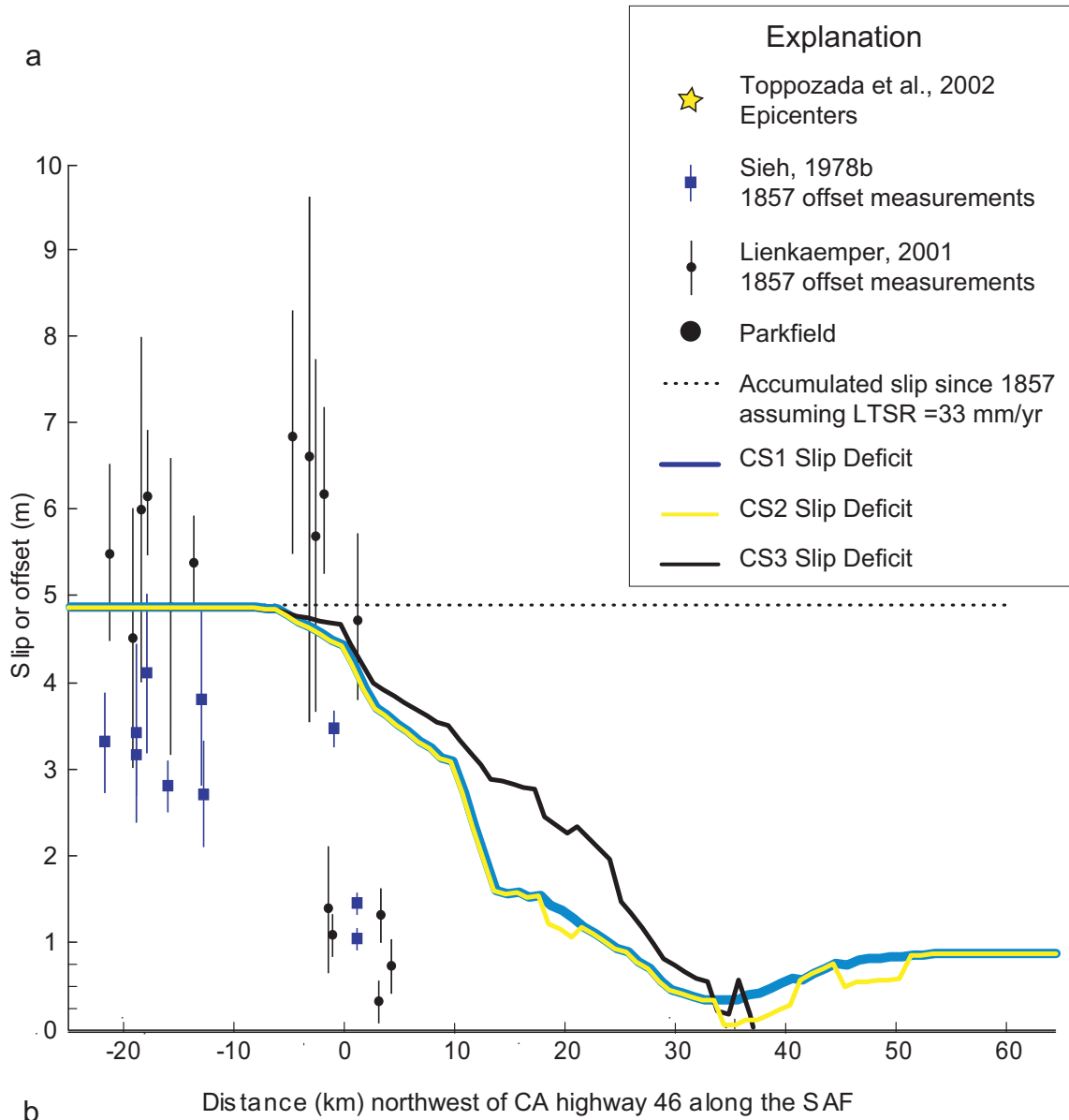


Figure 2.4. Slip deficit growth along the SAF through time since 1857. This was calculated using the CS2 coseismic slip estimation. The times of the six Parkfield earthquakes are noted. These events take a relatively instantaneous bite out of the slip deficit, but the slip deficit continues to grow (especially on the southeast portion of the Parkfield segment). Color represents slip deficit: blue is less than 2m, yellow is 2-3 m, and red is 3-5 m.

Figure 2.5. A) Slip deficit estimations along the SAF (text; figure 3; supplemental tables) and measurements of offset (with error bars) attributed to slip released in the 1857 Fort Tejón earthquake (Sieh, 1978b; Lienkaemper, 2001). B) Epicenters of historical Parkfield earthquakes, locations as reported by Topozada et al., 2002. Distance northwest of Highway 46 along the SAF and topography along the SAF trace.



1857 earthquake as measured by Lienkaemper, 2001 and Sieh, 1978b (figure 2.5). The slip deficit is larger by a meter to several meters than the few small 1857 offsets measured in the southeast portion of the Parkfield segment (figure 2.5). Thus, the slip deficit in southeast Parkfield and Cholame may be as great as or may have surpassed the slip released along these segments in 1857.

Discussion

The slip deficit along the SAF abruptly decreases across the southeast portion of the Parkfield segment. Moreover, northwest of the town of Parkfield the slip deficit appears to be less than 1 meter. While historical changes in fault behavior define the boundaries of the transitional Parkfield segment, the central portion of the Parkfield segment may represent the northwestern terminus for large Central SAF ruptures as implied by the high gradient in slip deficit there (figures 2.3c and 2.5). Parkfield foreshocks probably played a role in the nucleation and rupture of the great Fort Tejón earthquake of 1857 (figure 2.2; e.g., Sieh, 1978a; Meltzner and Wald, 1999). However, the northwest extent of the 1857 rupture is uncertain. Sieh, 1978b refers to Wood, 1955, to suggest that the 1857 rupture may have extended as much as 80 km northwest of the town of Cholame. Additionally, paleoseismic excavations 21 km northwest of Cholame (at Parkfield) did not expose clear evidence of large magnitude surface ruptures (Chapter 1). These previous observations and the low slip deficit result northwest of Parkfield, CA suggest that large SAF ruptures from the southeast may not extend deeply northwest into the Parkfield segment.

Numerous studies have suggested that the Parkfield and Cholame segments could rupture together in a $\sim M7$ event (e.g., Sieh and Jahns, 1984; Harris and Archuleta, 1988; Arrowsmith et al., 1997; Murray and Langbein, in review; Lienkaemper, in review). Figure 2.5 shows the three slip deficit estimations presented here and measurements of offset landforms that slipped in the 1857 event (Sieh, 1978b; and Lienkaemper, 2001). Sieh, 1978b suggests that about 3.5 m of slip was released along the northwestern Cholame segment in 1857. This result is corroborated by Young et al., 2002 who attribute 3.0 \pm 0.70 m of offset (exposed in a paleoseismic trench) to the 1857 event (about 60 km SE of Hwy 46). If 3.5m of slip were released in 1857, then the slip deficit has exceeded 1857 slip by 1.5 m in the northwestern Cholame segment. If the Lienkaemper, 2001 interpretation of 1857 slip (~ 6 m) is more accurate, then the slip deficit has not yet reached the 1857 slip. On the Parkfield segment, both Lienkaemper, 2001 and Sieh, 1978b agree that slip in 1857 was much less: between 0.5 and 1.5m. Moreover, they were only able to find such offsets a few km northwest of Highway 46. Clearly the slip deficit since 1857 exceeds 1.5m along this portion of the Parkfield segment (figure 2.5). These observations imply that this part of the SAF could be ready to slip again in a large ($\sim M7$) event (e.g., Sieh and Jahns, 1984; Arrowsmith, et al., 1997). Based upon full slip deficit recovery, we would expect that slip from a Parkfield-Cholame rupture would decrease rapidly from Highway 46 to the northwest along the Parkfield segment and that slip northwest of the town of Parkfield, CA might be indistinguishable from a typical Parkfield event. Such an event could rupture for nearly 100 km SE of Parkfield into the Carrizo segment (Arrowsmith, et al., 1997).

The slip deficit calculated here is highly dependant upon the assumptions that the 1857 event is a suitable starting point and that the long-term SAF slip rate of 33 mm/yr is appropriate for this portion of the SAF. Sims, 1987 inferred that the late Holocene slip rate may be significantly less ($26.3 \pm 3.9/-3.3$ mm/yr). If this is correct, slip may be accommodated along structures adjacent to the main SAF trace at Parkfield (e.g., the Southwest Fracture Zone). Moreover, it also suggests the slip deficit along the Parkfield segment could be 0.5-1.5 m less than what is reported here. Nevertheless, slip released in the 1857 earthquake has been exceeded along the Cholame and southeastern Parkfield segments. If the SAF is to recover this slip deficit, we anticipate a change in fault behavior from what has been observed historically along this portion of the fault. Possible changes include periods of rapid aseismic slip, more quickly recurring moderate Parkfield events, large (M7) Central SAF ruptures, or some combination thereof.

Conclusions

Since 1857, a slip deficit has grown along the Cholame and Parkfield segments of the south-central San Andreas Fault. Apparently, the slip deficit has exceeded slip released in the 1857 Fort Tejón earthquake along the Cholame segment and on the southeast portion of the Parkfield segment. In order to recover this deficit we should anticipate a change in fault behavior along the Cholame and southeast Parkfield segment.

Acknowledgements

We thank Jim Lienkaemper and Tousson Topozada for their correspondence. We especially thank Jessica Murray for correspondence and access to the results of her

2001 model of spatially-variable slip along the Parkfield segment of the SAF. The US National Science Foundation (EAR-0310357) supported this investigation.

References

- Agnew, D.C. and K.E. Sieh (1978). A Documentary Study of the Felt Effects of the Great California Earthquake of 1857, *Bulletin of the Seismological Society of America* **68**, 1717-1729.
- Allen, C. R. (1968). The tectonic environments of seismically active and inactive areas along the San Andreas Fault system, *Proceedings of conference on geologic problems of San Andreas Fault system*, (edited by W. R. Dickinson and A. Grantz), *Stanford University Publications in the Geological Sciences* **11**, 70-82.
- Arrowsmith, JR., K. McNally, and J. Davis (1997). Potential for Earthquake Rupture and M7 Earthquakes along the Parkfield, Cholame, and Carrizo Segments of the San Andreas Fault, *Seismological Research Letters* **68**, no. 6, 902-916.
- Bakun, W.H. and A.G. Lindh (1985). The Parkfield California, Earthquake Prediction Experiment, *Science* **229**, 619-624.
- Bakun, W.H. and T.V. McEvilly (1984). Recurrence Models and Parkfield, California Earthquakes, *Journal of Geophysical Research* **89**, 3051-3058.
- Burford, R.O. and Harsh, P.W. (1980). Slip on the San Andreas fault in central California from alignment array surveys, *Bulletin of the Seismological Society of America* **70**, p. 1233-1261.
- Crosby C.J. (2004). Digital database of faulting accompanying the 1966 Parkfield, California earthquake, *US Geological Survey Open File Report* **2004-1437**.

- Harris, R.A. and R.J. Archuleta (1988). Slip Budget and potential for a M7 earthquake in Central California, *Geophysical Research Letters* **15**, 1215-1218.
- King, N.E., P. Segall, and W. Prescott (1987). Geodetic Measurements near Parkfield, California, 1959-1984, *Journal of Geophysical Research* **92**, 2747-766.
- Jennings, C. W., (1977). Geologic map of California, *California Division of Mines and Geology*, Geologic Data Map No. 2, scale 1:750,000
- Langbein, J., R. Borchardt, D. Dreger, J. Fletcher, J.L. Hardebeck, M. Hellweg, C. Ji, M. Johnson, J.R. Murray, R. Nadeau, M.J. Rymer, and J.A. Treiman (2005). Preliminary report on the 28 September 2004, M 6.0 Parkfield, California Earthquake, *Seismological Research Letters* **76**, no. 1, 10-26.
- Lienkaemper, J.J. (2001). 1857 Slip on the San Andreas Fault Southeast of Cholame, California, *Bulletin of the Seismological Society of America* **91**, no. 6, 1659-1672.
- Lienkaemper, J.J., Baker, B., and McFarland, F.S (in review). Surface Slip Associated with the 2004 Parkfield (CA) Earthquake Measured on Alinement Arrays.
- Lienkaemper, J.J. and W.H. Prescott (1989). Historic Surface Slip along the San Andreas Fault near Parkfield, California, *Journal of Geophysical Research* **94**, 17647-17670.
- Meltzner, A.J. and D.J. Wald (1999). Foreshocks and Aftershocks of the Great 1857 California Earthquake, *Bulletin of the Seismological Society of America* **89**, 1109-1120.

- Murray, J., P. Segall, P. Cervelli, W. Prescott, J. Svarc (2001). Inversion of GPS Data for Spatially Variable Slip-rate on the San Andreas Fault near Parkfield, CA, *Geophysical Research Letters* **28**, 359-362.
- Murray, J. and J. Langbein (in review). Slip on the San Andreas Fault at Parkfield over two earthquake cycles and the implications for seismic hazard.
- Noriega G.R., J.R. Arrowsmith, L.B. Grant, and J.J. Young (BSSA, in press). Stream Channel Offset and Late Holocene Slip Rate of the San Andreas Fault at the Van Matre Ranch Site, Carrizo Plain, California.
- Segall, P. and Y. Du (1993). How Similar were the 1934 and 1966 Parkfield Earthquakes?, *Journal of Geophysical Research* **98**, 4527-4538.
- Segall, P. and R. Harris (1987). Earthquake Deformation Cycle on the San Andreas Fault near Parkfield, California, *Journal of Geophysical Research* **92**, 10,511-10,525.
- Segall, P. and R. Harris (1986). Slip Deficit on the San Andreas Fault at Parkfield, California, as Revealed by Inversion of Geodetic Data, *Science* **233**, no. 4771.
- Sieh, K.E., (1978a). Central California Foreshocks of the Great 1857 Earthquake, *Bulletin of the Seismological Society of America* **68**, 1731-1749.
- Sieh, K.E. (1978b). Slip along the San Andreas Fault associated with the great 1857 earthquake, *Bulletin of the Seismological Society of America* **68**, 1421-1448.
- Sieh, K.E. and R.H. Jahns (1984). Holocene activity of the San Andreas fault at Wallace Creek, California, *Geological Society of America Bulletin* **95**, p. 883-896.
- Sims, J.D., (1987). Late Holocene slip rate along the San Andreas Fault near Cholame, California, *Geological Society of America Abstracts with Programs*, 451.

- Titus, S.J., C. DeMets, B. Tikoff (2005). New slip rate estimates for the creeping segment of the San Andreas Fault, California, *Geology* **33**, no. 3, 205-208.
- Toké et al. (in review). Paleoseismic implications for fault behavior along the Parkfield segment of the San Andreas Fault (SAF)
- Topozada, T.R., D.M. Branum, M.S. Reichle, and C.L. Hallstrom (2002). San Andreas Fault Zone, California: M>5.5 Earthquake History, *Bulletin of the Seismological Society of America* **92**, 2555-2601.
- Wells, D.L. and K.J. Coppersmith (1994). New Empirical Relationships among Magnitude, Rupture Length, Rupture Width, Rupture Area, and Surface Displacement, *Bulletin of the Seismological Society of America* **84**, no. 4, 974-1002.
- Wood, H.O. (1955). The 1857 Earthquake in California, *Bulletin of the Seismological Society of America* **45**, 47-67.
- Young, J. J., JR. Arrowsmith, L. Colini, and L.B. Grant (2002). 3-D excavation and measurement of recent rupture history along the Cholame segment of the San Andreas Fault, *Bulletin of the Seismological Society of America: Special Issue on Paleoseismology of the San Andreas fault* **92**, 2670-2688.
- Zielke, O. and JR. Arrowsmith (in progress). Digital database of active breaks in the SAF along the 1857 rupture

CONCLUSIONS AND RECOMMENDATIONS

The primary paleoseismic conclusion from Chapter 1 was that trench-observed tectonic deformation was most consistent with deformation from a combination of aseismic fault creep and M6 ruptures (such as the 2004 Parkfield event). This is significant because the exposed sedimentary record spans more than 2000 years, suggesting that the historically observed fault behavior may be a long-term phenomenon. The primary conclusion from the post-1857 slip budget analysis, Chapter 2, was that a major change in the pattern of strain release occurs along the central Parkfield segment (>18 km northwest of Highway 46; figure 2.1 and figure 2.5). If this strain release pattern persists through time, then the conclusions of Chapter 1 and 2 are consistent and may suggest that only creep and moderate Parkfield earthquake have occur along the central Parkfield segment and along the SAF to the northwest. However, the slip budget (figure 2.5) also suggests that at this paleoseismic site (located 21 km northwest of Highway 46) a slip deficit of 1-2 m exists. This suggests that slip must be released at a more rapid rate than historically observed to balance the slip budget. Moreover, in this paleoseismic study we were unable to rule out the possibility of large prehistoric rupture along this portion of the fault and it is plausible that the entire slip deficit could be released in a single event.

Much uncertainty remains about the characteristics of large-magnitude earthquakes along the central San Andreas Fault. Understanding the characteristics of such ruptures (rupture extent and offset) is important because it may allow us to better assess where the greatest ground motions would occur in future events. Lingering

uncertainties about the rupture behavior of the Parkfield segment should be addressed with further paleoseismic study along the entire length of this segment. Because the slip budget suggests a gradational change in strain release across the segment, it would be valuable to test whether a corresponding variation in rupture size can be identified paleoseismically by looking for a gradational change in event offsets across the segment. This task presents three large challenges: 1) identification of sites suitable for preserving single-event offsets, 2) the ability to differentiate between offsets attributed to persistent aseismic creep and ruptures, and 3) the delocalization of SAF deformation along the Parkfield segment (e.g., the southwest fracture zone; figure 1.4). At a minimum, continued paleoseismic study of the segment should constrain the northwestern extent of large ruptures along the central San Andreas Fault.

APPENIDIX A
TECTONIC GEOMORPHOLOGY

Preface of Appendix A

To confirm the position of the most-recently tectonically-active trace of the San Andreas Fault (SAF) and select a site for paleoseismic study I documented tectonic landforms (on the scale of 10's of meters) from Carr Hill to Middle Mountain (~10 km of mapping) in the central portion of the Parkfield segment. My research did not focus on analyzing the shallow SAF structure or the development of Middle Mountain; however such analysis is addressed in a structural geology thesis by Maurits Thayer (in preparation). Here I present the following:

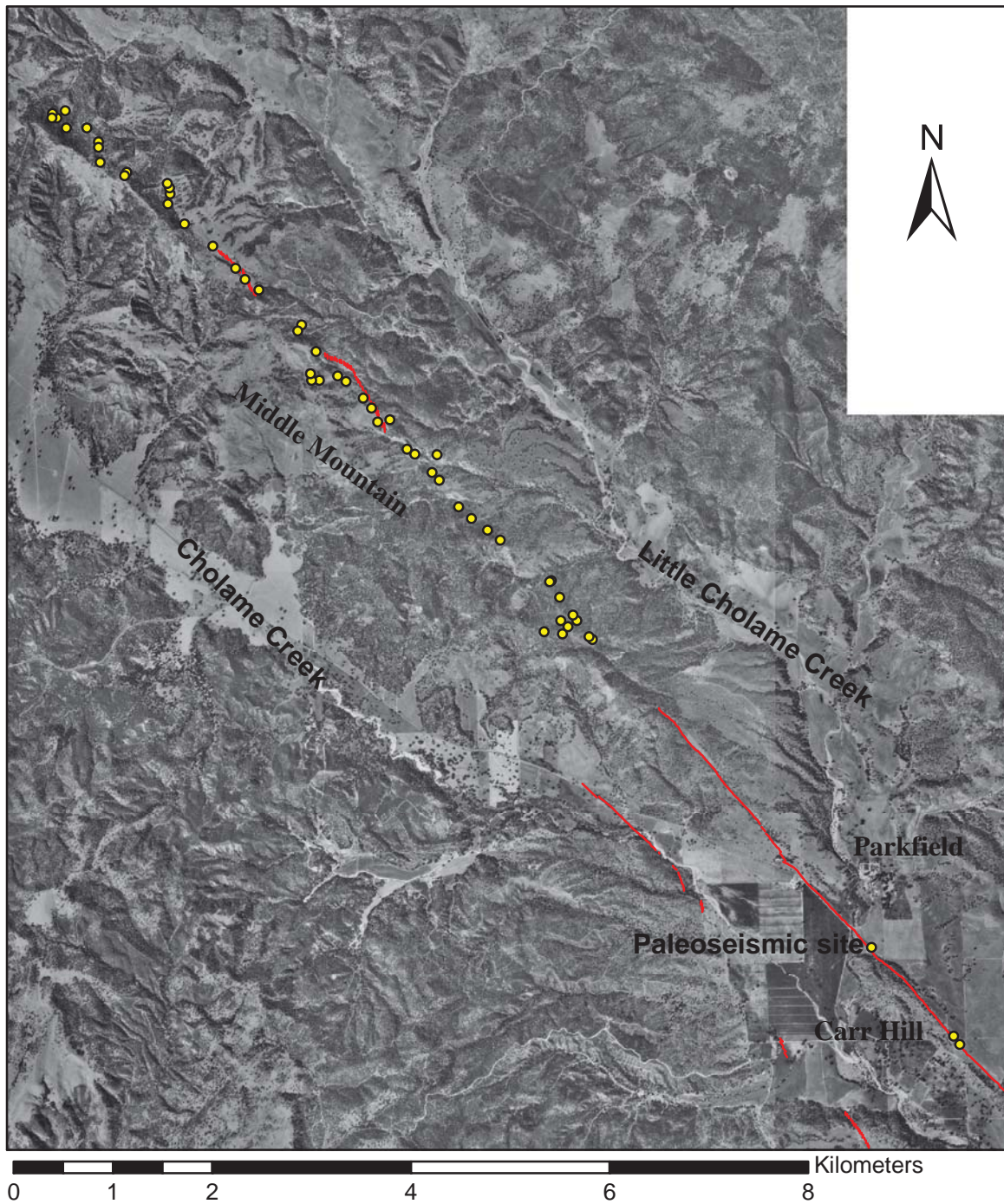
- A1) Description of general tectonic geomorphology
- A2) A map of the locations of documented tectonic landforms
- A3) A table of the documented tectonic landforms

Recently, the Southern California SAF LIDAR scan collected high resolution digital elevation data (< 1m) from Parkfield to the southeast along the San Andreas fault. This data will provide superior data for analyses of the tectonic geomorphology, shallow SAF structure, suitable paleoseismic sites, and comparison to past and future ruptures (e.g., the 2004 Parkfield event) at Parkfield and all along the southern San Andreas fault.

Appendix A1.

From Carr Hill to Middle Mountain the main trace of the SAF is delineated by tectonically produced landforms (Appendices A2 and A3) including sags, linear ridges, linear troughs, right-laterally offset stream channels, shutter ridges, hillside benches, and land slides along Middle Mountain. I mapped tectonic landforms along this central stretch of the Parkfield segment of the SAF in search of sites for paleoseismic investigation. Along this portion of the fault, the area near Carr Hill contains a series of well-developed tectonic landforms including a tectonically formed sag pond within a fluvial terrace of the Little Cholame Creek (figure 1.4). I chose to conduct the paleoseismic investigation (Chapter 1) at this site because of the location's superior combination of recent deposition, localized deformation, tectonic scarps, and accessibility for excavation. Several interesting paleoseismic sites were considered along Middle Mountain, but these sites had limited accessibility and may not have contained the same quantity/quality of recently preserved stratigraphy.

A clear relationship was seen between the mapped landforms and the 2004 Parkfield rupture (e.g., figure 1.12). Unfortunately, the 2004 rupture mapping was not published at the time of this manuscript and thus they are not compared here. This will likely be done with lidar-produced geomorphic mapping and the anticipated publication of the 2004 earthquake rupture map. Appendix A3 is a table of the mapped tectonic land from locations. To obtain data (e.g., photos) referenced in this table, but not presented herein please contact the author.



Appendix A2. Locations of recently-active tectonic landforms from Carr Hill to the northwest along Middle Mountain in the central Portion of the Parkfield segment. Yellow circles are locations of tectonic landforms. Together, they indicate the location of the most-active trace of the SAF. Appendix A3 provides the corresponding attribute table to this map (A3 ID numbers increase from east to west). See A1 for a description of the geomorphology of this section of the fault. 1966 rupture: red line (Crosby, 2004) Scale is 1:65000, background is DOQQ aerial photography. UTM zone 11, NAD 83

<u>ID</u>	<u>Easting</u>	<u>Northing</u>	<u>Elev</u>	<u>Waypoint</u>	<u>Photo</u>	<u>Trend</u>	<u>Length</u>	<u>Width</u>	<u>Relief</u>	<u>Trate</u>	<u>Descript</u>
1	732604	3974189	481	ST1	Y	317	x	x	x	1	small trough and small sag just SE of Carr Hill and a small rd leading the the Hearst-Cook property
2	732541	3974276	472	ST2	Y	310	x	x	x	1	deep linear trough along E side of Carr Hill
3	731716	3975164	457	SURVEY1	x		x	x	x	1	totalstation setup point for surveying of the sag pond and pressure ridge trench sites
4	728909	3978261	628	F1	16	350	40	10	-1m	3	southeasternmost USGS equipment accompanies a notch in the hill ridge
5	728874	3978290	644	LT29	116	315	25	10	-2m	4	notch in ridge crosses between USGS creep meters
6	728751	3978450	623	LT28	114,115	315	60	5	0-1m	4	long narrow bench along very hummocky hillslope
7	728715	3978508	616	LT27	113	335	20	8	-1m	4	bench containing a trough and small sag depression
8	728662	3978391	684	WINDG1	n	x	x	x	x	4	wind gap along middle mtn ridge top, perhaps a paleochannel uplifted by SAF deformation
9	728609	3978321	647	SAG014	118	345	10	4	1-2m	5	elongate sag above elevation of suspected geomorphic lineaments
10	728590	3978454	665	HOLE	19	x	x	x	10's of m	5	very deep ravine closed depression high on middle ridge, a small sag pond, lots of bones
11	728581	3978689	595	LT26	Y	325			0-3m	2	fan dammed by a shutter ridge
12	728498	3978855	561	LT25	112	305	40	7	-1m	4	linear trough along hummocky slope, may be an old scarp?
13	728478	3978840	559	SAG013	111	300	6	4	2-3m	5	small rounded sag depression on hummocky hillslope QIs?
14	728426	3978342	686	SAG015	119	0	12	10	-2m	5	large rounded sag in hummocky terrain, appears man made
15	727985	3979263	614	LT24	110	320	50	20	-1m	5	wide banch situated in hummocky terrain, containing a sag depression
16	727853	3979360	616	SCARP+B	x	x	x	x	x	x	a scarp and a bench
17	727692	3979481	619	LT23	109	340	50	30	1-2m	5	wide bench situated in hummocky terrain, containing a sag depression
18	727565	3979597	609	BENCH4	x						a bench

19	727369	3979866	624	LT22	108	325	60	10	1-2m	3	linear trough containing two small sag depressions.
20	727345	3980118	615	SAG7	x						a sag
21	727297	3979940	650	LT21	107	325	25	5	0-1m	4	bench on hummocky slope with a small trough running through it.
22	727125	3980128	638	LT20	106	310	30	10	1-4m	4	a notch separating two units, a clay rich well cemented unit to the east and a softer sandier unit the west
23	727046	3980175	661	LT19	105	320	30	15	1-2m	4	bench tilted into the hillslope creating a trough, Qls head scarp?
24	726871	3980474	631	LT18	104	320	40	7	x	4	trough and bench, very subtle features.
25	726752	3980452	638	LT17	Y					1	Grabben
26	726692	3980588	649	LT16	103					1	USGS equipment
27	726606	3980688	652	LT15	28					1	Offset Channel
28	726431	3980858	658	LT14	102	315	70	10	1-4m	3	trough and a likely shutter ridge followed by a bench.
29	726348	3980910	662	LT13	101	305	50	40	hummocky	5	hummocky bench
30	726163	3980867	699	SAG012	100	25	15	5	~1m	5	elongate sag depression in hummocky terrain Qls?
31	726131	3981156	691	BENCH7	97	340	35	25	-flat	4	wide bench just off ridge top along hummocky slope, leading to a trough. Granite outcrop nearby.
32	726089	3980867	696	SAG011	99	x	10	10	1-2m	5	rounded sag depression in hummocky terrain Qls? Man Made?
33	726077	3980933	685	SAG010	98	x	8	8	~1m	5	rounded sag depression in hummocky terrain Qls?
34	725987	3981426	720	BENCH6	x						a bench
35	725950	3981366	698	LT11	96	325	60	5	-flat	5	long narrow bench on hummocky hillslope.
36	725556	3981779	732	LT10	94	315	12	5	1-2m	5	trough along the base of a steep slope in very hummocky terrain. (trough is not well defined)
37	725415	3981883	747	LT09	93	325	30	10	~4m	2	a deep linear trough in hummocky terrain
38	725325	3981993	753	LT08	92	325	60	10	-flat	2	long and wide bench bounded by a trough and ridge on the NW side
39	725092	3982220	792	LT07	91	325			x	2	series of tectonic landforms
40	724812	3982441	780	SAG08	90	270	10	5	1-2m	5	sag in hummocky terrain
41	724665	3982742	774	SAG07	88	270	20	7	1-3m	5	sag in hummocky terrain
42	724657	3982804	773	SAG06	87	x	15	15	1-4m	5	round sag in hummocky terrain

43	724640	3982642	787	LT06	89	315	100	25	hummocky	5	hummocky long/wide bench uphill of three sag depressions
44	724636	3982848	794	SAG05	87	x	15	15	1-4m	5	round sag in hummocky terrain
45	724229	3982958	796	LT05	86	310	60	5	~flat	4	long narrow bench along hillslope just below LT04 contains a 1m trough that is semi-crescent-shaped
46	724209	3982927	809	LT04	85	315	60	5	~flat	4	long narrow bench along hillslope
47	723962	3983061	832	SAG04	84	325	10	7	~3m	4	deep sag on Kester property
48	723944	3983266	796	SAG02	82	345	10	5	~1m	5	subtle sag along road in hummocky terrain
49	723944	3983213	807	SAG03	83	305	15	5	1-2m	5	crescent shaped sag in hummocky terrain
50	723826	3983404	785	SAG01	81	x	12	12	x	5	rounded sag depression in hummock terrain QIs?
51	723621	3983408	798	LB1	?	322	60	5	~3m	2	long linear trough
52	723608	3983580	761	NOTCH1	x	x	x	x	x	x	notch in ridge
53	723528	3983507	792	LT03	80	320	100	15	undulating	3	a hummocky bench followed by a ridge and trough along the hillslope to the SE
54	723484	3983551	795	LT01	78	320	80	10	~1m	4	subtle trough in a narrow bench leads to another crescent-shaped bench; heavily vegetated with shrubs
55	723475	3983509	798	LT02	79	320	80	12	~flat	4	long subtle bench without a pronounced trough; old oaks, but no shrubs

*Appendix A3. Datum is NAD 83, UTM Zone 11

*Trate = tectonic rating 1-5, 1 being most confident in formation via tectonic deformation

APPENDIX B

PALEOSEISMIC STRATIGRAPHY

Stratigraphic unit descriptions for Miller Sag Trench (MST)
Refer to text, trench logs and photo mosaics.

Unit Description

PR

Mottled clay and silt with some sand, sparse carbonate nodules, and occasional pebbles. This unit is defined as a mixed zone resulting from root bioturbation and agricultural tilling. The unit extends across the upper 10-20 cm of both walls of the trench exposure. Color: 2.5Y 4/2 (gray/brown).

MSEUD

Mottled mix of clay, silt, sand and some pebbles. The uppermost unit beneath the present day sag expression. The unit is undifferentiated because of heavy mixing due to bioturbation of both burrows and to a greater extent roots within the sag pond. Color varies.

MSE1

Very fine sand and silt with pedogenic clay development. MSE1 is only exposed to the northeast of fault zone 1 and is the lowest unit exposed in that portion of the trench. It is tabular with a slight down warping towards fault zone 1. The unit is consistent in composition across the exposure. It is capped by a thin, 2-8 cm, clay layer containing sparse charcoal. Color: 5Y 4/2 (brownish grey).

MSE2

MSE2 is fine silt that is dissected by multiple sand and gravel paleochannels of the Little Cholame Creek and/or the offset stream channel. MSE 2 is found to the northeast of fault zone 1 and is warped downward by fault zone 1. Channel deposits vary in size from sand to cobbles. Cobbles were sub-rounded to rounded and included mafic clasts of Franciscan origin and sandstones including quartz arenites and greywackes with 1-2mm weathering rinds. Large pebbles included arkosic sandstones, Franciscan, gabbros, and marble. Smaller pebbles consisted of granite, chert, and quartz. Color: 5Y 4/2 (brownish grey).

MSE3

Thick clayey sand and silt containing small carbonate nodules. MSE3 has a lower mixing interface with MSE2 containing some small pebbles from MSE2. The unit is thinned and folded down into fault zone 1 and is not continuous across the fault zone. Near fault zone 1 the unit can be divided into subunits based upon an obvious variation in color and clay content. Color: 7.5YR 7/1 (light grey).

MSE4

Organic rich clayey silt, some small carbonate nodules, locally bioturbated by burrows. MSE 4 is folded downward, thinned and discontinued across fault zone 1. Color: 7.5YR 5/1 (dark brown/grey).

MSE5

Silty fine sand, which is apparently down warped and dropped by fault zone 1. MSE5 is siltier to the northeast of fault zone 1. Color: 5Y 7/2.

MSE6

Brown gray clay, 10YR 4/1, to the southwest of fault zone 1.

MSE7

Organic rich unit of mottled clay and silt with widespread carbonate nodules. Down dropped and thickens over fault zone one indicating deposition was coincident with deformation along fault zone 1. MSE 6 and MSE7 could be lumped into one thickening unit across fault zone 1, but has been separated here based upon clay content (MSE 6 is more clay rich). Alternatively, with much more logging time, the units could be broken into many smaller subunits representing on lapping sag pond deposition as the sag subsided tectonically. Color: 10YR 4/1 (mottled brown and grey).

MSE8

Clayey silt deposited over fault zone 1 and thickens towards fault zone 2 where it is truncated. Top of unit is clay with discontinuous charcoal, probably an in situ burn. Color: 7.5YR 6/1 (light grey/brown).

MSE9

Thin sandy silt, thickens from fault zone 1 to fault zone 2 where it is truncated. Some root bioturbation within sag. Color: 5YR 6/2 (tan/gray).

MSE10

Dark, organic rich, silty clay, which, thickens from fault zone 1 to fault zone 2 where it is truncated. Charcoal is abundant. Color: 10YR 6/1 (gray/green).

MSE11

Thin layer of tan silty sand, overlain by undifferentiated MSEUD so this could be an influx of sand related to local deposition within the sag or it could be Little Cholame Creek over bank deposit. Truncated by fault zone 2. Color: 7.5 YR 6/2 (tan).

MSE12

Lowest unit exposed between fault zone 2 and 4, and only on the northwest wall. Silty clay tilted down towards fault zone 3/sag pond. Color: 10YR 4/1 (brown/gray/green).

MSE13

Silty clay tilted down towards fault zone 3. Color: 5YR 5/2 (pale brown).

MSE14

Clayey sand and silt. Tilted down towards fault zone 3. Color: 10YR 4/2 (brown).

MSE15

Organic rich clay. Deformed by splay of fault zone 2 on southeast wall and tilted down towards fault zone 3. Color: 10YR 5/2 (dark brown).

MSE16

Clayey silty sand that becomes more clayey as it is tilted down towards fault zone 3. Is also deformed by splay of fault zone 2 on southeast wall. Color: 2.5Y 4/2 (light brown).

MSE17

Clayey sandy silt that is tilted and down faulted by fault zone 3. Color: 5Y 2.5/2 (brownish grey).

MSE18

Fine silty clayey sand. It is folded and down warped by fault zone 3. Color: 7.5YR 4/2 (brown).

MSE19

Mottled layer of dark clay with intermixed silt that becomes thinner and more homogeneous dark clay as it is faulted and down warped by fault zone 3. Color: 10R 4/2 (red/brown).

MSE20

Silty clayey very fine sand is deformed across fault zone 3, consistent with the units below. Truncated by fault zone 4. Color: 2.5Y 4/2 (yellowish brown).

MSE21

Clayey sandy silt, which becomes more clayey towards fault zone 3. Separated from MSE20 by a thin clay band containing sparse charcoal (a possible burn horizon). Faulted down by fault zone 3 in the same manner as units below. Truncated by fault zone 4. Color: 2.5Y 5/2 (orange/brown).

MSE22

Silty clay, which is darker and more organic right towards the bottom of the exposure. Some charcoal present, near bottom of current sag depression. Truncated by fault zone 4. Color: 5GY 4/1 (gray brown).

MSE23

Dark green clay, sag deposit. Truncated by fault zone 4. Color: 5GY 4/1 (green brown).

MSE24

Upper distinguishable unit of current sag pond. Some charcoal, mottled clay and silt, truncated by fault zone 4. Color varies.

MSWUD

Heavily burrowed and bioturbated, lumped as one unit because of its current state, but once consisted of silts, sands and gravels. This southwest side of the sag pond is much drier than the northeast side, allowing more burrow related bioturbation. Tan, gray, and brown.

MSW1

Dark silty sandy clay, lowest of the southwestern units. Tilted down towards fault zone 4. Color: 7.5YR 4/3 (dark brown).

MSW2

Fine silty sand that is bioturbated to the southwest, tilted down towards fault zone 4. Color: 10YR 4/3 (tan).

MSW3

Clayey sandy silt between laminated burn horizon (MSW4) and sand (MSW2), discontinuous because of bioturbation. Tilted down towards fault zone 4. Color: 5YR 4/4 (brown grey).

MSW4

Laminated silty clay with laminated charcoal. Tilted towards fault zone 4. Discontinuous because of bioturbation. Color: 10YR 6/4 (gray brown).

MSW5

Fine to coarse sand with some small pebbles, heavily bioturbated towards the southwest and cannot be traced across entire exposure. Tilted towards fault zone 4. Color: 5YR 3/4 (brown).

MSW6

Dark clayey silt that grades to brown as it is bioturbated towards the southwest. Tilted, sheared and faulted by fault zone 4. Color: 2.5YR 2.5/2 (dark grey).

MSW7

Brown sandy silt is apparently warped down into fault zone 4 and faulted several times. Color: 2.5Y 4/2 (brown).

Stratigraphic unit descriptions for Phoebe' s Trench (PT).

Unit	Description
PR	Mottled clay and silt with some sand, sparse carbonate nodules, and occasional pebbles. This unit is defined as a mixed zone resulting from root bioturbation and agricultural tilling. The unit extends across the upper 10-20 cm of both walls of the trench exposure. Color: 5Y 4/2 (gray/brown).
PTW1	Clayey silt with moderate root-bioturbation and some carbonate nodules. Color: 10YR 4/1 (gray/brown).
PTW1.5	Very thin matted unit of decayed organic material, topped by a thin horizon of sand, carbonate nodules, and sparse pebbles. Apparently vertically offset by the primary fault zone. Color: 10YR 4/1.
PTW2	Silty sand intermixed with dark organic-rich units of the west side of the primary fault zone. Color: 5YR 6/2 (light tan).
PTW3	Organic rich clayey silt mixed with sparse sand and carbonate nodules. Color: 5YR 2.5/2 (dark brown).
PTW4	Mottled clay with sands and silt (pedogenic clay). Color varies.
PTW5	Clay with carbonate nodules, color: 2.5Y 5/2 (green/brown/gray).
PTE0	Dark organic-rich mottled clay mixed with sparse sand pockets, carbonate nodules, clay shear zones, roots, pebbles, and small cobbles.

- PTE1
Thick bioturbated mixture of silt, sand, clay, and gravel. Fresh and old Kordivinas. Thins towards deformation zone. Color: 10YR 8/2 (pale tan to orange).
- PTE2
Sand silt that thins and pinches out towards the deformation zone. Color: 2.5Y 6/6 (orange, rust color).
- PTE3
Coarse gravel lenses of varying thickness and extent, paleochannels of Little Cholame Creek lumped as one unit. Clasts include Monterey, Franciscan, and quartz pebbles. Color: 7.5YR 7/3 (tan/gray).
- PTE4
Fine sand lenses, with some gravels. More paleochannels. Could be lumped with PTE3. Color: 2.5Y 4/4.
- PTE5
Laminated clay with thin charcoal horizon. Color: 5Y 4/2.
- PTE6
Fine sand and silt. Varies in thickness through the fault zone. Color: 5Y 4/4 (brown).
- PTE7
Laminated clay with thin charcoal horizon. Color: 5Y 4/2.
- PTE8
Clayey sand. Color: 2.5Y 4/2 (brown).
- PTE9
Laminated clay with thin charcoal horizon. Color: 5Y 4/2.
- PTE10
Very fine clayey sand. Color: 2.5Y 4/2 (brown).
- PTE11
Dark brown/gray unit composed of charcoal (thick). Excellent reference layer through fault zone splays as it is crisply faulted. Color: 10Y 2/1.
- PTE12
Fine sand with some clay. Color: 2.5Y 4/4.

PTE13

Dark brown/gray thick clay and charcoal. Color: 10YR 2/2

PTE14

Light brown and grey clay with carbonate nodules. Color: 5GY 4/1

PTE15

Sandy silty gray clay. Color: 5G 4/1

PTE16

Matrix supported well-sorted small pebble gravel layer, poorly exposed at base of trench.

APPENDIX C
RADIOCARBON SAMPLES

Radiocarbon Samples collected, but not analyzed from MST and PT; Refer to table 1.2 for analyzed radiocarbon samples.

Sample #	Wall	Unit	Description
04-MST -25	SE	MSE19	charcoal from laminated silt
04-MST -27	NW	MSE15	charcoal pieces collected from silt
04-MST -29	SE	MSE20	charcoal pieces collected from a sandy layer
04-MST -28	SE	MSE21	charcoal form laminated clay at base of MSE21.
04-MST -31	SE	MSE24	charcoal from upper active sag near deformation zone 4.
04-MST -10	SE	MSE4	bulk sample from dark organic-rich layer
04-MST -18	SE	MSE6	bulk sample with an abundance of charcoal
04-MST -8	SE	MSE4	large wood sample from organic rich unit. (root?)
04-MST -19	SE	MSE6	charcoal from organic-rich subunit of MSE6.
04-MST -23	SE	MSE7	charcoal from clayey silt
04-MST -35	SE	MSEUD	bulk sample with abundance of charcoal
04-MST -16	SE	MSW7	small charcoal pieces from sand in deformation zone 4
04-MST -34	SE	MSW6	bulk sample from organic-rich unit near deformation zone 4
04-MST -5	NW	MSW4	large charcoal sample from laminated in situ clayey silt burn layer
04-MST -3	SE	MSE9	charcoal from dark organic-rich unit
04-MST -2	NW	MSE3	wood (root/bioturbation?)
04-MST -6	SE	MSE3	charcoal from MSE3 mixing zone with MSE2
04-MST -7	SE	MSE2	detrital wood from top of MSE 2 gravel lens
04-MST -11	NW	MSE4	bulk sample
04-MST -14	SE	MSE6	bulk sample
04-MST -15	NW	MSE7	bulk sample
04-MST -12	SE	MSE9	bulk sample
04-MST -13	NW	MSE9	bulk sample
04-MST -20	SE	MSE2	charcoal from sand lens
04-MST -21	SE	MSE9	charcoal from dark clay
04-MST -4	SE	MSE5	large piece of wood
04-PT-2	NW	PTE 5B	Charcoal from an in situ clayey silt burn layer
04-PT-4	NW	PTE 4B	Charcoal from an in situ clayey silt burn layer
04-PT-6	NW	PTE 7	Bulk sample from thick charcoal rich clayey silt layer
04-PT-5	NW	PTE 4B	Charcoal from an in situ clayey silt burn layer
04-PT-1	NW	PTE 3 (base)	Charcoal from an in situ clayey silt burn layer
04-PT-10	NW	PTW 0	Bulk sample from dark undifferentiable organic-rich deformation layer
04-PT-11	NW	PTW 0	Bulk sample from dark undifferentiable organic-rich deformation layer
04-PT-12	NW	PTE 0	Bulk sample from dark undifferentiable organic-rich deformation layer
04-PT-9	NW	PTW 3	Bulk sample from dark organic-rich layer SW of the deformation zone.

APPENDIX D

ASEISMIC SLIP RATE CALCULATIONS

Aseismic slip rates along the SAF and calculating aseismic slip since 1857

Explanation

*Aseismic slip rates (meters per year) were obtained from depth averaging the rates of Murray et al., 2001 for the Parkfield segment, we assume 27 mm/yr northwest of slack canyon (considering data from Titus et al., 2004 and Burford and Harsh, 1980)

Cumulative aseismic slip in meters, obtained by multiplying the slip rates by 148 years (2005-1857).

places	position northwest of highway 46 (km)	aseismic slip rate (m/y)*	cumulative aseismic slip (m)#
	-25	0.00000	0.0000
	-24	0.00000	0.0000
	-23	0.00000	0.0000
	-22	0.00000	0.0000
	-21	0.00000	0.0000
	-20	0.00000	0.0000
	-19	0.00000	0.0000
	-18	0.00000	0.0000
	-17	0.00000	0.0000
	-16	0.00000	0.0000
	-15	0.00000	0.0000
	-14	0.00000	0.0000
	-13	0.00000	0.0000
	-12	0.00000	0.0000
	-11	0.00000	0.0000
	-10	0.00000	0.0000
	-9	0.00000	0.0000
	-8	0.00000	0.0000
	-7	0.00000	0.0000
	-6	0.00000	0.0000
	-5	0.00000	0.0000
	-4	0.00000	0.0000
	-3	0.00000	0.0000
	-2	0.00000	0.0000
	-1	0.00000	0.0000
hwy 46	0	0.00000	0.0000
	1	0.00149	0.2206
	2	0.00298	0.4412
	3	0.00447	0.6618
	4	0.00488	0.7217
	5	0.00528	0.7816
	6	0.00569	0.8415
	7	0.00610	0.9028
	8	0.00651	0.9641
	9	0.00693	1.0254
	10	0.00719	1.0635
	11	0.00753	1.1142
	12	0.00770	1.1396
	13	0.00795	1.1762
	14	0.00820	1.2129
	15	0.00844	1.2495
	16	0.00880	1.3017
	17	0.00915	1.3538
	18	0.00950	1.4060
	19	0.01028	1.5216

	20	0.01106	1.6372
	21	0.01184	1.7527
Parkfield	22	0.01282	1.8979
	23	0.01380	2.0431
	24	0.01479	2.1883
	25	0.01592	2.3560
	26	0.01705	2.5238
	27	0.01819	2.6915
	28	0.01960	2.9015
	29	0.02102	3.1115
	30	0.02244	3.3215
	31	0.02311	3.4209
	32	0.02379	3.5203
	33	0.02446	3.6197
	34	0.02485	3.6774
	35	0.02524	3.7352
	36	0.02563	3.7930
	37	0.02563	3.7930
	38	0.02600	3.8480
	39	0.02600	3.8480
	40	0.02600	3.8480
	41	0.02600	3.8480
	42	0.02650	3.9220
	43	0.02650	3.9220
	44	0.02650	3.9220
	45	0.02650	3.9220
	46	0.02700	3.9960
	47	0.02700	3.9960
Slack Canyon	48	0.02700	3.9960
	49	0.02700	3.9960
	50	0.02700	3.9960
	51	0.02700	3.9960
	52	0.02700	3.9960
	53	0.02700	3.9960
	54	0.02700	3.9960
	55	0.02700	3.9960
	56	0.02700	3.9960
	57	0.02700	3.9960
	58	0.02700	3.9960
	59	0.02700	3.9960
	60	0.02700	3.9960

APPENDIX E

COSEISMIC SLIP CALCULATIONS

CS1

Calculating cumulative coseismic slip assuming only 6 Parkfield events and assuming the events prior to 1966 had similar surface ruptures as 2004.

Explanation CS1

* Event slip is assumed to be the surface slip presented in Lienkaemper et al., BSSA this issue. In this calculation we assume that Parkfield events prior to 1966 ruptured similar to 2004.

Event slip is assumed to be the surface slip as presented in Lienkaemper and Prescott, 1989.

Earthquakes

places	position northwest of highway 46 (km)	cm 1881*	cm 1901*	cm 1922*	cm 1934*	cm 1966#	cm 2004*	cm SUM	meters SUM
	-25					0	0.00		
	-24					0	0.00		
	-23					0	0.00		
	-22					0	0.00		
	-21					0	0.00		
	-20					0	0.00		
	-19					0	0.00		
	-18					0	0.00		
	-17					0	0.00		
	-16					0	0.00		
	-15					0	0.00		
	-14					0	0.00		
	-13					0	0.00		
	-12					0	0.00		
	-11					0	0.00		
	-10					0	0.00		
	-9					0	0.00		
	-8					0	0.00		
	-7			1		1	0.01		
	-6			2		2	0.02		
	-5	1	1	1	1	4	1	9	0.09
	-4	2	2	2	2	6	2	16	0.16
	-3	3	3	3	3	8	3	23	0.23
	-2	4	4	4	4	10	4	30	0.30
	-1	5	5	5	5	12	5	37	0.37
hwy 46	0	6	6	6	6	13	6	43	0.43

1	6	6	6	6	13	6	43	0.43
2	7	7	7	7	14	7	49	0.49
3	7	7	7	7	15	7	50	0.50
4	7	7	7	7	16	7	51	0.51
5	8	8	8	8	17	8	57	0.57
6	8	8	8	8	18	8	58	0.58
7	9	9	9	9	19	9	64	0.64
8	9	9	9	9	20	9	65	0.65
9	10	10	10	10	20	10	70	0.70
10	10	10	10	10	21	10	71	0.71
11	15	15	15	15	27	15	102	1.02
12	21	21	21	21	33	21	138	1.38
13	27	27	27	27	39	27	174	1.74
14	32	32	32	32	46	32	206	2.06
15	32	32	32	32	45	32	205	2.05
16	31	31	31	31	44	31	199	1.99
17	31	31	31	31	43	31	198	1.98
18	30	30	30	30	42	30	192	1.92
19	30	30	30	30	41	30	191	1.91
20	29	29	29	29	40	29	185	1.85
21	29	29	29	29	39	29	184	1.84
Parkfield22	28	28	28	28	38	28	178	1.78
23	27	27	27	27	37	27	172	1.72
24	26	26	26	26	35	26	165	1.65
25	25	25	25	25	33	25	158	1.58
26	23	23	23	23	31	23	146	1.46
27	22	22	22	22	29	22	139	1.39
28	20	20	20	20	27	20	127	1.27
29	19	19	19	19	26	19	121	1.21
30	17	17	17	17	24	17	109	1.09
31	16	16	16	16	23	16	103	1.03
32	15	15	15	15	22	15	97	0.97
33	14	14	14	14	21	14	91	0.91
34	13	13	13	13	20	13	85	0.85
35	12	12	12	12	19	12	79	0.79
36	11	11	11	11	18	11	73	0.73
37	10	10	10	10	17	10	67	0.67
38	9	9	9	9	16	9	61	0.61
39	8	8	8	8	15	8	55	0.55
40	7	7	7	7	14	7	49	0.49
41	6	6	6	6	13	6	43	0.43
42	5	5	5	5	12	5	37	0.37
43	4	4	4	4	11	4	31	0.31
44	3	3	3	3	10	3	25	0.25

CS2

calculating cumulative coseismic slip: CS2 = CS1 + additional Parkfield events identified by Topozada et al., 2002

places	position northwest of highway 46 (km)	cm	cm	cm	cm	cm	cm	cm	cm	cm	cm	m	SUM	
	-25	1877^	1881*	1901*	1908^	1922*	1922b^	1934*	1966#	2004*			0	0
	-24												0	0
	-23												0	0
	-22												0	0
	-21												0	0
	-20												0	0
	-19												0	0
	-18												0	0
	-17												0	0
	-16												0	0
	-15												0	0
	-14												0	0
	-13												0	0
	-12												0	0
	-11												0	0
	-10												0	0
	-9												0	0
	-8												0	0
	-7								1				1	0.01
	-6								2				2	0.02
	-5		1	1		1		1	4	1			9	0.09
	-4		2	2		2		2	6	2			16	0.16
	-3		3	3		3		3	8	3			23	0.23
	-2		4	4		4		4	10	4			30	0.3
	-1		5	5		5		5	12	5			37	0.37
hwy 46	0		6	6		6		6	13	6			43	0.43
	1		6	6		6		6	13	6			43	0.43
	2		7	7		7		7	14	7			49	0.49
	3		7	7		7		7	15	7			50	0.5
	4		7	7		7		7	16	7			51	0.51
	5		8	8		8		8	17	8			57	0.57
	6		8	8		8		8	18	8			58	0.58
	7		9	9		9		9	19	9			64	0.64
	8		9	9		9		9	20	9			65	0.65
	9		10	10		10		10	20	10			70	0.7
	10		10	10		10		10	21	10			71	0.71
	11		15	15		15		15	27	15			102	1.02
	12		21	21		21		21	33	21			138	1.38
	13		27	27		27		27	39	27			174	1.74
	14		32	32		32		32	46	32			206	2.06
	15		32	32		32		32	45	32			205	2.05
	16		31	31		31		31	44	31			199	1.99
	17		31	31		31		31	43	31			198	1.98
	18		30	30		30		30	42	30			192	1.92
	19	21	30	30		30		30	41	30			212	2.12
	20	21	29	29		29		29	40	29			206	2.06
	21	21	29	29		29		29	39	29			205	2.05
Parkfield	22		28	28		28		28	38	28			178	1.78
	23		27	27		27		27	37	27			172	1.72
	24		26	26		26		26	35	26			165	1.65
	25		25	25		25		25	33	25			158	1.58
	26		23	23		23		23	31	23			146	1.46
	27		22	22		22		22	29	22			139	1.39
	28		20	20		20		20	27	20			127	1.27
	29		19	19		19		19	26	19			121	1.21
	30		17	17		17		17	24	17			109	1.09

31	16	16		16	16	23	16	103	1.03
32	15	15		15	15	22	15	97	0.97
33	14	14		14	14	21	14	91	0.91
34	13	13		13	13	20	13	85	0.85
35	12	12	30	12	12	19	12	109	1.09
36	11	11	30	11	11	18	11	103	1.03
37	10	10	30	10	10	17	10	97	0.97
38	9	9	30	9	9	16	9	91	0.91
39	8	8	30	8	8	15	8	85	0.85
40	7	7	30	7	7	14	7	79	0.79
41	6	6	30	6	6	13	6	73	0.73
42	5	5		5	5	12	5	37	0.37
43	4	4		4	4	11	4	31	0.31
44	3	3		3	3	10	3	25	0.25
45	2	2		2	2	9	2	19	0.19
46	1	1		1	26	1	8	39	0.39
47					26		7	33	0.33
Slack Canyon									
48					26		6	32	0.32
49					26		5	31	0.31
50					26		4	30	0.3
51					26		3	29	0.29
52							2	2	0.02
53							1	1	0.01
54								0	0
55								0	0
56								0	0
57								0	0
58								0	0
59								0	0
60								0	0

Explanation of CS2

* Event slip is assumed to be the surface slip presented in Lienkaemper et al., BSSA this issue. In this calculation we assume that Parkfield events prior to 1966 ruptured similar to 2004.

Event slip is assumed to be the surface slip as presented in Lienkaemper and Prescott, 1989.

^ Topozada et al., 2002 identified events. Rupture extent and average extent were calculated using the empirical relationships of Wells and Coppersmith et al., 1994 (modified by Arrowsmith et al., 1997 for California strike slip earthquakes. See below for calculations

Empirical Calculations

Relationship between magnitude and rupture area (Arrowsmith et al., 1997)

Moment Magnitude = $3.9987 + 0.97471 \log(\text{rupture area})$

We assume a constant rupture depth of Topozada Identified
 events (date, estimated magnitudes, and location northwest of Hwy 46)

10 km	year	Magnitude (Mw)	loc
	5/30/1877	5.5	20.1
	4/27/1908	5.8	37.9
	8/18/1922	5.7	49.3

Rupture area Calculations = $10^{((Mw-3.9987)/0.97471)}$

date	Rupture area (km ²)
5/30/1877	34.69389009
4/27/1908	70.47528681
8/18/1922	55.64706127

Rupture Length = Rupture area/10km

date	Rupture length (km)
5/30/1877	3
4/27/1908	7
8/18/1922	6

Moment = $M_0 = 10^{((3/2)*(Mw+10.73))}$

date	moment (dyn/cm)
5/30/1877	2.21309E+24
4/27/1908	6.23735E+24
8/18/1922	4.4157E+24

Displacement = $[\text{Moment}/(u = 3*10^{11} \text{ dyn/cm})]/\text{rupture area}$

date	displacement (cm)
5/30/1877	21
4/27/1908	30
8/18/1922	26

CS3

calculating cumulative coseismic slip: CS3= 2004 and 1966 (Iienkaemper et al., this issue) and earlier Parkfield events calculated empirically (Topozada et al., 2002; Wells and Coppersmith, 1994; Arrowsmith et al., 1997)

places	position northwest of highway 46 (km)	cm 1877 ^	cm 1881 ^	cm 1901 ^	cm 1908 ^	cm 1922 ^	cm 1922b ^	cm 1934 ^	cm 1966 #	cm 2004*	cm SU M	meter s SUM
	-25										0	0
	-24										0	0
	-23										0	0
	-22										0	0
	-21										0	0
	-20										0	0
	-19										0	0
	-18										0	0
	-17										0	0
	-16										0	0
	-15										0	0
	-14										0	0
	-13										0	0
	-12										0	0
	-11										0	0
	-10										0	0
	-9										0	0
	-8										0	0
	-7								1		1	0.01
	-6								2		2	0.02
	-5								4	1	5	0.05
	-4								6	2	8	0.08
	-3								8	3	11	0.11
	-2								10	4	14	0.14
	-1								12	5	17	0.17
hwy 46	0								13	6	19	0.19
	1								13	6	19	0.19
	2								14	7	21	0.21
	3								15	7	22	0.22
	4								16	7	23	0.23
	5								17	8	25	0.25
	6								18	8	26	0.26
	7								19	9	28	0.28
	8								20	9	29	0.29
	9								20	10	30	0.3
	10								21	10	31	0.31
	11								27	15	42	0.42
	12								33	21	54	0.54
	13								39	27	66	0.66
	14								46	32	78	0.78
	15								45	32	77	0.77
	16								44	31	75	0.75
	17								43	31	74	0.74
	18								42	30	72	0.72
	19	21							41	30	92	0.92
	20	21							40	29	90	0.9
	21	21							39	29	89	0.89
Parkfield	22								38	28	66	0.66
	23								37	27	64	0.64
	24								35	26	61	0.61
	25								33	25	58	0.58
	26							37	31	23	91	0.91
	27							37	29	22	88	0.88
	28							37	27	20	84	0.84

	29				37	26	19	82	0.82
	30				37	24	17	78	0.78
	31				37	23	16	76	0.76
	32				37	22	15	74	0.74
	33				37	21	14	72	0.72
	34				37	20	13	70	0.7
	35			30	37	19	12	98	0.98
	36			30	37	18	11	96	0.96
	37			30		17	10	57	0.57
	38	37		30		16	9	92	0.92
	39	37		30	51	15	8	141	1.41
	40	37		30	51	14	7	139	1.39
	41	37		30	51	13	6	137	1.37
	42	37			51	12	5	105	1.05
	43	37			51	11	4	103	1.03
	44	37			51	10	3	101	1.01
	45	37			51	9	2	99	0.99
	46	37			51	26	8	123	1.23
	47	37			51	26	7	121	1.21
Slack Canyon	48	37			51	26	6	120	1.2
	49				51	26	5	82	0.82
	50		57		51	26	4	138	1.38
	51		57		51	26	3	137	1.37
	52		57		51		2	110	1.1
	53		57		51		1	109	1.09
	54		57		51			108	1.08
	55		57		51			108	1.08
	56		57		51			108	1.08
	57		57		51			108	1.08
	58		57		51			108	1.08
	59		57		51			108	1.08
	60		57		51			108	1.08

Explanation CS3

* Event slip is assumed to be the surface slip presented in Lienkaemper et al., BSSA this issue. In this calculation we assume that Parkfield events prior to 1966 ruptured similar to 2004.

Event slip is assumed to be the surface slip as presented in Lienkaemper and Prescott, 1989.

^ Topozada et al., 2002 identified events. Rupture extent and average extent were calculated using the empirical relationships of Wells and Coppersmith et al., 1994 (modified by Arrowsmith et al., 1997 for California strike slip earthquakes. See below for calculations

Empirical Calculations

Relationship between magnitude and rupture area (Arrowsmith et al., 1997)

$$\text{Moment Magnitude} = 3.9987 + 0.97471 \log(\text{rupture area})$$

We assume a constant rupture depth of 10 km
 events (date, estimated magnitudes, and location northwest of Hwy 46) Topozada Identified

10 km	year	Magnitude (Mw)	loc
	5-30-1877	5.5	20.1
	2-2-1881	6	42.8
	3/3/1901	6.4	63.6
	4/27/1908	5.8	37.9
	3/10/1922	6.3	49.3
	8/18/1922	5.7	49.3
	1/8/1934	6	30.8

$$\text{Rupture area Calculations} = 10^{((Mw-3.9987)/0.97471)}$$

date	Rupture area (km ²)
5-30-1877	35
2-2-1881	113
3/3/1901	291
4/27/1908	70
3/10/1922	230
8/18/1922	56
1/8/1934	113

$$\text{Rupture Length} = \text{Rupture area}/10\text{km}$$

date	Rupture length (km)
5-30-1877	3
2-2-1881	11
3/3/1901	29
4/27/1908	7
3/10/1922	23
8/18/1922	6
1/8/1934	11

$$\text{Moment} = M_0 = 10^{((3/2)*(M_w + 10.73))}$$

date	moment (dyn/cm)
5-30-1877	2.21309E+24
2-2-1881	1.24451E+25
3/3/1901	4.9545E+25
4/27/1908	6.23735E+24
3/10/1922	3.50752E+25
8/18/1922	4.4157E+24
1/8/1934	1.24451E+25

$$\text{Displacement} = [\text{Moment}/(u = 3*10^{11} \text{ dyn/cm})]/\text{rupture area}$$

date	displacement (cm)
5-30-1877	21
2-2-1881	37
3/3/1901	57
4/27/1908	30
3/10/1922	51
8/18/1922	26
1/8/1934	37

APPENDIX F

COSEISMIC SLIP CALCULATIONS

Slip budget comparisons reveal a slip deficit along the SAF (three variations are produced by three estimations of coseismic slip: CS1, CS2, and CS3)
refer to figures 3-5 and supplemental tables 1-4

Slip budget = (Expected slip = long-term slip rate*time) - (cumulative aseismic slip + cumulative coseismic slip)

places	position northwest of highway 46 (km)	Expected slip (m) (.033 meters/year * 148 years)	cumulative aseismic slip (m)	CS1 coseismic slip (m)	CS2 coseismic slip (m)	CS3 coseismic slip (m)	meters Slip Deficit CS1	meters Slip Deficit CS2	meters Slip Deficit CS3
							C-(D+E)	C-(D+F)	C-(D+G)
	-25	4.884	0.0000	0	0	0	4.8840	4.8840	4.8840
	-24	4.884	0.0000	0	0	0	4.8840	4.8840	4.8840
	-23	4.884	0.0000	0	0	0	4.8840	4.8840	4.8840
	-22	4.884	0.0000	0	0	0	4.8840	4.8840	4.8840
	-21	4.884	0.0000	0	0	0	4.8840	4.8840	4.8840
	-20	4.884	0.0000	0	0	0	4.8840	4.8840	4.8840
	-19	4.884	0.0000	0	0	0	4.8840	4.8840	4.8840
	-18	4.884	0.0000	0	0	0	4.8840	4.8840	4.8840
	-17	4.884	0.0000	0	0	0	4.8840	4.8840	4.8840
	-16	4.884	0.0000	0	0	0	4.8840	4.8840	4.8840
	-15	4.884	0.0000	0	0	0	4.8840	4.8840	4.8840
	-14	4.884	0.0000	0	0	0	4.8840	4.8840	4.8840
	-13	4.884	0.0000	0	0	0	4.8840	4.8840	4.8840
	-12	4.884	0.0000	0	0	0	4.8840	4.8840	4.8840
	-11	4.884	0.0000	0	0	0	4.8840	4.8840	4.8840
	-10	4.884	0.0000	0	0	0	4.8840	4.8840	4.8840
	-9	4.884	0.0000	0	0	0	4.8840	4.8840	4.8840
	-8	4.884	0.0000	0	0	0	4.8840	4.8840	4.8840
	-7	4.884	0.0000	0.01	0.01	0.01	4.8740	4.8740	4.8740
	-6	4.884	0.0000	0.02	0.02	0.02	4.8640	4.8640	4.8640
	-5	4.884	0.0000	0.09	0.09	0.05	4.7940	4.7940	4.8340
	-4	4.884	0.0000	0.16	0.16	0.08	4.7240	4.7240	4.8040
	-3	4.884	0.0000	0.23	0.23	0.11	4.6540	4.6540	4.7740
	-2	4.884	0.0000	0.3	0.3	0.14	4.5840	4.5840	4.7440
	-1	4.884	0.0000	0.37	0.37	0.17	4.5140	4.5140	4.7140
hwy 46	0	4.884	0.0000	0.43	0.43	0.19	4.4540	4.4540	4.6940
	1	4.884	0.2206	0.43	0.43	0.19	4.2334	4.2334	4.4734
	2	4.884	0.4412	0.49	0.49	0.21	3.9528	3.9528	4.2328
	3	4.884	0.6618	0.5	0.5	0.22	3.7222	3.7222	4.0022
	4	4.884	0.7217	0.51	0.51	0.23	3.6523	3.6523	3.9323
	5	4.884	0.7816	0.57	0.57	0.25	3.5324	3.5324	3.8524
	6	4.884	0.8415	0.58	0.58	0.26	3.4625	3.4625	3.7825
	7	4.884	0.9028	0.64	0.64	0.28	3.3412	3.3412	3.7012
	8	4.884	0.9641	0.65	0.65	0.29	3.2699	3.2699	3.6299
	9	4.884	1.0254	0.7	0.7	0.3	3.1586	3.1586	3.5586
	10	4.884	1.0635	0.71	0.71	0.31	3.1105	3.1105	3.5105
	11	4.884	1.1142	1.02	1.02	0.42	2.7498	2.7498	3.3498
	12	4.884	1.1396	1.38	1.38	0.54	2.3644	2.3644	3.2044
	13	4.884	1.1762	1.74	1.74	0.66	1.9678	1.9678	3.0478
	14	4.884	1.2129	2.06	2.06	0.78	1.6111	1.6111	2.8911
	15	4.884	1.2495	2.05	2.05	0.77	1.5845	1.5845	2.8645
	16	4.884	1.3017	1.99	1.99	0.75	1.5923	1.5923	2.8323
	17	4.884	1.3538	1.98	1.98	0.74	1.5502	1.5502	2.7902

	18	4.884	1.4060	1.92	1.92	0.72	1.5580	1.5580	2.7580
	19	4.884	1.5216	1.91	2.12	0.92	1.4524	1.2424	2.4424
	20	4.884	1.6372	1.85	2.06	0.9	1.3968	1.1868	2.3468
	21	4.884	1.7527	1.84	2.05	0.89	1.2913	1.0813	2.2413
Parkfield	22	4.884	1.8979	1.78	1.78	0.66	1.2061	1.2061	2.3261
	23	4.884	2.0431	1.72	1.72	0.64	1.1209	1.1209	2.2009
	24	4.884	2.1883	1.65	1.65	0.61	1.0457	1.0457	2.0857
	25	4.884	2.3560	1.58	1.58	0.58	0.9480	0.9480	1.9480
	26	4.884	2.5238	1.46	1.46	0.91	0.9002	0.9002	1.4502
	27	4.884	2.6915	1.39	1.39	0.88	0.8025	0.8025	1.3125
	28	4.884	2.9015	1.27	1.27	0.84	0.7125	0.7125	1.1425
	29	4.884	3.1115	1.21	1.21	0.82	0.5625	0.5625	0.9525
	30	4.884	3.3215	1.09	1.09	0.78	0.4725	0.4725	0.7825
	31	4.884	3.4209	1.03	1.03	0.76	0.4331	0.4331	0.7031
	32	4.884	3.5203	0.97	0.97	0.74	0.3937	0.3937	0.6237
	33	4.884	3.6197	0.91	0.91	0.72	0.3543	0.3543	0.5443
	34	4.884	3.6774	0.85	0.85	0.7	0.3566	0.3566	0.5066
	35	4.884	3.7352	0.79	1.09	0.98	0.3588	0.0588	0.1688
	36	4.884	3.7930	0.73	1.03	0.96	0.3610	0.0610	0.1310
	37	4.884	3.7930	0.67	0.97	0.57	0.4210	0.1210	0.5210
	38	4.884	3.8480	0.61	0.91	0.92	0.4260	0.1260	0.1160
	39	4.884	3.8480	0.55	0.85	1.41	0.4860	0.1860	-0.3740
	40	4.884	3.8480	0.49	0.79	1.39	0.5460	0.2460	-0.3540
	41	4.884	3.8480	0.43	0.73	1.37	0.6060	0.3060	-0.3340
	42	4.884	3.9220	0.37	0.37	1.05	0.5920	0.5920	-0.0880
	43	4.884	3.9220	0.31	0.31	1.03	0.6520	0.6520	-0.0680
	44	4.884	3.9220	0.25	0.25	1.01	0.7120	0.7120	-0.0480
	45	4.884	3.9220	0.19	0.19	0.99	0.7720	0.7720	-0.0280
	46	4.884	3.9960	0.13	0.39	1.23	0.7580	0.4980	-0.3420
	47	4.884	3.9960	0.07	0.33	1.21	0.8180	0.5580	-0.3220
Slack Canyon	48	4.884	3.9960	0.06	0.32	1.2	0.8280	0.5680	-0.3120
	49	4.884	3.9960	0.05	0.31	0.82	0.8380	0.5780	0.0680
	50	4.884	3.9960	0.04	0.3	1.38	0.8480	0.5880	-0.4920
	51	4.884	3.9960	0.03	0.29	1.37	0.8580	0.5980	-0.4820
	52	4.884	3.9960	0.02	0.02	1.1	0.8680	0.8680	-0.2120
	53	4.884	3.9960	0.01	0.01	1.09	0.8780	0.8780	-0.2020
	54	4.884	3.9960	0	0	1.08	0.8880	0.8880	-0.1920
	55	4.884	3.9960	0	0	1.08	0.8880	0.8880	-0.1920
	56	4.884	3.9960	0	0	1.08	0.8880	0.8880	-0.1920
	57	4.884	3.9960	0	0	1.08	0.8880	0.8880	-0.1920
	58	4.884	3.9960	0	0	1.08	0.8880	0.8880	-0.1920
	59	4.884	3.9960	0	0	1.08	0.8880	0.8880	-0.1920
	60	4.884	3.9960	0	0	1.08	0.8880	0.8880	-0.1920